LBL-2772

AN INVESTIGATION OF BAINITE TRANSFORMATION IN MEDIUM CARBON LOW ALLOY STEELS

B. Naga Prakash Babu
(D. Eng. Thesis)

August 1974

Prepared for the U.S. Atomic Energy Commission
under Contract W-7405-ENG-48

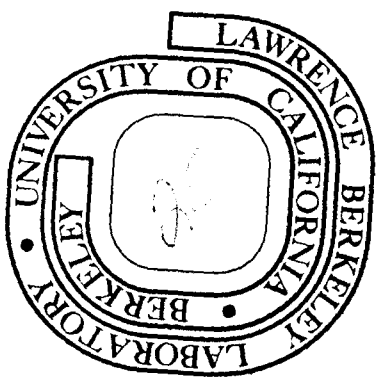

LBL-2772

DISCLAIMER

AN INVESTIGATION OF BAINITE TRANSFORMATION
IN MEDIUM CARBON LOW ALLOY STEELS

Contents

AN INVESTIGATION OF BAINITE TRANSFORMATION IN MEDIUM CARBON LOW ALLOY STEELS

B. Naga Prakash Babu

Inorganic Materials Research Division, Lawrence Berkeley Laboratory and Department of Materials Science and Engineering, College of Engineering; University of California, Berkeley, California

ABSTRACT

The effects of small additions of common alloying elements (C, Ni, Cr, Mn, Mo and Si) on the kinetics of the bainite reaction in 4340 steel were studied. The 4340 steel was selected as a base because it had the necessary pearlitic hardenability and this enabled studies of the bainite reaction to be made without interference from the proeutectoid or pearlite reactions. A rapid magnetic permeability method was developed to facilitate this investigation. It consisted of quenching the sample from an austenitizing temperature to a subcritical temperature in an isothermal bath which was held within the field of an inductor coil. The increase in permeability accompanying austenite decomposition increased the inductance of the coil, and this changed the resonant period of oscillation of the circuit. An automatic continuous recording of the period provided a convenient and accurate method for following the austenite decomposition. Computer aided methods were used to analyze the isothermal reaction data and to plot the time-temperature-transformation (TTT) diagrams.

An acceleration of the bainite reaction just above the M_s temperature gave an S-shaped curve for the bainite reaction in all the steels studied. In some of the steels, separate C-curves for the upper and lower bainite were observed in the initial stages of transformation, but these

overlapped in the later stages. All the alloy additions (wt%) except additions of Mo increased the incubation times for bainite reaction. Silicon, up to 2% addition was as effective as Ni or Cr, and 1% Ni + 1% Cr addition was more effective than either a 2% Ni or 2% Cr addition in increasing the incubation period. All the alloying elements except Mo shifted the bainite curves to longer times and lowered the kinetic B_s and B_f temperatures. Molybdenum, when added alone, accelerated the bainite reaction and raised the B_s and M_s temperatures, but when added together with Ni or Cr, retarded the bainite reaction. Manganese, up to 2% addition was more effective than Ni or Cr in improving the bainite hardenability. The effect of a 2% alloy addition was not equal to 2 times the effect of 1% addition. The ratios of times for 5% transformation for 2% vs 1% additions of Ni, Cr and Mn are 1.3, 15.5 and 20 respectively. The effect of combined additions on bainite hardenability was not linear, but mixed additions had an additive effect in lowering the B_s temperature. An equation was derived to calculate the B_s temperature directly from the composition.

In 4340 and 4340 modified with Ni, Cr, Mn and Mo, a distinct change in the experimental activation energy of decomposition occurred around 350°C. This indicates that the initial transformation product may change from upper bainite to lower bainite, or vice versa, at about 350°C. Transmission electron microscopy studies of the morphology of bainite in 4340 + 0.1% C steel showed that mixed bainites formed in the temperature range where the two C-curves of upper bainite and lower bainite overlap. Thus, depending on the transformation temperature, upper bainite may form first followed by lower bainite or vice versa. The classical forms

of bainite containing carbides were formed in 4340 + 0.1% C steel. G. Lai (private communication) has shown the upper bainite that formed in silicon modified steels was devoid of carbides.

Partial transformation to bainite produced significant amounts of retained austenite in all the steels studied, with Si modified steels showing considerably larger amounts of retained austenite. For the same carbon content, the amount of retained austenite obtained at any particular reaction temperature increased with the increase in silicon content and for the same silicon content, it increased with increasing carbon content.

I. INTRODUCTION

The nature of the bainitic transformation, even 40 years after its discovery,[1] continues to be the subject of debate.[2] Although the morphology of bainite has been well characterized,[3] its growth kinetics and mechanisms are still not completely resolved. The bainite reaction occurs at an intermediate temperature range of austenite decomposition, overlapping with the proeutectoid and pearlite reactions at high temperatures, and with the martensite reaction at low temperatures. From a practical viewpoint, it is important to understand the relative merits of various types and morphologies of bainite as compared to martensite in their influence on the fracture toughness of the heat treated steels.

From a microstructural viewpoint, bainite is defined as a non-lamellar aggregate of ferrite and carbide with an acicular morphology. Since the early metallographic studies,[1] at least two variants have been recognized. These two classical variants of bainite are usually called upper and lower bainite. Upper bainite consists of ferrite laths with carbides precipitated along the lath boundaries. Its presence has a detrimental effect on the fracture toughness of martensitic steels, and heat treatments that produce this structure should be avoided. This is sometimes difficult in complex parts with varying section sizes. In lower bainite the carbides are precipitated within ferrite plates and at an angle to the major axis of the plate. It is considered to be comparable in fracture toughness to

tempered martensite. In designing alloys of optimum hardenability* for specific applications, factors affecting bainitic hardenability, particularly upper bainitic hardenability, should be considered in addition to those affecting pearlitic hardenability. Precise knowledge of the location and shape of the lower and upper bainite reactions is important from a hardenability viewpoint.

The alloying elements which comprise the composition of steel and the solid state reactions which they undergo determine the structure and, therefore, the properties of steel. These detailed reactions, which are important in the economic design of superior steels, are not yet fully understood. Very little work has been done on the effect of alloying elements on the kinetics of the bainite reaction. This is in contrast to the large volume of kinetic data available on the proeutectoid ferrite and pearlite reactions. A systematic study of the influence of alloying elements, individually and in combination, on the shape and position of time-temperature-transformation (TTT) curves in steel has been a formidable task, because of the tedious and laborious nature of the techniques used. The present investigation had several objectives. One of the objectives was to develop a rapid experimental technique for the study of transformation kinetics. A magnetic permeability technique was developed which consists of quenching the sample from an austenitizing

---

*The term "hardenability" as defined by Grossman means the ability to generate martensite, and the term "pearlitic hardenability" means the ability to avoid the formation of pearlite and thus making possible bainite and martensite transformations. In the same vein, the term "bainitic hardenability" has been used to mean the ability to avoid the formation of bainite to produce martensite, and the term "upper bainitic hardenability" refers to the ability of the steel to avoid the formation of upper bainite so that it can be transformed to lower bainite and martensite.

temperature to a subcritical temperature in an isothermal bath and holding it within the magnetic field of an inductor coil. The increase in permeability accompanying austenite decomposition increases the inductance of the coil, and this changes the resonant frequency of the circuit. An automatic continuous recording of the corresponding period provides a convenient and accurate method for following the austenite decomposition.

To test the above technique and to facilitate the evaluation of the effect of alloying elements on bainite reaction, it was necessary to choose a steel in which the pearlite or proeutectoid reactions did not interfere with the bainite reaction. A commercial low alloy steel, AISI 4340 steel was selected for this purpose. Additional amounts of Mn, Ni, Cr, Mo and Si were added to the base composition in order to study the effect of alloying elements on the bainite reaction. The magnetic method was used to follow the isothermal decomposition of austenite in the bainite and martensite temperature ranges of the steels. A computer aided analysis was employed to provide accurate quantitative values of the kinetics of transformation.

It is not always possible to distinguish by optical methods between the two variants of bainite. The morphological study[3] conducted using replica and thin-foil transmission electron microscopy techniques has revealed that a structural transition exists between the two variants of bainite. Kinetic methods used in recent years for studying the bainite reaction[4-7] have shown that in plain carbon steels, at

about 350°C, there is a sharp change in the activation energy of decomposition. This change is said to correspond to the transition between upper and lower bainite. However, both kinetic and morphological studies of the bainitic reaction have not been carried out in the same steel. One objective of this investigation was to conduct such a study to see whether the transition temperature obtained by kinetic methods is the same as the temperature at which the structural transition is observed.

It is reasonable to assume that upper and lower bainites have different reaction kinetics and thus there may be a corresponding discontinuity in the TTT curves. It is of interest then to determine whether such a discontinuity could be detected by accurate determination of the TTT curves in the vicinity of the transition from upper to lower bainite.

The subject of bainite transformation is rightly referred[8] to as a microcosm of metallurgy since it covers the whole range of transformation and precipitation reactions including diffusion controlled and shear nucleation. Understanding the mechanism of bainite formation is essential in explaining its structural features. In this investigation an attempt was also made to understand the factors causing the structural differences in the two variants of bainite.

II. MATERIAL PREPARATION AND EXPERIMENTAL METHODS

A. Material Preparation

The basic material used in this investigation was a commercial aircraft quality AISI 4340 steel. Its chemical composition in wt% was: 0.39 carbon, 0.70 manganese, 0.28 silicon, 0.76 chromium, 1.70 nickel, 0.20 molybdenum and 0.22 copper. The steel was received in the form of 5/8 in. thick bar stock and in a fully annealed condition. To obtain modified compositions of 4340 steel, the bar stock was sectioned into several short lengths. Each length was individually vacuum melted with the desired alloy addition into a 4 lb ingot. Table I lists the alloy compositions. It is to be noted that heat No. 741-23 was a remelt of 4340 with no alloy addition. The ingots were homogenized in vacuum either for 72 hr at 1100°C or for 24 hr at 1200°C.

Chemical analysis, when performed, was done only for the element that was added to the base 4340 steel in making up the heat. The results of the chemical analyses are compared with the expected values in Table II. It is apparent that there is virtually no loss of any added element during melting and homogenizing.

The ingots after homogenizing were softened by holding at 600°C for 4 hr. Specimens for isothermal treatments were prepared by cutting 0.06 in. thick strips from the ingots and then cold rolling the strips to 0.03 in. thickness. From the rolled lengths, samples with dimensions of 2 in. by 0.56 in. by 0.03 in. were prepared.

Table I. List of alloys prepared and their composition (given in wt%).

Heat Number	Alloy Composition
736-1	4340 + 0.1% C
736-2	4340 + 1.0% Ni
736-3	4340 + 2.0% Ni
736-4	4340 + 1.0% Cr
741-24	4340 + 2.0% Cr
741-26	4340 + 1.0% Mn
741-27	4340 + 2.0% Mn
736-7	4340 + 1.0% Si
741-25	4340 + 2.0% Si
736-8	4340 + 3.0% Si
741-16	4340 + 0.10% C + 3.0% Si
741-17	4340 + 0.20% C + 3.0% Si
736-6	4340 + 0.5% Mo
736-14	4340 + 1.0% Ni + 1.0% Cr
736-15	4340 + 1.0% Ni + 0.5% Mo
736-16	4340 + 1.0% Cr + 0.5% Mo
736-17	4340 + 1.0% Ni + 1.0% Cr + 0.5% Mo
741-23	Remelt of 4340

Table II. Results of chemical analysis (given in wt%).

Alloy	Composition of the Analyzed Elements						Expected Composition
	C	Mn	Cr	Ni	Mo	Si	
4340 + 0.10% C	0.48						0.49 C
4340 + 1.0% Ni				2.72			2.70 Ni
4340 + 2.0% Ni				3.71			3.70 Ni
4340 + 1.0% Cr			1.72				1.76 Cr
4340 + 0.5% Mo					0.73		0.73 Mo
4340 + 1.0% Si						1.24	1.28 Si
4340 + 3.0% Si						3.22	3.28 Si
4340 + 2.0% Cr			2.69				2.76 Cr
4340 + 2.0% Si						2.22	2.28 Si
4340 + 1.0% Mn		1.78					1.70 Mn
4340 + 2.0% Mn		2.74					2.70 Mn

B. Magnetometric Technique

1. Introduction

Since the pioneering work of Davenport and Bain in 1930,[1] a tremendous amount of information on the isothermal transformation behavior of steel has been generated. Numerous papers and several compilations of collated time-temperature transformation (TTT) diagrams have been published. However, the original metallographic methods developed by Davenport and Bain to study pearlitic and bainitic transformations are time consuming and laborious and require considerable skill in the metallographic examination of a series of samples reacted isothermally for various periods of time. In general, these methods lack accuracy, and consistency is difficult to insure from sample to sample.[9] The microscopic method commonly referred to as the quench-temper technique described by Greninger and Troiano[10] for the determination of martensite formation ranges is also subject to limitations. This technique is restricted to steels of high bainitic hardenability, because it is virtually impossible to distinguish between tempered martensite and lower bainite, when these constituents are present together.[11]

Several investigators have attempted to follow the course of austenite transformation by methods involving the measurement of some physical property that changes during transformation, such as a physical dimension, the electrical resistance,[12] a magnetic property[13,14] or the hardness.[15] Most TTT diagrams have been determined by the combined application of metallographic and dilatation methods, the former to determine the initial stages of transformation, and the latter to follow the subsequent progress during transformation. Measuring the dilation

of long, thin specimens has been criticized[16] as not truly being a measure of the volume fraction transformed, particularly in the case when acicular products are formed. The electrical resistivity method has also been criticized[9] since it is not a simple function of the transformation, but instead involves other factors, such as particle size and lattice coherency.

Magnetic permeability methods have been used by relatively few investigators. The type of apparatus previously used involved either an electrical transformer[14] or an electromagnet having a secondary search coil.[17] The sample was held isothermally between the poles of a transformer or within the airgap of a magnet. The induced emf in the secondary winding due to the magnetic change in the sample was recorded visually or photographically. The magnetic method developed in the present investigation is an evolution of the above magnetic techniques with the advantages that it is simple, more sensitive, and can be used to study austenite transformations at all temperatures and in time periods ranging from 2 sec to many hours. Details of this method are given in the following sections.

2. Experimental Apparatus

The apparatus consisted of a vertical tube furnace for austenitizing the sample, an isothermal quenching system for holding the sample at the desired subcritical temperature, a sensing coil, and an electronic system to measure and record the extent of transformation in the sample. A sketch of the furnace, quenching system, and the sensing coil is shown in Fig. 1. A block diagram of the electronic system is shown in Fig. 2. A photograph of the apparatus is given in Fig. 3.

a. Tube furnace. The mullite tube furnace, 1 in. in internal diameter and 33 in. long, and mounted vertically, had a uniform hot zone over a 2 1/2 in. length. This uniform zone was 7 in. from the bottom of the tube. The sample was attached with a tantalum wire to the end of a long Hastelloy rod (both of which are non-magnetic), which passed through a water cooled vacuum seal at the top of the furnace. The vertical movement of the rod inside the tube was guided by a sliding heat shield. Both ends of the tube were water cooled. The bottom end could be closed and sealed with a lid for evacuation. During the evacuation of the tube, the sample was held in the bottom cold zone. The long cold zone at the top of the furnace was needed to hold the part of the rod that became hot when the sample was being attached to the rod outside the bottom opening of the furnace.

b. Isothermal quenching system. The system contained an inconel tube, 1 in. in internal diameter and 18 in. long, mounted coaxially with the tube furnace. The quenching medium (quenching oil for temperatures up to 200°C, and molten salt for higher temperatures) was circulated through the tube by an impeller pump located at the base of the reservoir. The quenching medium was gravity fed to the pump through a central hole in the reservoir. The impeller shaft passed through this hole and was driven by a variable speed motor mounted at the top of the reservoir. The level of the quenching medium in the reservoir was maintained low enough to facilitate its gravity return from the inconel tube.

The system was insulated to minimize heat losses during the circulation of the quenching medium. The temperature of the medium was controlled as it was circulating by controlling the power input to the heating coil that surrounded the reservoir.

c. Sensing coil and electronic system. The sensing coil, 5 in. long and 2 in. in internal diameter, surrounded the inconel tube. It had an inductance of 90 mH, and oscillated at the resonant frequency of the circuit which was around 1.4 kHz. After austenitizing, the Hastelloy rod was thrust downward, placing the sample simultaneously into the circulating quench medium and within the field of the inductor coil. The increase in permeability of the sample, which resulted from increasing amounts of transformation from non-magnetic austenite to low temperature phases which are magnetic, caused an increase in the inductance (L) of the coil. The inductance of the coil determined the resonant period of ocillation (P) of the electrical circuit. A variable frequency oscillator (hereafter referred to as VFO) was used to measure the period. The output of the VFO was fed into a divider counter, which divided the frequency or in effect multiplied the period of oscillation by 1600. The control timing decoder monitored the count of the divider counter and provided start, stop, and reset signals to a time interval counter and a punch command to a paper tape punch, as indicated in Fig. 2. Considering the resonant frequency of the circuit at some instant to be 1.428 kHz, the resonant period as measured by the VFO was 0.0007003 sec/cycle. The resonant period as measured by the divider counter, which multiplied the output of the VFO by 1600, was equal to 1.12045 sec/cycle. In other words, it took 1.12045 second for the divider counter to count 1600. Thus, between start and stop signals, i.e., between counts 0000 and 1000 of the divider counter (or in a time interval of 0.70028 sec), the time interval counter with a 1 mHz time base had averaged the period of oscillation of the VFO over 998 cycles. When the count reached 1100,

i.e., after 0.77 sec from the start of the count, a punch command was sent to the tape punch, and the output from the time interval counter was recorded by the punch. Thus, the fastest recording time interval was every 0.77 sec.

It should be noted from Fig. 2 that the timing decoder obtains its time signal from the resonant period as measured by the divider counter. Thus, the recording interval is determined by the resonant period. When the resonant period changes because of the changes in inductance of the sensing coil, the recording interval will also change. For the size of the sample used the resonant period was found to change by a maximum of 0.00002 sec/cycle for complete transformation of the sample. Accordingly, the recording interval would change from 0.77 sec to 0.79 sec. This error was considered negligible, and was ignored especially since the error is trivial when considering the early stages of transformation. However, a correction can be made for the above error by using a multiple period averaging counter or an independent time signal which could be fed into the circuit.

To ensure the thermal stability of the system, the VFO was stored in a constant temperature container. The sensing coil was also maintained at a constant temperature by surrounding it with a water cooled copper jacket. Amidst external fields and stray capacitance, the system was stable enough to measure 1/10 of 1% transformation.

3. Experimental Procedure

To prevent oxidation and decarburization, the samples were austenitized in a vacuum of 8×10^{-5} Torr or better. Carbon analysis on samples, prior to and after austenitization showed no evidence of decarburization. Also, microhardness tests of a reacted sample indicated no surface decarburization.

It was important to know the cooling rate of the sample upon quenching into the isothermal bath. Temperature measurements were made by using a thermocouple consisting of 0.002 in. chromel and alumel wires, spotwelded to the opposite sides of the sample at its center. At first, a laminar flow of the quenching medium was used. The measurements showed that a 0.03 in. thick sample required 6 sec and a 0.01 in. thick sample required 4 sec to cool and stabilize at the temperature of the quenching medium. But by using counter current turbulent flow, the times were reduced to 2 sec and 1 sec, respectively.

The experimental procedure consisted of the following steps:

(1) The sample was held in the cold zone at the bottom of the furnace, the lid was closed and the tube was evacuated.

(2) The quenching medium was circulated and allowed to stabilize at the desired temperature.

(3) The electronic system was turned on, and allowed to warm up.

(4) After a good vacuum in the tube was obtained, the sample was raised into the hot zone and was austenitized at 900°C for 15 min.

(5) At the end of 15 min, the ceramic tube was isolated from the evacuating system.

(6) The latch holding the bottom lid was released.

(7) The tape punch was turned on.

(8) An inert gas was let into the tube to force the bottom lid open.

(9) The sample was then quenched and held in the inconel tube, within the field of the coil.

Initially, the tape punch recorded the period at intervals of 0.77 sec. In the later stages of transformation, recording was done at intervals of 7.77 sec or 77 sec. In the six digit printout, the last five digits gave the measured period, while the first digit was coded to indicate the recording intervals.

4. Analysis of Data

For a given alloy, the magnetic permeability is a function of temperature, strain, and structure of the phases present.[18] To interpret the data obtained at different temperatures, a calibration was needed for each alloy to account for the temperature and structure dependence of the magnetic permeability. To obtain quantitative values of the kinetics of the austenite decomposition, it was necessary to know for each alloy the value of ΔP for 100% transformation at each reaction temperature.

In alloy steels, in the upper part of the bainite range, it is known that the bainite reaction stabilizes short of complete austenitic transformation.[19] In some alloy steels, the bainite reaction is very slow and it can take several hours before the reaction is completed or stabilized short of completion. Thus it was time consuming and sometimes impossible to follow the reaction to completion in order to determine

the value of ΔP for 100% transformation. For the steels used in this study, complete transformation to martensite could be achieved by quenching the samples in water to room temperature and then refrigerating them in liquid nitrogen. The samples with fully martensitic structure were used to determine the calibration curves for the different steels. In doing so, it was assumed that tempered martensitic structure has magnetic properties similar to those of bainitic structures.

To test this assumption, fully bainitic structures were obtained in a few steels by transforming in the lower part of the bainite range for sufficient periods of time. The completion of the transformation was determined by the tapering off of the steady increase in ΔP, and was verified by optical metallography. The steady values of ΔP were noted in each case. These values were compared with the ΔP value obtained for fully martensitic samples by holding them at the same temperature at which the fully bainitic samples were transformed. Comparison of the values was made for samples of the same composition. The values agreed within 5%.

The sample previously transformed to 100% martensite was held in the field of the sensing coil, and the resulting change in period was measured. The sample was then heated to higher temperatures, held at each temperature for about 30 min, and the corresponding ΔP values were noted. The ΔP vs temperature relation was derived for each of the steels studied. The results are presented in Figs. 4 and 5.
The value of ΔP for 100% transformation in any steel for a particular reaction temperature was read from the corresponding calibration curve.

The need to determine the calibration curve for each alloy composition is shown in Figs. 4 and 5. Three important points should be noted from these figures. (1) All the alloying elements, when added to 4340 decreased the permeability of 4340 steel (measured here as the change in the resonant period of oscillation of the circuit effected by the presence of the sample transformed to 100% martensite in the magnetic field of the sensing coil). (2) The amount of this decrease was dependent on the element added, e.g., 1% Cr addition reduced the permeability of 4340 more than 1% Ni addition. (3) The dependence of ΔP on temperature was not the same for all compositions. For certain compositions, the value of ΔP was fairly constant over the whole range of temperatures studied (20°C to 400°C). Thus, composition has a major effect on the magnetic properties of a steel. These experimentally derived calibration curves are in agreement with that found for the general dependence of initial permeability with temperature.[18]

For small changes in inductance L, the relation between resonant period of oscillation, P and L in the equation $P = 2\pi\sqrt{LC}$ (where C is the capacitance) is substantially linear, as shown in Fig. 6. The change in L with the volume fraction transformed is not necessarily linear. To determine this relation, samples of different thicknesses, but with the other dimensions the same, were transformed to 100% martensite by quenching to room temperature, and in each case the resulting change in period, ΔP corresponding to the change in inductance ΔL was noted. Because the other dimensions were maintained, the change in thickness of the specimens could be correlated to their change in weight and in turn, the volume fraction transformed. For example, the

strength of the signal of a 2 gm specimen that is 100% transformed should be equivalent to that of a 4 gm specimen that is 50% transformed. The experimentally derived dependence of ΔP with weight is shown in Fig. 7. This relationship was not linear, but could be described quite well by the equation, $\Delta P = 34430(1-e^{-0.13K})$. A 100% transformation "value" of ΔP established a value for K to represent the 100% volume fraction. Based on this, other values of ΔP could be converted into their corresponding volume fractions of the transformed phase.

A computer program written by C. E. Ericsson[20] was used to decode the paper tape output, to correct the non-linearity of the change in ΔP vs volume fraction transformed, to convert the corrected change in ΔP to absolute volume fractions, to plot the kinetics of transformation of the isothermal curves, and finally, to plot the initial TTT diagrams. Using computer methods, the kinetic data were re-plotted according to two different empirical rate equations, namely the Zener equation[21] and the Austen and Rickett equation.[22]

C. Microscopy

1. Optical Metallography

Sections to be used for metallography were cut from the isothermally transformed samples of selected steels. They were mounted in Koldmount and ground on successively finer papers to 600 grit and then polished to 1μ using a diamond paste followed by 0.05μ alumina slurry. All specimens were etched in a 2% nital solution.

2. Electron Microscopy

Thin foils for transmission electron microscopy were also prepared from the isothermally transformed samples. The 0.03 in. thick strip samples were chemically thinned to 0.005 in. in an H_2O_2 + HF solution and then electropolished in a chromic-acetic acid solution using the window technique. The foils were examined in a Siemans Elmiskop IA operated at 100 kV.

III. RESULTS AND DISCUSSION

A. Magnetometric Technique

The magnetic permeability method permitted continuous measuring of the fraction of austenite decomposed in the alloys as they were isothermally transformed. The initiation (incubation) and finish times of the isothermal reactions and their associated kinetics can thus be determined. The decomposition products can be identified by observing the kinetics of the transformation and by correlating the kinetics with the microstructure.

The martensitic reaction was recognized by its athermal behavior and by the rapid rate at which it formed. Below the M_s temperature, the rapid martensite reaction was followed by the time dependent bainite reaction, the beginning of which was signified by an inflection point in the isothermal reaction curve. At the M_s temperature, only 1% of the austenite transformed rapidly to martensite, and the rest transformed slowly to bainite.

The magnetic technique provides a direct experimental method for determining the M_s temperature and the temperatures required for different amounts of martensite to form. From isothermal reaction curves, the various percentages of martensite obtained at the different reaction temperatures can be easily determined.

Above the M_s temperature, the isothermal reaction was characterized by an incubation period during which there was no detectable transformation, followed by a period during which there was a time dependent decomposition of austenite. These kinetic features of bainite reaction

are similar to those of a nucleation and growth process. With proper calibration, the amount of untransformed austenite remaining after the bainite reaction had stabilized, or when the bainite reaction was interrupted by quenching, could be determined. Also, the amount of austenite that transformed while cooling to room temperature could be measured. By measuring the permeability of the sample before and after refrigeration in liquid nitrogen, the amount of austenite transformed during refrigeration could also be measured.

The validity of the quantitative values derived by using the magnetic permeability method was evaluated in two ways. (1) A few samples that had been partially transformed to bainite were examined optically. The amount of bainite formed was estimated by averaging over a large area of the sample. The values so obtained were close to the values obtained using the magnetic method. (2) The magnetic method used to determine the bainitic and martensitic regions of the TTT diagram of 4340 steel provided transformation data consistent with the diagram reported in the literature for this steel. The experimentally determined diagram is given in Fig. 10. The diagram reported in the literature[23,24] for 4340 steel is reproduced in Fig. 9. The two are very similar except for a few differences in the lower bainite range. These differences will be discussed in the next section.

Like any other indirect method to follow the austenite decomposition, the magnetic method required that a proper calibration be made to determine the quantitative values of kinetics. There was bound to be some error in the quantitative estimations. The main source of error

was in correlating ΔP with phase change. The tempering occurring during the transformation would cause a higher ΔP than what would be caused by transformation alone. The error was, however, minimal in estimating the start and early stages of the transformation, because, at the beginning of the transformation, the value of ΔP changed from zero to a positive value. After evaluating the reliability of the magnetic method, the method was further used to study the detailed kinetics of the bainite reaction in the modified 4340 steels. The isothermal reaction curves and the TTT diagrams for the different steels are presented in Figs. 8A thru 8N and Figs. 12A thru 12N. The isothermal reaction data are plotted in both linear and log forms. The plot of log percent transformed vs log time delineated the early stages of the transformation, whereas, the linear plot of percent transformed vs time gave a better picture of the later stages of the transformation.

B. Kinetic Features of Bainite Reaction

In the TTT diagram recently published for 4340 steel[23,24] (reproduced in Fig. 9) the bainite range is shown as a smooth C-shaped curve. The present investigation showed significant differences in the shape and kinetics of the lower bainite region. As shown in Fig. 10, the incubation period for the formation of lower bainite decreased at temperatures just above M_s and gave an S-shaped curve for the bainite reaction. This acceleration of austenite decomposition at temperatures just above M_s has been observed previously.[5,25,26] This observation was not unique to 4340 steel since it was found to occur in all the modified 4340 steels, Figs. 12A thru 12N.

The bainite curve extending below the M_s into the martensitic range was C-shaped. Below the M_s, the bainite reaction began almost immediately. The rapid onset, which is well established in the literature, is attributed to the increased nucleation rate of the bainite reaction by the strain effects associated with the austenite to martensite transformation. Decreasing the temperature below the M_s produced more martensite and less bainite, and the bainite formed slower the lower the temperature, thus giving rise to a C-curve for bainite. The decreased rate of bainite transformation at temperatures well below M_s is apparently due to the lower diffusion rates of carbon.

The reaction curves for the formation of bainite obtained in all the steels are similar to those of a nucleation and growth process. However, other kinetic features are analogous to those of the martensitic transformation. A definite temperature usually designated B_s exists, above which austenite does not transform by bainitic mode.[19] Below the B_s temperature, the amount of austenite transformed to bainite is a function of reaction temperature. The extent of decomposition increases from close to 0 at B_s to 100% at some lower temperature (called B_f). In alloy steels, the B_s temperature is the lower shelf of the metastable austenitic bay that is frequently found below the pearlite transformation ranges. The austenite, if held in the bay for long periods of time, should transform by proeutectoid and pearlitic modes. In plain carbon steels, there is only one C-curve describing the complete range of austenite decomposition. The presence of kinetic B_s is obscured by competition from the pearlite and proeutectoid reactions.

The existence of a separate transformation curve for bainite

is revealed only when the proeutectoid and pearlite reactions are sufficiently retarded by alloy additions that do not appreciably affect the bainite reaction kinetics.

As different reaction kinetics are involved in the formation of upper and lower bainites, there should be separate C-curves for the two variants of bainite. The retardation of one reaction relative to the other should separate the two overlapping C-curves.

Two different overlapping C-curves have been identified for upper and lower bainite in certain alloys.[6,26,27] However, no discontinuity is observed in the TTT curve in the bainite range in 4340 steel austenitized at 900°C (Fig. 10). By raising the austenitizing temperature from 900°C to 1200°C a considerable retardation of the upper bainite reaction is produced (see Fig. 11). This shifting of the upper bainite reaction relative to the lower bainite reaction revealed the existence of two overlapping C-curves for the two variants of bainite. Similar displacements of the two C-curves in the TTT diagrams were observed in many of the modified 4340 steels (austenitized at 900°C) in the present investigation. However, the two C-curves were not separated from each other by an austenitic bay similar to that observed between the pearlite and bainite reactions.

C. Effect of Austenitizing Temperature on the Kinetics of Bainite Formation

There are conflicting data in the literature concerning the effect of austenitizing conditions on the bainite reaction. Davenport, et al.[28] found that on increasing the austenite grain size from ASTM 7-8 to 2-3 in a low alloy steel, the rate of bainite reaction was unaffected. Cottrel and Ko,[29] investigating low alloy hypoeutectoid steels, found that the bainite reaction rate was increased with increasing austenitizing temperature from 950°C to 1300°C. Barford and Owen[30] investigating hypereutectoid Fe-Mn-C alloys found that the rate of transformation of austenite to both upper and lower bainite was substantially reduced by increasing the prior austenite grain size. Graham and Axon[31] found that increasing the austenite grain size accelerated the lower bainite reaction in a plain carbon steel. It is difficult to separate the effects of the increased austenite grain size and the increased chemical homogeneity within the austenite grains on the bainite reaction with an increase in austenitizing temperature. This could be the reason for the conflicting results.

In the present investigation, the effect of austenitizing temperature on bainitic hardenability in 4340 steel was also examined. The TTT diagrams for the bainite range of 4340 steel determined by austenitizing at 900°C and 1200°C are shown in Figs. 10 and 11. It is evident that the incubation period increased and the transformation rate decreased when the austenitizing temperature was increased from 900°C to 1200°C for the upper bainite reaction. The incubation period and transformation rate for the lower bainite reaction were virtually unaffected. The times

to 0.5%, 25% and 50% transformation at different reaction temperatures for the two austenitizing conditions are listed in Table III. The ratio of the times to 50% transformation after austenitizing at 1200°C and 900°C was about 2.2 for higher transformation temperatures and was about 1.0 for lower transformation temperatures. When the austenitizing temperature was increased from 900°C to 1200°C, the rate of upper bainite reaction was considerably reduced, while the rate of lower bainite reaction was virtually unaffected.

These differences in the behavior of the two variants of bainite can be attributed to the differences in their nucleation characteristics. Nucleation of upper bainite occurs predominantly at the austenite grain boundaries. Thus, a higher austenitizing temperature resulting in increased grain size with reduced grain boundary area, should retard its nucleation rate. (This is analogous to the retardation of proeutectoid ferrite and pearlite reactions when the austenite grain size is increased). Lower bainite nucleates both at the austenite grain boundaries and within the austenite grains and thus would be less affected by the decreased grain boundary area.

The retardation of the upper bainite reaction for the higher austenitizing treatment might also be attributed to the increased solution of carbides at higher austenitizing temperatures. This should result in a decrease of the M_s temperature due to increased alloy concentration in the matrix. However, it was found that the higher austenitizing temperature resulted in an increase in the M_s temperature of about 25°C (there was no apparent effect on the M_f temperature).

Table III. Effect of austenitizing temperature on kinetics of bainite reaction in 4340 steel.

Reaction Temperature	$t^*_{0.5}$		t_{25}		t_{50}	
	Austenitizing Temperature		Austenitizing Temperature		Austenitizing Temperature	
	900°C	1200°C	900°C	1200°C	900°C	1200°C
500°C	12 sec	93 sec				
450°C	15 sec	77 sec	85 sec	200 sec	123 sec	270 sec
400°C	28 sec	75 sec	108 sec	208 sec	146 sec	270 sec
375°C	46 sec	40 sec	154 sec	162 sec	208 sec	216 sec
350°C	62 sec	35 sec	177 sec	192 sec	270 sec	270 sec

*Time to 0.5% transformation.

The increase in the M_s temperature was believed to be due to the increase in grain size, which would result in a decreased flow strength of the prior austenite. The decreased resistance of the austenite matrix to the deformation accompanying the formation of martensite probably caused the increase in the M_s temperature discussed above. These results are in agreement with conclusions reached by Breinan and Ansell.[32] Sastri and West[33] have also observed an increase in M_s temperature of about 25°C by increasing the austenitizing temperature from 800°C to 1200°C.

D. Influence of Alloy Content on the Kinetics of Bainite Formation

To avoid interference from the proeutectoid and pearlite reactions in studying the bainite reaction, it was necessary to choose an alloy like 4340 steel, in which a metastable austenitic bay separates the proeutectoic and pearlite reactions from the bainite reaction. It is unfortunate that such a bay does not exist in a binary Fe-C alloy or in simple ternary alloys with an alloy content less than that of 4340 steel. The 4340 steel already contains small amounts of different alloying elements. It was thought that the addition of common alloying elements, one at a time, in small amounts, to the base 4340 steel should delineate their relative effects on the bainite reaction. To understand the interaction effects, combined additions of the alloying elements were also studied. Compositions of the various steels used are given in Table I. The total alloy addition did not exceed 3%. Thus, the modified alloys could still be regarded as low alloy steels. Whereas the amounts of Mn, Ni and Cr added was either 1 or 2% and up to 3%, a much smaller amount

(0.5%) of Mo was added. Molybdenum, when present in larger concentrations is known to form stable carbides, which are difficult to dissolve under normal austenitizing conditions.

An examination of the TTT diagrams of 4340 and modified 4340 steels reveals that (for single alloy additions) Mo, unlike all the alloying elements, reduced the induction period, accelerated the bainite reaction, and raised M_s temperature by about 40°C. It is known[34,35] that the type of carbide formed at elevated temperatures in medium carbon steels containing molybdenum changes from orthorhombic M_3C (cementitic type) carbide to face centered cubic $M_{23}C_6$ carbide, when the amount of molybdenum present exceeds about 0.4%. It is possible that the carbides formed in 4340 + 0.5% Mo steel (total Mo content is 0.73%) were $M_{23}C_6$ type carbides. Bridge et al.[36] have shown that solvus temperatures of $M_{23}C_6$ carbides is about 1000°C, and that the rate of dissolution of these carbides is extremely slow. The decrease in bainitic hardenability with 0.5% Mo additions was thus probably due to decreased alloy concentration in the matrix because of incomplete solution of carbides.

However, 0.5% Mo effectively shifted the bainite reaction to <u>longer</u> times and to <u>lower</u> temperatures when added to 4340 + 1.0% Ni, 4340 + 1.0% Cr and 4340 + 1.0% Ni + 1.0% Cr steels. Compare the TTT diagrams of the following midified 4340 steels, (1) 4340 + 1.0% Ni vs 4340 + 1.0% Ni + 0.5% Mo, (2) 4340 + 1.0% Cr vs 4340 + 1.0% Cr + 0.5% Mo and (3) 4340 + 1.0% Ni + 1.0% Cr vs 4340 + 1.0% Ni + 1.0% Cr + 0.5% Mo. No undissolved carbides were found in any of these steels in optical micrographs. Thus, the increased Ni or Cr contents in the base 4340 composition changed the phase fields of the different carbides so that

the carbides formed dissolved easily at the austenitizing temperature used.

All the alloy additions (except single additions of Mo) shifted the bainite curves to longer times and lowered the kinetic B_s and B_f temperatures. The B_s (defined as 1% transformation to bainite), B_{25} (25% transformation to bainite), B_{50}, B_{75} and B_f temperatures of the steels as derived from the TTT diagrams are listed in Table IV. An analysis of these data revealed that the B_s temperature was depressed by 30°C per 0.1% addition of carbon, by 30-35°C per 1% addition of Ni, by 60-65°C per 1% addition of Cr, by 60°C per 1% addition of Mn, by 65°C per 0.5% addition of Mo, and by 40-45°C per % addition of Si up to 2% Si addition. The effect of Si in depressing the B_s temperature leveled out a 2% Si addition. For combined additions, the effect of the various alloying elements in lowering the B_s temperature was additive, thus it is possible to calculate the B_s temperature directly from the composition. An equation was derived to do this, and it is as follows:

$$B_s\ (°C) = 839 - 300\%\ C - 60\%\ Mn - 33\%\ Ni - 63\%\ Cr - 130\%\ Mo - 43\%\ Si\ \ldots \quad (1)$$

A similar equation was derived by Steven and Haynes[11] using the experimental data found in the literature. It is as follows:

$$B_s\ (°C) = 830 - 270\%\ C - 90\%\ Mn - 37\%\ Ni - 70\%\ Cr - 83\%\ Mo\ \ldots \quad (2)$$

A factor for Si was not included in the second equation, apparently for lack of data. The values of B_s temperature calculated using the two equations are compared with experimentally determined values for

Table IV. Bainite formation temperatures for the steels studied.

Steel	Experimental Data					Calculated Values of B_s Temp., °C using Eq. (2)
	B_s Temp., °C	B_{25} Temp., °C	B_{50} Temp., °C	B_{75} Temp., °C	B_f	
4340	530	480	470	450	430	517
4340 + 0.1% C	500	460	450	440	400	
4340 + 1.0% Cr	470	425	412	400	~370	447
4340 + 1.0% Ni	495	455	445	415	380	480
4340 + 1.0% Mn	470	424	405			427
4340 + 1.0% Si	485	450	400	325		
4340 + 2.0% Cr	405	360	345			377
4340 + 2.0% Ni	465	430	420	395		443
4340 + 2.0% Mn	408					337
4340 + 2.0% Si	445	410	365			
4340 + 1.0% Ni + 0.5% Mo	430	390	380	365	~330	439
4340 + 1.0% Cr + 0.5% Mo	405	380	370	360		406
4340 + 1.0% Ni + 1.0% Cr	430	370	360	430	~305	410
4340 + 1.0% Ni + 1.0% Cr + 0.5% Mo	375	340	330			369
4340 + 3.0% Si	440	400	325			410

the commercial steels listed in Table V. For most of the steels, it can be seen that the correlation with experimentally determined values is better when the B_s temperatures are calculated using Eq. (1) than Eq. (2).

From Table IV, it is seen that in the base 4340 and in 4340 modified with Cr, Ni, Mn additions, B_{50} was about 50-60°C and B_f was about 100-120°C less than the B_s temperature. In these steels, the austenite decomposition was incomplete when transformed between B_s and B_f temperatures, but most of the remaining austenite transformed to martensite during cooling to room temperature. At temperatures below B_f, the austenite could be transformed to bainite completely within reasonable lengths of time. In silicon modified 4340 steels, B_{50} was 80° to 115°C lower than the B_s depending on the silicon content, and the austenite decomposition was incomplete at all reaction temperatures. Thus, the B_f temperature could not be determined. Therefore, an "apparent B_f temperature" was assumed for these steels to be about 110°C below the B_s. At temperatures near the B_s, the austenite does not completely transform.[19] Part of this austenite transforms to martensite during cooling to lower temperatures. The austenite retained below the "apparent B_f" was in a more finely dispersed form than the austenite that did transform to martensite. The morphology of bainite and the stability of retained austenite in these steels will be discussed in later sections.

Alloying elements differ in the nature and magnitude of their effects on isothermal transformation of austenite. Their effects on bainite transformation were of two forms.

(1) All the alloying elements used in this investigation shifted the bainite reaction to lower temperatures but by different amounts. The effect was additive when combined additions were made. The shifting of bainite reaction to lower temperatures means that bainite formed in these modified steels is fine. The range over which upper bainite reaction can occur is greatly restricted thus lower bainite formation is promoted.

(2) The effects of the alloying elements on the incubation time differed significantly from each other, some affecting the upper bainite reaction more than the lower bainite, while others affecting both about equally. The times for 1% transformation (considered to be the incubation period) and for 5% transformation (where sufficient amounts of bainite have formed) at temperatures corresponding to the upper bainite nose are listed in Table VI. Examples of effects are:

(a) 0.1% C was more effective than 1% additions of Ni, Cr, Mn or Si in increasing the incubation period.

(b) Silicon up to 2% addition, was as effective as Ni or Cr in increasing the incubation period. Beyond 2%, the effect due to Si appeared to level off.

(c) The increase in incubation period was greater with 1% Ni and 1% Cr addition than with either 2% Ni or 2% Cr addition. This indicates a positive interaction effect between Ni and Cr as far as bainite incubation period is concerned.

(d) The addition of 1% Ni and 0.5% Mo was more effective in increasing the incubation period than the addition of 1% Cr and 0.5% Mo.

Table V. Experimental and calculated values of B_s temperature for some commercial low alloy steels.

Steel and Composition	B_s, °C Experimental Values	Calculated Values of B_s Temperature, °C	
		Using Eq. (1)	Using Eq. (2)
300-M (0.41 C, 0.79 Mn, 0.75 Cr, 1.85 Ni, 0.43 Mo, 1.59 Si)	440*	436	492
D6AC (0.46C, 0.68 Mn, 0.98 Cr, 0.58 Ni, 0.83 Mo, 0.25 Si)	460*	460	486
En 25 (0.32 C, 0.56 Mn, 0.74 Cr, 2.37 Ni, 0.51 Mo, 0.27 Si)	510**	507	511
En 26 (0.38 C, 0.56 Mn, 0.74 Cr, 2.42 Ni, 0.46 Mo, 0.15 Si)	505**	499	498
En 30A (0.35 C, 0.44 Mn, 1.43 Cr, 4.23 Ni, 0.13 Mo, 0.14 Si)	430**	455	429
En 100 (0.40 C, 1.38 Mn, 0.53 Cr, 0.74 Ni, 0.16 Mo, 0.24 Si)	520**	522	510

*Obtained from Ref. 20.

**Obtained from Ref. 37.

Table VI. Times to 1% and 5% transformation at reaction temperatures corresponding to upper bainite nose for the different steels.

Steel	Temp., °C	$t^{*}_{1.0}$, sec	$t^{**}_{5.0}$, sec
4340	450°C	17	25
4340 + 0.1% C	460°C	100	130
4340 + 1.0% Ni	430°C	62	130
4340 + 1.0% Cr	380°C	85	110
4340 + 1.0% Mn	450°C	50	192
4340 + 1.0% Si	450°C	50	
4340 + 2.0% Ni	420°C	61	170
4340 + 2.0% Cr	380°C	50	1700
4340 + 2.0% Mn	350°C	150	3922
4340 + 2.0% Si	425°C	85	
4340 + 3.0% Si	400°C	80	
4340 + 1.0% Ni + 1.0% Cr	375°C	200	850
4340 + 1.0% Cr + 0.5% Mo	400°C	150	450
4340 + 1.0% Ni + 0.5% Mo	380°C	210	400
4340 + 1.0% Ni + 1.0% Cr + 0.5% Mo	350°C	600	2000

*Time to 1% transformation.
**Time to 5% transformation.

That is, for the same total weight of alloying additions Ni + Mo is more effective than Cr + Mo combination in retarding bainite formation.

(e) Up to 2% additions, manganese was more effective than Ni or Cr in retarding the rate of bainite formation.

(f) The rate of bainite formation was retarded in a non-linear manner by increasing amounts of an alloying element. For example, the retarding effect of a 2% addition was not equal to 2 times the effect of 1% addition. The ratios of the times (to 5% transformation) for 2% addition with those for 1% addition were 1.3 for Ni, 15.5 for Cr and 20 for Mn. Thus, for Ni, increased addition had smaller effects on bainite hardenability whereas larger additions of Mn and Cr apparently lead to multiple effects.

(g) The addition of 2% Cr was more effective in retarding the bainite reaction than either a 2% Ni or 1% Ni and 1% Cr addition. (Compare this with (c) above.)

The observation that Ni is more effective in the presence of Cr than by itself is in agreement with that of Brophy and Miller's result.[38] The effects of combinations of two or more alloying elements on the isothermal transformation of austenite are complex, and a great deal of systematic work is required to determine to what extent the effects of one element are intensified or weakened by the presence of another. A detailed study of this topic should lead to the establishment of the most effective combinations of alloying elements for different purposes. It is hoped that the rapid magnetic technique developed in this investigation will greatly facilitate such a study.

E. Analysis of Isothermal Reaction Data

Two empirical rate equations were used to analyze the experimental data. These equations are:

$$\log \log\left(\frac{a}{a - y}\right) = n \log t - n \log k - 2.3 \text{ (Zener)}^{21} \quad . \quad . \quad . \qquad (1)$$

and

$$\log \frac{y}{a - y} = n \log t - \frac{k}{2.3} \text{ (Austen and Rickett)}^{22} \quad . \quad . \quad . \qquad (2)$$

where a is the fraction of austenite transformed when the reaction is stabilized (a was unity for reaction temperatures below the kinetic B_f temperature, and was less than unity for temperatures between the B_s and B_f temperatures), y is the fraction transformed at time t, k is a temperature-dependent rate constant, and n is a constant dependent upon the morphology of the reaction products and the nucleation characteristics. Experimental data which conform to the above equations will lie on straight lines on plots of $\log \log\left(\frac{a}{a - y}\right)$ vs $\log t$ or $\log\left(\frac{y}{a - y}\right)$ vs $\log t$.

Both Zener and Austen-Rickett plots for some steels studied in this investigation are shown in Figs. 13A through 13C and 14. Values of index n were obtained from the slopes of the linear parts of the curves. Austen-Rickett plots gave slightly larger value for n compared to Zener plots. Also, the Austin-Rickett equation correlated more closely with the experimental results of any one reaction to a higher degree of transformation than did the Zener equation. Beyond 50-70% of the total transformation, the correlation between the experimental data and the two equations became poor. The two equations could not be used to analyze the transformation curves obtained in the vicinity of the M_s temperature

because the bainite reaction at these temperatures had an early accelerated stage.

Values of the Zener index n obtained for different modified 4340 steels (excluding silicon additions) are given in Fig. 15 as a function of the isothermal reaction temperature. The indices for transformation temperatures above 350°C are within the range 1.0-2.0, whereas those for temperatures below 350°C lie within the range 2.0-3.0. This distinctive change in the value of n around 350°C is probably associated with the transition from upper to lower bainite. However, there was no significant trend in the variation of n with composition within the range of compositions studied. Similar changes in the values of Zener index n observed by Radcliffe and Rollason[5] for plain carbon steels were in the range 1.8-2.6 for temperatures above 350°C, whereas for temperatures below 350°C they were in the 3.0-4.0 range.

The Zener index values obtained for the 2% and 3% silicon modified 4340 steels were in the range 1.0 to 2.0, indicating that the reaction was predominantly upper bainitic in the complete range of reaction temperatures studied.

The temperature dependence of the rate constant k in Eq. (1) can be expressed as:

$$\frac{1}{k} = c \exp\left(\frac{-Q}{RT}\right) \quad , \ldots . \qquad (3)$$

where c is a constant, T is the reaction temperature in absolute degrees, and R is the gas constant. The empirical activation energy, Q, can be determined in a number of ways.[39] A direct way is to determine the

values of k at different reaction temperatures and to plot $\log\left(\frac{1}{k}\right)$ vs the reciprocal of the absolute temperature. The slope of this graph is $\frac{Q}{2.303R}$. If R is taken to be 1.98 cal, Q is measured in cal/mol. However, it is more convenient to use the time to a given fraction transformed method. The equation on which this method is based can be derived by substituting the Arrhenius relationship for the constant k (Eq. (3)) into Eq. (1). This results in a rate equation of the form

$$\log \log\left(\frac{a}{a - y}\right) = n \log t - n \log c - \frac{nQ}{2.303RT} - 2.3$$

For transformations below the kinetic B_f temperatures (a=1), and for a fixed amount of transformation the equation reduces to the following form:

$$\log t_y = \frac{Q}{2.303RT} + \log c + c' ,$$

where t_y is the time to reach y percent transformation and c' is another constant. Kinetic data conforming to this equation will lie on a straight line when plotted in the form of $\log t_y$ vs $\frac{1}{T}$. The slope of the line is $\frac{Q}{2.303R}$.

In many of the modified 4340 steels studied in this investigation, the bainite reaction range between M_s and B_f was very restricted, in some cases it was only 20-30°C and hence an accurate activation energy measurement could not be made. Thus, the reaction data for 4340, 4340 + 0.1% C and 4340 + 1.0% Si steels in which the range between M_s and B_f was at least 100°C are plotted in Fig. 16 in the form of $\log t_{25}$ vs $\frac{1}{T}$, where t_{25} is the time to reach 25% transformation. Since the location of the lower C-curve was not clear in the TTT diagrams for

4340 and 4340 + 1.0% Si steel, only the data obtained at higher temperatures were considered in these two steels. For 4340 + 0.1% C steel, the data fell on two straight lines. This was expected since two curves were observed in the TTT diagram. The values of Q obtained from measurements of the slopes of these plots are given in Table VII. The Q values obtained from high temperature data are for upper bainite, and the Q values obtained from lower temperature data are for lower bainite. The Q values obtained from the data for 4340 + 1.0% Ni steel are also given in Table VII.

The results available in the literature regarding the values of activation energy calculated in this manner for the bainite reaction are conflicting. The rates of formation of upper and lower bainite have been studied employing either electrical resistivity[5,6,27] or hot-stage microscope[7,63] techniques. Hot stage microscopy work appears to indicate that the activation energy for the formation of upper bainite is smaller than that of lower bainite (17-22 kcal/mol for lower bainite and 3 to 8 kcal/mol for upper bainite). Radcliffe and Rollason[5] using electrical resistivity have shown that in plain carbon steels, the activation energy for the formation of upper bainite is large (18-32 kcal/mol) and is greater than that for the formation of lower bainite (7-13 kcal/mole). They conclude that the activation energies for upper and lower bainite formation are approximately those of carbon diffusion in austenite, and ferrite respectively. The discrepancy between the activation energies determined by these different techniques is difficult to rationalize. Both techniques have been criticized,[8] resistivity studies for being complicated by tempering occurring during the transformation and hot-stage

Table VII. Values of "Q".

Steel	Q, cal/mol	
	Lower Bainite	Upper Bainite
4340		11,185
4340 + 0.1% C	4512	7,416
4340 + 1.0% Ni	4858	10,759
4340 + 1.0% Si		9,688

microstructural studies for not being able to resolve the boundaries of individual units of bainite. The activation energy values obtained using the magnetic method in the present study for upper and lower bainite reactions were both relatively small. The activation energy for upper bainite was higher than that of lower bainite. Both values were far lower than the activation energy for carbon diffusion in austenite, which is well over 30 kcal/mol. So, it is suggested that the diffusion of carbon in ferrite might be the rate controlling process in the formation of both forms of bainite.

F. Stabilization of Bainite Reaction and Retention of Austenite

It is well known that partial transformation of austenite to bainite results in an increase in the amount of austenite retained at room temperature.[40-43] The retained austenite is enriched in carbon and is highly stable. The amount of austenite retained is determined both by reaction temperature and by alloy content. Hehemann and co-workers[19] showed that a silicon steel (0.60 C, 1.98 Si, 0.3 Cr) retained substantially greater amounts of austenite than did 4340 steel when transformed to upper bainite. However, the amount of retained austenite was considerably lower in both steels if lower bainite formed. Using transmission microscopy techniques, Oblak and Hehemann[44] observed that upper bainite formed at 400°C in the silicon steel (0.60 C, 0.86 Mn, 0.31 Cr, 2.00 Si) was free of carbides. Instead, it contained austenite trapped between the laths of ferrite. The same steel, when transformed at 275°C, exhibited a lower bainite morphology (ε carbide in ferrite) with no detectable amounts of retained austenite.

The amounts of austenite retained at room temperature after partial transformation to bainite at different reaction temperatures observed in this study are listed in Table VIII. The state of bainite reaction at the time of interruption (as to whether it was stabilized or progressing) is also indicated in the table. It can be noted that the silicon modified 4340 steels retained much larger amounts of austenite than the other steels. The results obtained for two other high silicon steels studied, namely, 4350 + 3.0% Si and 4360 + 3.0% Si steels are also given in Table VIII. However, contrary to the published results, the silicon modified 4340 steels retained significant amounts of austenite as part of bainite at all reaction temperatures, both above and below the M_s temperature. The bainite contained no carbides.[47] Films and sometimes islands of austenite were observed trapped between the bainitic ferrite laths. Following Oblak and Hehemann,[44] this structure was classified as upper bainite. The morphology of bainite obtained in these steels will be discussed in a later section.

The kinetics of transformation curves obtained for silicon modified 4340 steels, given in Figs. 8D through 8F show that most isothermal reactions have stabilized within an hour. In silicon modified 4350 and 4360 steels, the bainite reaction was considerably slower, stabilizing only after several hours. The M_s temperatures for 4340 + 3.0% Si, 4350 + 3.0% Si and 4360 + 3.0% Si steels were approximately 280°C, 250°C and 220°C respectively, and decrease with increasing carbon content. Thus, transformation to bainite without interference from the martensite reaction was possible at temperatures as low as 220°C in case of 4360 + 3.0% Si steel. At these low temperatures, the reaction rates

Table VIII. Amounts of austenite retained at room temperature after partial transformation to bainite.

Steel	Reaction Temp., °C	% Transformed at Reaction Temperature	State of Reaction at Interruption	% Austenite Retained at Room Temperature
4340+1.0%Ni	429	71	Stabilized	10
	465	15	Stabilized	5
4340+2.0%Ni	315	76	Progressing	1
	349	53	Progressing	9
	398	62	Progressing	10
4340+1.0%Cr	422	26	Stabilized	9
4340+2.0%Cr	313	60	Progressing	13
	350	35	Progressing	12
4340+1.0%Ni+1.0%Cr	351	59	Progressing	8
	369	29	Progressing	10
4340+1.0%Ni+1.0%Cr+0.5%Mo	322	65	Progressing	9
4340+1.0%Si	304	77	Stabilized	20
	352	64	Stabilized	28
	407	45	Stabilized	40
4340+2.0%Si	299	63	Stabilized	26
	351	51	Stabilized	40
	408	33	Stabilized	22

Table VIII. Continued.

Steel	Reaction Temp., °C	% Transformed at Reaction Temperature	State of Reaction at Interruption	% Austenite Retained at Room Temperature
43 0+3.0%Si	307	51	Stabilized	36
	350	46	Stabilized	44
	381	38	Stabilized	51
4350+3.0%Si	300	50	Stabilized	42
	350	40	Stabilized	55
4360+3.0%Si	300	45	Stabilized	50
	350	35	Stabilized	60

were very slow, and it took over 24 hrs for the bainite reaction to stabilize.

The amounts of retained austenite in the silicon steels were measured after cooling to room temperature, and also after refrigerating in liquid nitrogen (-195°C). (All the samples used for these measurements were cooled from the reaction temperature after the reaction had fairly stabilized with time.) The results obtained for the five high silicon steels studied are plotted as percent retained austenite at room temperature vs reaction temperature, as shown in Figs. 17A through 17E. The following inferences can be drawn from these results:

(1) At reaction temperatures below the M_s, the bainite reaction was preceded by the martensite reaction. The fraction of austenite transforming to bainite decreased with decreasing temperature below the M_s. The amount of austenite retained was approximately proportional to the amount of bainitic ferrite formed.

(2) In all the high silicon steels, the amount of austenite retained on cooling to room temperature increased with increasing reaction temperature above 300°C and reached a maximum value at about 100°C below the B_s temperature. Beyond this point, the amount of retained austenite decreased rather steeply.

(3) Note from Figs. 17A through 17C that the amount of retained austenite generally increased with the increase in silicon content. Not linear, the increase appeared to saturate beyond a certain silicon content.

(4) Also, from Figs. 17C through 17E it can be inferred that for the same silicon content, the amount of retained austenite increased with increasing carbon content.

(5) The retained austenite obtained at lower reaction temperatures was highly stable, and did not transform on refrigerating at -195°C as did some of the retained austenite obtained at higher reaction temperatures.

Austenite decomposition is stabilized at the reaction temperature because of the carbon enrichment of austenite. Its retention at room temperature, however, can be explained partly by the lowering of M_s temperature below room temperature due to carbon enrichment. Austenite retention can also be understood in terms of thermal and mechanical stabilizations.[45,46] Thermal stabilization is attributed to modifications that might occur in the substructure of the untransformed austenite. For instance, the dislocations in the austenite lattice may be locked by solute atmospheres. As a result, the interface motion required for martensitic transformation may be inhibited. On the other hand, mechanical stabilization is caused by the strengthening of austenite following the bainite transformation.

As the transformation temperature is lowered, the strength of austenite increases and so does its resistance to deformation that accompanies its transformation to bainitic ferrite. Thus, the strength of both bainitic ferrite and retained austenite increases with decreasing reaction temperature. It is likely that the bainitic ferrite formed at lower reaction temperatures is strong enough to resist the expansion that would accompany the martensitic growth in the adjacent austenite. The austenite is thus elastically constrained between ferrite grains and does not transform even after refrigerating at -195°C. The bainitic ferrite formed at higher reaction temperatures

is considerably weaker and can be plastically deformed to accommodate the transformation of trapped austenite to martensite.

The stability of the retained austenite is also determined by its morphology. If the trapped austenite is in blocky form, it is likely that the center is less deformed than the outer portions. The central portion should be thus less stable. In high silicon steels, after the transformation in the B_s-apparent B_f temperature range, two morphologies of austenite were retained. They were, (1) the austenite that was trapped between individual ferrite laths in a fine form and (2) the austenite that was trapped between growing bainite colonies in a blocky form. Note from Figs. 17A through 17E that on refrigerating, some of the retained austenite obtained in this temperature range, transformed. It will be shown in a later section that it are the blocky austenite that transformed. not the fine type.

G. Morphology of Bainite in Steels without Silicon Additions

The morphology of bainite in steels containing added Si was significantly different from that in the other steels. In high silicon steels, the upper bainite was associated with large amounts of retained austenite, and this morphology will be discussed further in the next section. In the other steels, the classical form of upper bainite containing carbides was formed. A preliminary examination showed that the morphology of bainite was relatively similar in all the low silicon steels. Thus, detailed morphological study of bainite was conducted in only one of the steels.

The discontinuity in the TTT curves for the bainite range observed around 350°C in many of the modified 4340 steels has been previously mentioned. In one of the steels, namely, 4340 + 0.1% C steel, two separate C-curves could be clearly distinguished in the early stages of the transformation, and they seemed to overlap in the later stages (Fig. 12A). The lower C-curve was actually S shaped, because of the acceleration of bainite reaction at temperatures just above M_s. Obviously, the upper C-curve described the upper bainite reaction and the lower one described the lower bainite reaction. Both types of bainite should form in the temperature range where the two C-curves overlap. The two C-curves intersected at about 350°C. In Section E it was shown that there was a distinctive change both in the value of Zener index n and in the value of experimental activation energy around 350°C. These changes were considered to be associated with the transition between upper and lower bainites. Since bainite has been usually defined on a microstructural basis, it is instructive to correlate the structural differences between upper and lower bainite with their kinetic behavior. Therefore, the morphology of bainite formed at reaction temperatures above, below and at 350°C was studied.

Optical micrographs of specimens isothermally transformed at 329°C, 350°C, 379°C and 429°C are shown in Figs. 18 and 19. An examination of these micrographs failed to reveal any discontinuous change of microstructures with temperature, indicating that significant insight into the structural differences between upper and lower bainite cannot be gained at magnifications possible with an optical microscope. The study of these structures using transmission electron microscopy was more

rewarding. The results are presented in the following sections.

1. Isothermal Transformation at 329°C

The structure obtained was predominantly that of lower bainite and it occurred in two forms. (1) Bainitic ferrite was acicular, and had the appearance of laths or plates. The cementite was precipitated within the ferrite laths as discrete particles and at an angle of about 55-65° to the major axis of ferrite lath. Composite pictures taken from two different areas of the thin foil are shown in Figs. 20 and 21. Frequently, the lower bainite plate contained several substructural units. In these subunits, rod-like carbides were found and the lengths of the carbides appeared to be restricted by the width of the subunits. Such a structure is marked A in Fig. 20. (2) There were extensive regions of ferrite, each region containing many parallel cementite particles. Such a structure is marked B in Figs. 20 and 21. The lath boundaries of bainitic ferrite were not clear. Thus, it was difficult to say whether the carbides were precipitated within the ferrite laths or at the boundaries. However, the carbide morphology was similar to that found in lower bainite. (One row of parallel short rods of carbide was seen displaced from another row). It is likely that these structures are analogous. Shackleton and Kelly[3] have also observed similar regions of ferrite containing many parallel carbides and have identified them as lower bainite.

Adjacent to the lower bainite areas, some carbides were longer, stringer like, and were precipitated along the lath boundaries of ferrite. See regions marked C, Figs. 20 and 22. Such a structure is typical of upper bainite. The upper bainite formed was very fine, and

the lath size of upper bainitic ferrite was comparable to that of a subunit in a lower bainitic plate. It was interesting to observe small amounts of upper bainite formed amidst extensive regions of lower bainite. A selected area diffraction pattern obtained from a typical lower bainite area is given in Fig. 23, showing both cementite and ferrite reflections.

2. Isothermal Transformation at 350°C

A composite picture taken from a representative area of the thin foil is presented in Fig. 24. There are significant amounts of upper bainite mixed with lower bainite, and these two forms sometimes occur in adjacent areas. The morphology of lower bainite was similar to that observed at 329°C. The lower bainite plate, like the one marked A in Fig. 24, was often seen to be composed of several subunits. Large areas of ferrite containing parallel carbides, like the one shown in Fig. 25(a) were also observed. Upper bainite structure was easy to recognize when the lath boundaries were well delineated with the carbide stringers found along the lath boundaries such as in regions marked B in Figs. 24 and 25(b). In some upper bainite regions a few carbides were found within the ferrite laths. This is an interesting observation. Such a structure is marked A in Fig. 26. An analysis of the structure suggests that the upper bainite is actually formed by repeated nucleation of a more basic substructural unit. This mechanism of formation of upper bainite will be discussed further in a later section.

3. Isothermal Transformation at 379°C

Transformation at 379°C produced large amounts of upper bainite mixed with considerable amounts of lower bainite. The mixed structure is illustrated in a composite picture given in Fig. 27. The structure was generally coarser than that obtained at lower temperatures. The classical upper bainite with cementite precipitated at ferrite lath boundaries was frequently observed (A). Lower bainite with cementite precipitated at a characteristic angle within the ferrite plate was occasionally observed (B). Frequently, the ferrite lath boundaries were not clear and thus classification of the structure was difficult. There were certain regions of ferrite (C) in which the carbide appeared as dark, irregular lumps. This structure may be classified as upper bainite, since the carbides were not as dense and as evenly distributed as they were in the lower bainite region. The irregular distribution of carbides was probably caused by the irregular nucleation of sub-structural units of upper bainite.

4. Isothermal Transformation at 429°C

The structure (Fig. 28) was similar to that obtained at 379°C, except that there was more upper bainite. Also, the carbides were coarser, and the distribution was more uneven. The lath boundaries were again not visible. Apparently, there were only very slight orientation differences between individual units, and normal recovery processes occurring at these high reaction temperatures might have annihilated the lath structure. This made it difficult to distinguish some areas (A) from lower bainite. Since the carbides in these regions (A) were shorter and more evenly distributed, these areas could probably be classified as lower bainite.

In some areas (B), recognized as upper bainite, the carbide stringers were long and continuous giving the appearance of pearlite. But in most areas, the carbides were discrete and unevenly distributed.

It can be noted from the TTT diagram for 4350 steel, given in Fig. 12A that the B_f temperature was around 400°C and as such the transformation to bainite was incomplete at 429°C. Magnetic measurements showed that most of the untransformed austenite transformed to martensite on cooling to room temperature and thus gave rise to light etching areas (A) in the optical micrograph of the structure obtained at 429°C shown in Fig. 19(b). The regions marked C in Fig. 28 and A in Fig. 29(a) correspond to the light etching areas (A) in Fig. 19(b). This part of the foil was thicker owing to differential thinning of the specimen. However, the martensite laths formed within the previously untransformed austenite are clearly visible in Fig. 29(a). It was interesting to observe that the colonies of untransformed austenite were at the prior austenite grain boundaries.

Above the B_f temperature, the amount of austenite transforming to bainite decreased with increasing reaction temperature. Transformation at 462°C produced only 30% of bainite. An optical micrograph of a specimen isothermally transformed at 462°C for 1 hr is given in Fig. 29(b). Note that the austenite that remained untransformed at the reaction temperature transformed to martensite when cooled to room temperature.

5. Summary of Observations

The structures changed from being predominantly lower bainitic at 329°C to predominantly upper bainitic at 429°C. At the intermediate temperatures, the structures contained varying amounts of upper and lower bainite, i.e., the transition was

gradual and occurred over a temperature range. These observations were in agreement with the kinetic data. The two C-curves for upper and lower bainite though separated initially were actually overlapping in the later stages of transformation. Both variants of bainite formed in the overlapping zone. The relative amounts depended upon the transformation temperature, and probably on the curvature of the overlapping C-curves. In the lower C-curve, the initial transformation product was lower bainite, and in the upper C-curve it was upper bainite. At the point of intersection of the two C-curves, that is at 350°C, both forms of bainite probably formed simultaneously. The overlapping nature of the two C-cruves and the observation that both upper and lower bainite form in the overlapping zone tends to indicate that the mechanisms of formation of the two forms of bainite may be very similar. The various mechanisms proposed for the formation of bainite will be reviewed in a later section.

H. Morphology of Bainite in Steels Containing Added Silicon

It was pointed out in an earlier section that in the high silicon steels, the bainite reaction was stabilized short of complete austenite decomposition at all reaction temperatures (Figs. 8D through 8F). Also, significant amounts of austenite were retained after the samples were cooled from the reaction temperatures to room temperature. For example, after transforming at 300°C and cooling to room temperature, about 18% austenite was retained in 4340 + 1.0% Si steel, about 35% austenite was retained in 4340 + 3.0% Si steel, and as much as 50% austenite was retained in 4360 + 3.0% steel. Typical microstructures of these steels

transformed below 300°C are shown in Figs. 30(a), 31(a) and 32(a). (The structures were generally light etching as compared to the bainitic structures obtained in low-silicon steels.) The retained austenite present in 4340 + 1.0% Si steel could not be identified optically. However, islands of austenite trapped within the bainitic laths were observed in 4340 + 3.0% Si and 4360 + 3.0% Si steel. These regions are marked by arrows (B) in Figs. 31(a) and 32(a). Thin foil electron microscopy is necessary to delineate the existence and distribution of retained austenite unequivocally.

Transmission electron microscopy work[47] on 4340 + 3.0% Si steel transformed at 278°C revealed that the structure was predominantly upper bainitic, and that the upper bainite was an aggregate of ferrite and austenite, and carbides were not present. Most of the carbon was probably dissolved in the retained austenite. The few plates of lower bainite that were observed contained ε carbide. The austenite retained as part of upper bainite formed at 278°C is revealed clearly in the precision dark field micrograph given in Fig. 33. Also presented in Fig. 34 are a bright field micrograph and the corresponding dark field micrograph of an austenite reflection for the upper bainite formed at 307°C. The austenite was unevenly distributed, and occurred with varying thicknesses. Frequently, austenite was in the form of films surrounding the ferrite laths (A) and in some areas (B), the thickness of the retained austenite was about the same as that of the ferrite lath. Islands of austenite 2-3 microns wide (C), were occasionally observed. Both the ferrite and austenite were highly dislocated. Tangled dislocations could be seen in the trapped islands of austenite.

Occasionally, austenite films were observed inside the laths. This observation appears to substantiate an earlier inference that the bainitic ferrite forms by nucleation of small substructural units. In a low silicon steel, carbides would have occurred instead of austenite films. It is obvious that the source of carbide precipitation in upper bainite is carbon enriched austenite trapped between ferrite laths. It is also apparent that in the formation of upper bainite the carbon enrichment of austenite occurs first, and is followed by the precipitation of carbide from the carbon enriched austenite.

Separate C-curves for the two variants of bainite were observed in the TTT diagram obtained for 4340 + 3.0% Si steel (Fig. 12E). Transformation at 278°C produced a few plates of lower bainite and large amounts of upper bainite. The upper bainite C-curves appeared to extend below 320°C and overlapped the lower C-curve. A lower bainite plate is shown by an arrow (A) in the optical micrograph given in Fig. 31(a). A transmission micrograph of one such lower bainite plate containing ϵ carbide is given in Fig. 35. Lower bainite plates similar to the above were not observed in optical micrographs of specimens transformed at temperatures higher than about 320°C.

To determine whether the retained austenite obtained in these steels would decompose on holding at higher temperatures, the bainitic structure obtained by transforming a 4340 + 3.0% Si steel specimen transformed at 278°C was tempered for 1 hr at 600°C. An optical micrograph of the resulting structure is given in Fig. 31(b). The structure was dark etching due to the presence of carbides because the retained austenite had decomposed. The islands of austenite appeared to have

been replaced by aggregates of carbide particles, and the austenite films had been replaced by stringers of carbide. In general, the distribution of carbides appeared to describe the morphology of retained austenite as it was prior to the tempering treatment.

The amount of austenite retained on cooling to room temperature increased with increasing reaction temperature as shown in Figs. 17A through 17E. The maximum amount of retained austenite in 4340 + 3.0% Si steel was about 50% and was obtained by transforming at 380°C. An optical micrograph of this structure is given in Fig. 32(b). The maximum amount of retained austenite in 4360 + 3.0% Si steel was about 60%, obtained by transforming at about 350°C. This structure is shown in Fig. 36(b). Blocky regions of untransformed austenite (B) can be noted in both the figures. The bainitic ferrite laths appeared to grow side by side, in colonies from the grain boundaries. Their growth would stop either by impingement at the grain boundary or on encountering a similarly growing packet of ferrite laths. The colonies of bainite (marked A in Fig. 36(b)) closely resembled the pearlite colonies. A transmission micrograph[47] of bainite formed at 354°C in 4360 + 3.0% Si steel is shown in Fig. 37. This specimen was refrigerated in liquid nitrogen prior to thinning. Magnetic measurements showed that the amount of retained austenite was reduced from 60% to 40% because of the refrigeration treatment. The bainite structure marked A in the transmission micrograph (Fig. 37) and corresponding to a typical area marked A in the optical micrograph (Fig. 36(b)) consisted of bainitic ferrite and austenite. It was very similar to the one obtained in 4340 + 3.0% Si steel transformed at 278°C, except that the austenite laths or films were considerably

thicker. There were many blocky regions (B) containing martensite. The blocky austenite that remained untransformed at reaction temperature, and also on cooling to room temperature must have transformed to martensite during the refrigeration treatment. On the other hand, the austenite laths or films trapped between the bainitic ferrite laths were unable to transform even at liquid nitrogen temperature. The way in which the shape and size of austenite determines its stability has been discussed in an earlier section.

In recent years, the mechanical properties of steels with bainitic structures have been explored. Whether the bainitic or martensitic structure has better toughness when compared at the same strength level has been argued, and conflicting data exist in literature. Holloman et al.[48] and Herres and Lorig[49] in the past, and Huang and Thomas[50] recently have observed that the impact toughness of bainite is inferior to that of tempered martensite. Opposite results have been reported by Irvine and Pickering,[51] Pascover and Matas,[52] and by Liu.[53] The bainitic structures explored by these investigators were all classical type, i.e., acicular ferrite and carbide aggregates. The mechanical properties of bainitic structures containing large amounts of retained austenite have not been investigated. Preliminary investigations[54] on 4340 + 3.0% Si steel showed that the bainitic structure formed at 300°C which contained about 35% retained austenite had a yield strength of over 200 ksi, and ultimate strength of 250 ksi, and plane strain fracture toughness of 95 ksi $in.^{1/2}$. These properties are comparable to those of expensive maraging steels. The bainitic structures obtained in high silicon steels thus appear to have good combinations of strength and toughness and warrant further study.

I. Mechanism of Bainite Formation

Several mechanisms for the formation of bainite have been proposed but none has gained universal acceptance. Central to the controversies on the bainite reaction are the growth mechanism of the bainitic ferrite and the sources of bainitic carbide. Ko and Cottrell[55] were the first to propose that lower bainite formed initially as supersaturated ferrite by a shear mechanism and that carbides subsequently precipitated from this ferrite. Hehemann and co-workers[7,19,56] later proposed that both forms of bainite formed by shear. In the formation of upper bainite, carbon is first partitioned to the adjacent austenite and later the carbide precipitates from the carbon-enriched austenite. According to Hehemann, bainite grows at rates more rapid than allowed by volume diffusion. The bainite is assumed to form by repeated nucleation of subunits and the subunits attain a limiting size rather rapidly. Thus, experimental growth rates actually refer to the nucleation rate of these units. Surface relief[7,55,57] accompanying the formation of upper and lower bainites tends to support the shear mechanism of bainite formation. Since Widmanstatten ferrite has also been observed to exhibit surface relief,[58] the surface tilts may not constitute sufficient evidence for a diffusionless transformation. Christian[59] believes that surface tilts are observed when the diffusivity of the solute greatly exceeds that of the solvent, as in these interstitial solid solutions. Thus, it is reasonable to conclude that the observation of surface relief, by itself, is not conclusive evidence that bainite forms by a shear mechanism.

The alternative model proposed is based on diffusion controlled (or interface controlled) growth of bainite. Kinsman and Aaronson[2] describe bainite as the product of a non-lamellar eutectoid reaction, and as growing (without the participation of a shear mechanism) at rates of the order of or less than that allowed by volume diffusion. Individual bainite plates are said to lengthen at a rate controlled by diffusion of carbon in austenite and thicken by a diffusion mechanism involving cooperative growth of ferrite and cementite into austenite.[2]

In analyzing the shear and the diffusion models for the formation of bainite, it is seen that carbide precipitation is essential in the diffusion model, whereas it is only ancillary in the shear model.[2] Lai[47] found that upper bainite formed in 4340 + 3.0% Si steel used in the present study was free of carbides. Previous investigators[44,60] also found that the upper bainite is silicon steels was free of carbides. Thus, the existence of carbides is not crucial to bainite formation. Further, the values of activation energies obtained for both forms of bainite in the present study were much less than that for carbon diffusion in austenite. Based on this evidence, the shear mechanism appears to be more probable.

Various investigators[55,61] have suggested that the carbon content of the bainitic ferrite when it first forms is the same as that of the parent austenite. Thus, according to the shear model, the bainitic ferrite forms in a substantially supersaturated condition. Hehemann[2] claims that the rate at which carbon precipitates from this supersaturated ferrite is responsible for the difference in morphology between upper and lower bainite. Rapid carbide precipitation will give rise to small

carbide particles within the ferrite laths and thus give a lower bainitic morphology. If the precipitation of carbides is slow, substantial partition of carbon to austenite trapped between ferritic laths can occur, and cementite may subsequently precipitate from this enriched austenite, resulting in an upper bainite morphology. The above explanation is supported by an analysis of crystallographic relationships between ferrite and carbide which indicates that carbide is precipitated from carbon-enriched austenite in upper bainite and from supersaturated ferrite in lower bainite.[3,62] Also, the observation that carbides in lower bainite are precipitated rather uniformly and with interparticle spacings comparable to those found in tempered martensite tends to indicate that the bainitic ferrite forms initially in a supersaturated condition.

Based on the observation[44] that in high silicon steels, austenite was retained only at reaction temperatures above 350°C, Hehemann attempted to explain the differences between upper and lower bainite by assuming that above 350°C ε carbide does not precipitate from supersaturated ferrite because at those temperatures the incubation period required for precipitation of cementite permits all or most of the carbon to partition to austenite. Below 350°C, however, ε carbide will precipitate rapidly. This model requires that the transition from lower to upper bainite should occur at 350°C, independent of composition of the steel. This model is incorrect because: (1) In the high silicon steels used in the present investigation, substantial amounts of retained austenite were obtained associated with upper bainite at reaction temperatures well below 350°C. (2) In 4340 + 0.1% C steel, both forms of bainite were observed above and below 350°C. (3) In 4340 + 3.0% Si steel

transformed at 278°C, small amounts of lower bainite containing ε carbide and large amounts of upper bainite containing retained austenite were found.[47] (4) There is no direct experimental evidence that ε carbide does not precipitate at temperatures above 350°C but will precipitate below 350°C.

Recognizing the limitations of the above model in explaining some of the observations in the present study, a slightly different model is proposed here. In this model, it is assumed that following the formation of supersaturated bainitic ferrite, the type of bainite is determined by the relative kinetics of carbide precipitation within the ferrite and of partitioning of carbon to the adjacent austenite. At higher reaction temperatures, the diffusivity of carbon is high enough to permit a rapid and complete partitioning of carbon to take place before the carbides have a chance to nucleate within the ferrite. At lower reaction temperatures, carbon diffuses much more slowly, and the carbides nucleate much faster. This results in rapid precipitation of carbides within the ferrite, and very little carbon can diffuse to the adjacent austenite. However, after some lower bainite has formed, the diffusion kinetics of carbon in the remaining austenite may be altered. It is known that the formation of bainite is accompanied by severe deformation of both bainitic ferrite and the adjacent austenite. The increased dislocation density will greatly enhance carbon diffusion in ferrite. It is possible that the carbon may now partition to the adjacent austenite at an accelerated pace, and may do so before the carbides have a chance to nucleate within the ferrite. Thus, at lower reaction temperatures, formation of upper bainite can follow the formation of lower bainite. In the upper transformation range, as upper bainite

forms, there is carbon enrichment in untransformed austenite. This means, as suggested by Pickering,[63] that the rate of diffusion of carbon away from the bainitic ferrite-austenite interface will be less rapid. Thus, it is likely that the precipitation of carbide can now occur within the ferrite, giving rise to a lower bainitic morphology.

The relative dominance of upper and lower bainite reactions is determined not only by the diffusion rates of carbon but also by the nucleation rates of carbides. Alloy composition plays a major role in determining these factors. Among the common alloying elements, silicon appears to have a distinctive influence. It is suggested[2,44] that the presence of silicon greatly reduces the chances of cementite precipitation. It is, however, reasonable to assume that silicon also affects the nucleation rate of ε carbide. The assumption is that the solubility of silicon in both the carbides is very low, and it is higher in ε carbide than in cementite. Thus, the lower bainite formed in high silicon steels always contains ε carbide. Since ε carbide does not precipitate from carbon-enriched austenite,[2,44] the upper bainite formed in high silicon steels always contains large amounts of retained austenite.

In the high silicon steels studied, it was found that the amount of austenite retained after transforming at about 300°C and cooling to room temperature increased with increasing silicon content. At these temperatures (around 300°C), both forms of bainite formed in these steels. Thus, at 300°C, the amount of lower bainite (containing ε carbide) formed decreased and the amount of upper bainite (containing austenite) formed increased with the increasing silicon content.

Alloy content, reaction temperature, transformation strains--all influence the diffusion rates of carbon and the nucleation rates of carbides. In low silicon steels, the carbides nucleate rather rapidly. Hence, at lower reaction temperatures, only lower bainite may form or upper bainite can form only after large amounts of lower bainite have formed. In high silicon steels on the other hand, the carbide nucleation is greatly inhibited. Upper bainite can form even at lower reaction temperatures or upper bainite can form following the formation of even small amounts of lower bainite.

IV. SUMMARY AND CONCLUSIONS

The effects of small additions of common alloying elements (C, Ni, Cr, Mn, Mo and Si) on the kinetics of bainite formation in a 4340 steel were studied. A rapid magnetic permeability method was developed to facilitate this study. Computer aided methods were used to analyze the isothermal reaction data and to plot the TTT diagrams. The isothermal reaction data were analyzed using two empirical rate equations (Zener[21] and Austen-Rickett[22] equations). The morphology of bainite was studied using optical and transmission electron microscopy techniques in a few steels. Some important observations made in these studies are summarized below.

1. The TTT diagram of the 4340 steel, that was determined using the magnetic method was similar to the published TTT diagram, except for significant differences in the lower bainite region. An acceleration of the austenite decomposition just above M_s gave an S-shaped curve for the bainite reaction in all the steels studied.

2. In some of the steels studied, separate C-curves for the two variants of bainite were observed in the early stages of the transformation but they overlapped in the later stages.

3. In 4340 steel, on increasing the austenitizing temperature from 900°C to 1200°C, the incubation period increased and the transformation rate decreased for the upper bainite reaction. The incubation period and transformation rate for the lower bainite reaction were unaffected. The M_s temperature increased by about 25°C, while the M_f temperature remained the same.

4. Molybdenum when added to 4340, unlike other alloying elements studied, reduced the incubation period, accelerated the bainite reaction, and raised the M_s temperature. However, when added together with Ni or Cr, Mo shifted the bainite reaction to longer times and to lower temperatures.

5. All the alloy additions (except single additions of Mo) shifted the bainite curves to longer times and lowered the kinetic B_s and B_f temperatures. For combined additions, the effect of the various elements in lowering the B_s temperature was additive. An equation was derived to calculate the B_s temperature directly from the composition, and it is as follows.

$$B_s(°C) = 839 - 300\%\ C - 60\%\ Mn - 33\%\ Ni - 63\%\ Cr - 130\%\ Mo - 43\%\ Si$$

6. In increasing the incubation period for bainite reaction, (a) 0.1% C was more effective than 1% additions of Ni, Cr, Mn or Si, (b) Si up to 2% addition was as effective as Ni or Cr, (c) 1% Ni + 1% Cr addition was more effective than either 2% Ni or 2% Cr, and (d) for the same total weight of alloying additions, Ni + Mo combination was more effective than Cr + Mo.

7. In retarding the bainite reaction, (a) up to 2% additions, Mn was more effective than Ni or Cr, (b) the addition of 2% Cr was more effective than either 2% Ni or 1% Ni + 1% Cr addition, (c) the effect of a 2% addition was not equal to 2 times the effect of 1% addition, but it was much smaller in case of Ni and much larger in case of Mn or Cr.

8. For 4340 and modified 4340 steels (excluding Si additions), there was a distinct change in the value of Zener index n and in the value of experimental activation energy around 350°C.

9. The Zener index values obtained for the 2% and 3% silicon modified 4340 steels were those that are characteristic of upper bainite reaction.

10. The activation energy obtained for upper bainite reaction was higher than that obtained for lower bainite reaction. Both were small compared to the activation energy for carbon diffusion in austenite.

11. Partial transformation of austenite to bainite produced significant amounts of retained austenite. The silicon modified 4340 steels retained much larger amounts of austenite than the other steels.

12. In the high silicon steels studied, the bainite reaction was stabilized short of complete austenite decomposition at all reaction temperatures. Large amounts of austenite were retained as part of bainitic structure at all reaction temperatures both above and below the M_s temperature.

13. In all the high silicon steels, the amount of retained austenite (retained on cooling the sample to room temperature after the reaction had fairly stabilized) increased with increasing reaction temperature above 300°C and reached a maximum value at about 100°C below the B_s temperature. For the same carbon content, the amount of retained austenite obtained at any particular reaction temperature increased with the increase in silicon content. For the same silicon content, it increased with increasing carbon content. The retained austenite obtained at lower reaction temperatures did not transform on refrigerating in liquid nitrogen as did some of the retained austenite obtained at higher reaction temperatures.

14. A morphological study of bainite formed at various reaction temperatures in 4350 steel (a low silicon steel) revealed that the structures changed from being predominantly lower bainitic at 329°C to predominantly upper bainitic at 429°C. The transition between upper and lower bainite was gradual and occurred over a temperature range. The classical forms of bainite containing carbides were formed in this steel.

15. In high silicon steels, upper bainite containing large amounts of retained austenite was formed. Two types of austenite were retained, namely (a) the austenite that was trapped between individual ferrite laths in a fine form and (b) the austenite that was trapped between growing bainite colonies in a blocky form.

ACKNOWLEDGEMENTS

The author gratefully acknowledges the constant encouragement and guidance given during the course of this investigation by Professors E. R. Parker and V. F. Zackay. He would also like to express his gratitude to to Professor K. M. Htun (University of Hawaii) and Professor J. W. Morris, Jr. and Professor Hauser for a critical review of the manuscript. Special thanks are extended to Dr. G. Lai for many discussions and help in transmission electron microscopy.

The author is thankful to the technical support staff of the Inorganic Materials Research Division, in particular, to D. Ott, E. Edwards and D. Newhart for their help in the design and fabrication of the experimental apparatus used in this investigation. Thanks are also due to Gloria Pelatowski (preparation of line drawings), Doug Kreitz and Phila Witherell (technical photography), and Jean Wolslegel, Shirley Ashley and M. S. Bhat (manuscript preparation). Last, but not least, the author is thankful to his wife for her constant encouragement and help in carrying out this investigation.

This work has been done under the auspices of the U. S. Atomic Energy Commission through the Inorganic Materials Research Division of the Lawrence Berkeley Laboratory.

REFERENCES

1. E. S. Davenport and E. C. Bain, Trans. AIME 90, 117 (1930).

2. R. F. Hehemann, K. R. Kinsman and H. I. Aaronson, Met. Trans. 3, 1077 (1972).

3. D. N. Shackleton and P. M. Kelly, Physical Properties of Martensite and Bainite, I.S.I Spec. Report. No. 93 (The Iron and Steel Institute, London, 1965), p. 126.

4. P. Vasudevan, L. W. Graham and H. J. Axon, J. Iron Steel Inst. 190, 386 (1958).

5. S. V. Radcliffe and E. C. Rollason, J. Iron Steel Inst. 191, 56 (1959).

6. J. S. White and W. S. Owen, J. Iron Steel Inst. 197, 241 (1961).

7. R. H. Goodenow, S. J. Matas and R. F. Hehemann, Trans. AIME, 227, 651 (1963).

8. R. W. K. Honeycombe and F. B. Pickering, Met. Trans. 3, 1099 (1972).

9. J. Burke, The Kinetics of Phase Transformations in Metals (Pergamon Press, 1965), p. 37.

10. A. B. Greninger and A. R. Troiano, Trans. ASM 28, 537 (1940).

11. W. Steven and A. G. Haynes, J. Iron Steel Inst. 183, 349 (1956).

12. F. B. Rote, W. C. Truckenmiller and W. P. Wood, Trans. ASM 30, 1359 (1942).

13. H. S. Smith, Trans. AIME 116, 342 (1935).

14. C. Nagler and W. P. Wood, Trans. ASM 30, 491 (1942).

15. R. L. Rickett and F. C. Kristufek, Trans. ASM 41, 1113 (1949).

16. W. Hume-Rothery, The Structures of Alloys of Iron (Pergamon Press, 1966), p. 176.

17. B. Yakovlev, Metallovedeniei Ternicheskaya Obrabotka Metallov 8, 57 (1966).

18. R. M. Bozorth, Ferromagnetism (D. Van Nostrand Co., New York, 1951), p. 59 and 714.

19. R. F. Hehemann, Phase Transformations (American Society for Metals, Ohio, 1970), p. 409.

20. C. E. Ericsson, An Isothermal Study of Bainitic and Martensitic Transformations in some Low Alloy Steels using a New Magnetic Permeability Technique (M. S. Thesis), LBL-2279, December 1973.

21. C. Zener, J. Appl. Phys. 20, 950 (1949).

22. J. B. Austin and R. L. Rickett, Trans. AIME 135, 396 (1939).

23. Atlas of Isothermal Transformation Diagrams (United States Steel Corporation, 1963), p. 103.

24. Isothermal Transformation Diagrams of Nickel Alloy Steels (The International Nickel Company, 1970), p. 7.

25. R. T. Howard and M. Cohen, Trans. AIME 176, 384 (1948).

26. O. Schaaber, J. Metals 7, 559 (1955).

27. J. Barford, J. Iron and Steel Inst. 204, 609 (1966).

28. A. S. Davenport, et al., Trans. AIME 145, 301 (1941).

29. S. A. Cottrell and T. Ko, J. Iron and Steel Inst. 173, 224 (1953).

30. J. Barford and W. S. Owen, J. Iron and Steel Inst. 197, 146 (1961).

31. L. W. Graham and H. J. Axon, J. Iron and Steel Inst. 191, 361 (1959).

32. E. M. Breinan and G. S. Ansell, Met. Trans. 1, 1513 (1970).

33. A. S. Sastri and D. R. F. West, J. Iron and Steel Inst. 203, 138 (1965).

34. R. F. Mehl and W. C. Hagel, Progress in Metals Physics (Pergamon Press, 1956), Vol. 6, p. 74.

35. E. C. Rollason, Fundamental Aspects of Molybdenum on Transformation of Steel (Climax Molybdenum of Europe, Limited), p. 19.

36. J. E. Bridge, Jr., G. V. Manihar and T. V. Philips, Met. Trans. 2, 2209 (1971).

37. Isothermal Transformation Diagrams for Nickel Steels, Metallurgia, 280 (June 1951).

38. G. R. Brophy and A. J. Miller, Trans. AIME 167, 654 (1946).

39. J. Burke, The Kinetics of Phase Transformations in Metals (Pergamon Press, 1965), p. 53.

40. R. I. Entin: The Decomposition of Austenite by Diffusional Processes, V. F. Zackay and H. I. Aaronson, eds. (Interscience, N. Y., 1962), p. 295.

41. J. Deliry, Mem. Sci. Rev. Met. 7-8, 524 (1965).

42. S. J. Matas and R. F. Hehemann, Trans. TMS-AIME 221, 179 (1961).

43. R. Le Houillier, G. Bégin and A. Dubé, Met. Trans. 2, 2645 (1971).

44. J. M. Oblak and R. F. Hehemann, Transformation and Hardenability in Steel (Climax Molybdenum Company, Ann Arbor, 1967), p. 15.

45. L. J. Habraken and M. Economopoulos, ibid, p. 69.

46. J. W. Christian, The Theory of Transformation in Metals and Alloys (Pergamon, New York, 1965).

47. G. Lai, unpublished work, University of California, Berkeley.

48. J. H. Holloman, L. D. Jaffe, D. E. McCarthy and M. R. Nortan, Trans. ASM 38, 807 (1947).

49. S. A. Herres and C. H. Lorig, Trans. ASM 40, 775 (1948).

50. Der-Hung Huang and G. Thomas, Met. Trans. 2, 1587 (1971).

51. K. J. Irvine and F. B. Pickering, J. Iron Steel Inst. 201, 518 (1963).

52. J. S. Pascover and S. J. Matas, ASTM Special Technical Publication No. 370, 1963, p. 30.

53. Y. H. Liu, Trans. ASM 62, 55 (1969).

54. B. N. P. Babu, unpublished work, University of California, Berkeley.

55. T. Ko and S. A. Cottrell, J. Iron and Steel Inst. 172, 307 (1952).

56. R. H. Goodenow, R. H. Barkalow and R. F. Hehemann, Physical Properties of Martensite and Bainite, Special Report 93, (The Iron and Steel Inst., London, 1965), p. 135.

57. G. R. Speich and M. Cohen, Trans. TMS-AIME 218, 1050 (1960).

58. A. P. Miodownik, J. Inst. Metals 83, 561 (1954-55).

59. J. W. Christian, The Decomposition of Austenite by Diffusional Processes, V. F. Zackay and H. I. Aaronson, eds. (Interscience, N. Y., 1962), p. 371.

60. T. G. Nilan, Transformation and Hardenability in Steel (Climax Molybdenum Company, Ann Arbor, 1967), p. 57.

61. C. Zener, Trans. AIME 167, 550 (1946).

62. K. J. Irivine and F. B. Pickering, Physical Properties of Martensite and Bainite, Special Report 93 (Iron and Steel Institute, London, 1965), p. 110.

63. F. B. Pickering, Transformation and Hardenability in Steel (Climax Molybdenum Company, Ann Arbor, 1967), p. 109.

FIGURE CAPTIONS

Fig. 1. Schematic of the tube furnace, the quenching system and the sensing coil.

Fig. 2. Block diagram of the electronic system.

Fig. 3. Photograph of the experimental apparatus.

Fig. 4. Calibration curves for change in period with temperature for 4340 and some modified 4340 steels.

Fig. 5. Calibration curves for change in period with temperature for modified 4340 steels.

Fig. 6. Plot of resonant periods of oscillation with change in inductance of the coil.

Fig. 7. Calibration curve for the amount of transformation with change in period.

Figs. 8A thru 8N Isothermal transformation curves for different steels austenitized at 900°C. In each figure, plot (a) is on a log-log scale and plot (b) is on a linear scale.

Fig. 8A. For 4340 steel.

Fig. 8B. For 4340 + 0.1% C steel.

Fig. 8C. For 4340 + 1.0% Mn steel.

Fig. 8D. For 4340 + 1.0% Si steel.

Fig. 8E. For 4340 + 2.0% Si steel.

Fig. 8F. For 4340 + 3.0% Si steel.

Fig. 8G. For 4340 + 1.0% Ni steel.

Fig. 8H. For 4340 + 2.0% Ni steel.

Fig. 8I. For 4340 + 1.0% Cr steel.

Fig. 8J. For 4340 + 2.0% Cr steel.

Fig. 8K. For 4340 + 1.0% Ni + 1.0% Cr steel.

Fig. 8L. For 4340 + 1.0% Ni + 0.5% Mo steel.

Fig. 8M. For 4340 + 1.0% Cr + 0.5% Mo steel.

Fig. 8N. For 4340 + 1.0% Ni + 1.0% Cr + 0.5% Mo steel.

Fig. 9. Time-temperature-transformation diagram of 4340 steel austenitized at 870°C as found in the literature.[23,24] Only bainite and martensite ranges are shown.

Fig. 10. Time-temperature-transformation diagram for 4340 steel austenitized at 900°C. Only bainite and martensite ranges were determined.

Fig. 11. Time-temperature-transformation diagram for 4340 steel austenitized at 1200°C.

Fig. 12A thru 12N Time-temperature-transformation diagrams for the different modified 4340 steels austenitized at 900°C.

Fig. 12A For 4340 + 0.1% C steel.

Fig. 12B For 4340 + 1.0% Mn steel.

Fig. 12C For 4340 + 1.0% Si steel.

Fig. 12D For 4340 + 2.0% Si steel.

Fig. 12E For 4340 + 3.0% Si steel.

Fig. 12F For 4340 + 1.0% Ni steel.

Fig. 12G For 4340 + 2.0% Ni steel.

Fig. 12H For 4340 + 1.0% Cr steel.

Fig. 12I For 4340 + 2.0% Cr steel.

Fig. 12J For 4340 + 1.0% Ni + 1.0% Cr steel.

Fig. 12K For 4340 + 0.5% Mo steel.

Fig. 12L For 4340 + 1.0% Ni + 0.5% Mo steel.

Fig. 12M For 4340 + 1.0% Cr + 0.5% Mo steel.

Fig. 12N For 4340 + 1.0% Ni + 1.0% Cr + 0.5% Mo steel.

Figs. 13A thru 13C Time for transformation at different temperatures for a few steels plotted according to (a) Zener equation[21] and (b) Austen-Rickett equation.[22]

Fig. 13A For 4340 + 0.1% C steel.

Fig. 13B For 4340 + 1.0% Ni steel.

Fig. 13C For 4340 + 2.0% Ni steel.

Fig. 14. Time for transformation at different temperatures for 4340 + 3.0% Si steel is plotted according to Zener equation.[21]

Fig. 15. Zener index "n" plotted against transformation temperature for 4340 steels modified with C, Ni, Cr and Mo additions. Note that n changes discontinuously at 350°C. Above 350°C, n lies within the range 1.0-2.0 and below 350°C, n varies from 2.0 to 3.0.

Fig. 16. Time for 25% transformation is plotted against the reciprocal of the transformation temperature in °K for (a) 4340 steel, (b) 4340 + 0.1% C steel and (c) 4340 + 1.0% Si steel. The values of the activation energy were determined from the slopes of these plots.

Figs. 17A thru 17E Variation in retained austenite is plotted against isothermal transformation temperature for the high silicon steels studied. The retained austenite was measured at room temperature after cooling from reaction temperature, and also after refrigerating in liquid nitrogen (-195°C).

Fig. 17A. For 4340 + 1.0% Si steel.

Fig. 17B. For 4340 + 2.0% Si steel.

Fig. 17C. For 4340 + 3.0% Si steel.

Fig. 17D. For 4340 + 2.0% Si steel.

Fig. 17E. For 4360 + 3.0% Si steel.

Fig. 18. Optical micrographs showing the microstructures of specimens of 4340 + 0.1% C steel isothermally transformed at (a) 329°C, (b) 350°C.

Fig. 19. Optical micrographs of specimens of 4340 + 0.1% C steel isothermally transformed at (a) 379°C and (b) 429°C. The light etching areas marked A in (b) are those of untransformed austenite transformed to martensite on cooling to room temperature. A transmission micrograph of such an area is given in Fig. 29(a).

Fig. 20. Transmission electron micrograph (composite picture) of 4340 + 0.1% C steel isothermally transformed at 329°C showing laths or plates of lower bainite with cementite precipitated within the ferrite laths at an angle of about 55-65° to the major axis of ferrite lath at A, a large area of ferrite containing many parallel cementite particles at B, and upper bainite regions consisting of carbides along the lath boundaries of ferrite at C.

Fig. 21. Transmission electron micrograph (composite picture) of 4340 + 0.1% C steel isothermally transformed at 329°C showing an extensive region of ferrite containing many parallel cementite particles at B.

Fig. 22. Transmission electron micrographs of 4340 + 0.1% C steel isothermally transformed at 329°C showing two different areas of the foil. Note the regions marked C in (a) and (b). These are upper bainite regions containing long and stringer like carbides along the lath boundaries of ferrite.

Fig. 23. Selected area diffraction pattern obtained from a typical lower bainite area in the thin foil specimen of 4340 + 0.1% C steel isothermally transformed at 329°C. The orientation relationship determined is $(112)_{\alpha} \| (100)$ Fe_3C.

Fig. 24. Transmission electron micrograph (composite picture) of a thin foil specimen of 4340 + 0.1% C steel isothermally transformed at 350°C showing a lower bainite plate composed of several structural units at A and regions of upper bainite at B.

Fig. 25. Transmission electron micrographs of 4340 + 0.1% C steel isothermally transformed at 350°C showing two different areas of the foil. A large area of ferrite containing parallel carbides (A) is shown in (a). A typical upper bainite area (B) containing carbide stringers along the ferritic lath boundaries and a lower bainite area (A) are shown in (b).

Fig. 26. Transmission electron micrograph of 4340 + 0.1% C steel isothermally transformed at 350°C showing another area of the foil. The upper bainite regions at A contain a few carbides within the ferrite laths. This indicates that the upper bainite actually forms by repeated nucleation of a more basic substructural unit.

Fig. 27. Transmission electron micrograph (composite picture) of a thin foil specimen of 4340 + 0.1% C steel transformed at 379°C

showing classical upper bainite with cementite stringers along the ferrite lath boundaries at A, the lower bainite at B and regions of ferrite containing irregular lumps of carbide at C.

Fig. 28. Transmission electron micrograph (composite picture) of a thin foil specimen of 4340 + 0.1% C steel isothermally transformed at 429°C showing areas containing shorter and evenly distributed carbides that could be classified as lower bainite at A, upper bainite areas giving the appearance of pearlite at B and regions of untransformed austenite transformed to martensite on cooling to room temperature at C. The region C is shown more clearly in Fig. 29(a). This part of the foil was thicker owing to differential thinning of the specimen, hence the dark contrast.

Fig. 29. (a) Transmission electron micrograph of 4340 + 0.1% C steel transformed at 429°C showing a region (A) containing martensite laths or plates. In this region the austenite that remained untransformed at the reaction temperature has transformed to martensite on cooling to room temperature. (b) Optical micrograph of 4340 + 0.1% C steel isothermally transformed at 462°C. Only 30% austenite transformed to bainite before the reaction stabilized at this temperature. The rest of the austenite transformed to martensite on cooling to room temperature. The martensite regions (A) are light etching, while the bainite regions (B) are dark etching.

Fig. 30. Optical micrographs of 4340 + 1.0% Si steel transformed at (a) 299°C and (b) 352°C. As per the magnetic measurements there should be 18% austenite in the structure shown in (a) and 30% austenite in the structure shown in (b). Obviously, the retained austenite present in these structures cannot be identified optically.

Fig. 31. (a) Optical micrograph of 4340 + 3.0% Si steel transformed at 278°C showing a light etching plate (identified as lower bainite in a corresponding transmission micrograph given in Fig. 35) at A and light etching blocky regions (identified as pools of austenite in a corresponding transmission micrograph given in Fig. 34) at B trapped between growing ferrite laths. Magnetic measurements show that about 35% austenite is present in this structure. (b) Optical micrograph of the above structure after it was tempered for 1 hr at 600°C. It appears that the austenite has decomposed by the tempering treatment. The resulting distribution of carbides appears to describe the morphology of retained austenite prior to the tempering treatment.

Fig. 32. (a) Optical micrograph of 4360 + 3.0% Si steel transformed at 247°C. The structure is similar to that shown in Fig. 31(a). Islands or pools of austenite are marked B. (b) Optical micrograph of 4340 + 3.0% Si steel transformed at 380°C. It can be noted that the structure is much coarser compared to that shown in Fig. 31(b).

As per magnetic measurements, the structures shown in (a) and (b) both contain about 50% austenite.

Fig. 33. A low magnification dark field of austenite reflection (transmission electron micrograph) of a thin foil specimen of 4340 + 3.0% Si steel transformed at 278°C. Diffraction pattern showing the ferrite and austenite spots and corresponding explanatory line drawing are also given. Note that the austenite occurs with varying thicknesses.

Fig. 34. A bright field micrograph and the corresponding dark field micrograph of an austenite reflection obtained from a different area of the thin foil specimen of 4340 + 3.0% Si steel transformed at 307°C. Note the films of austenite decorating the lath boundaries of ferrite at A, austenite regions with a thickness equal to the lath size of bainitic ferrite at B and a pool of austenite at C. Tangled dislocations can be seen in the trapped islands of austenite. An examination of the region A indicates that the bainitic ferrite forms by the nucleation of small subunits.

Fig. 35. (a) A transmission electron micrograph (composite) of 4340 + 3.0% Si steel transformed at 278°C showing a lower bainite plate containing ε carbide. (b) A higher magnification picture showing a part of the lower bainite plate.

Fig. 36. (a) Optical micrograph of 4350 + 3.0% Si steel transformed at 350°C (b) Optical micrograph of 4360 + 3.0% Si steel transformed at 350°C showing colonies of bainite at A and blocky regions of untransformed austenite at B. The bainitic ferrite laths appear to grow in colonies from the grain boundaries.

Fig. 37. Transmission electron micrographs of 4360 + 3.0% Si steel transformed at 350°C showing a bainite colony consisting of ferrite laths with austenite trapped between the laths at A and a blocky region of martensite at B. The specimen was refrigerated prior to thinning. The blocky austenite that remained untransformed at reaction temperature has transformed to martensite during the refrigeration, while the fine form of austenite that is trapped between the ferritic laths remains untransformed.

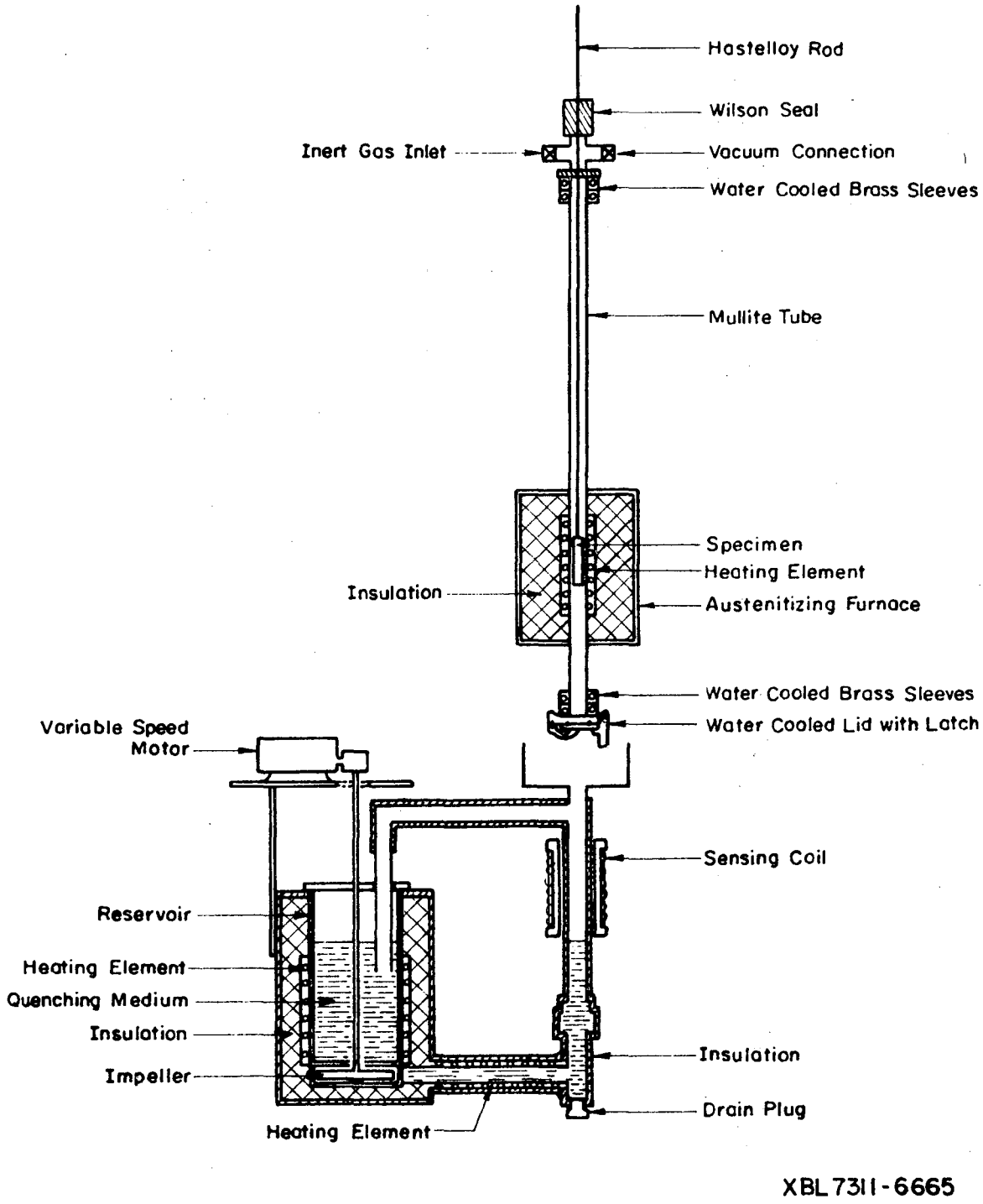
Hastelloy Rod
Wilson Seal
Inert Gas Inlet
Vacuum Connection
Water Cooled Brass Sleeves
Mullite Tube
Specimen
Heating Element
Insulation
Austenitizing Furnace
Water Cooled Brass Sleeves
Water Cooled Lid with Latch
Variable Speed Motor
Sensing Coil
Reservoir
Heating Element
Quenching Medium
Insulation
Impeller
Insulation
Drain Plug
Heating Element
XBL 7311-6665

Fig. 1

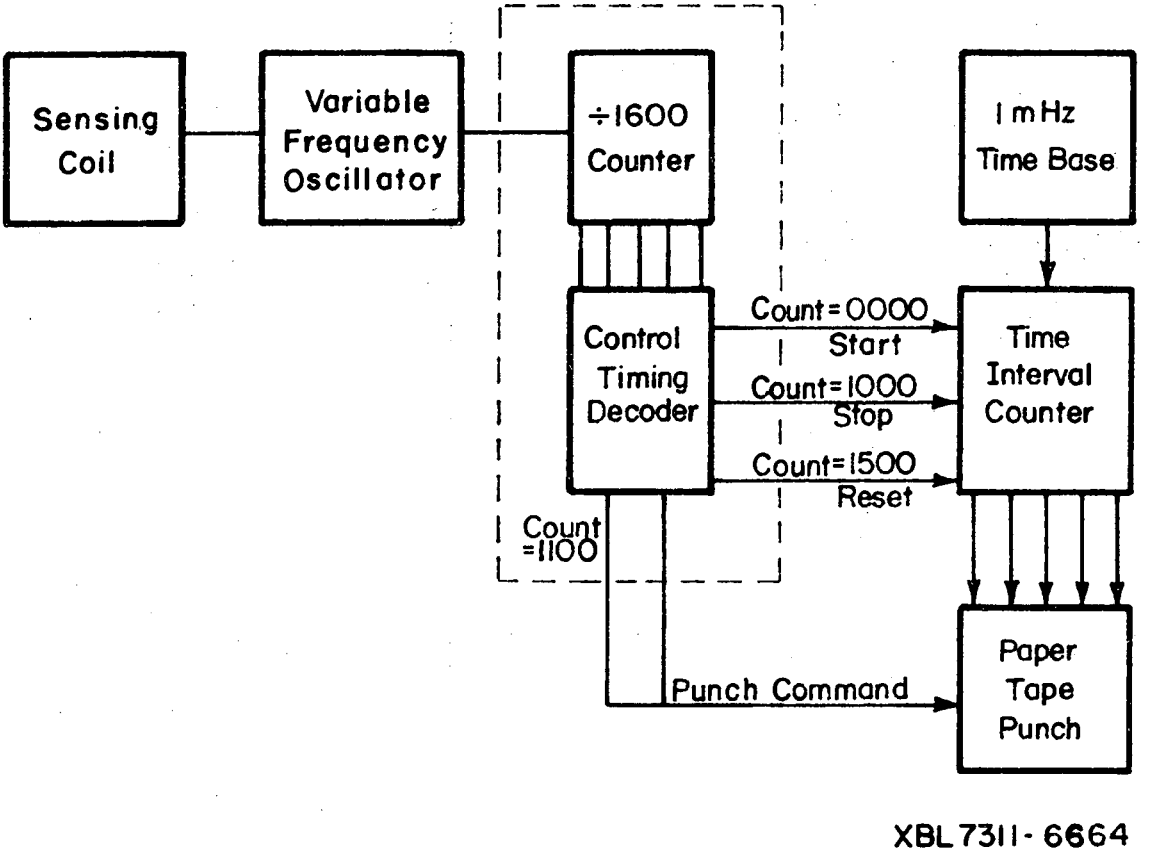
Sensing Coil
Variable Frequency Oscillator
÷1600 Counter
1 mHz Time Base
Control Timing Decoder
Count=0000 Start
Count=1000 Stop
Count=1500 Reset
Time Interval Counter
Count =1100
Punch Command
Paper Tape Punch
XBL7311-6664

Fig. 2

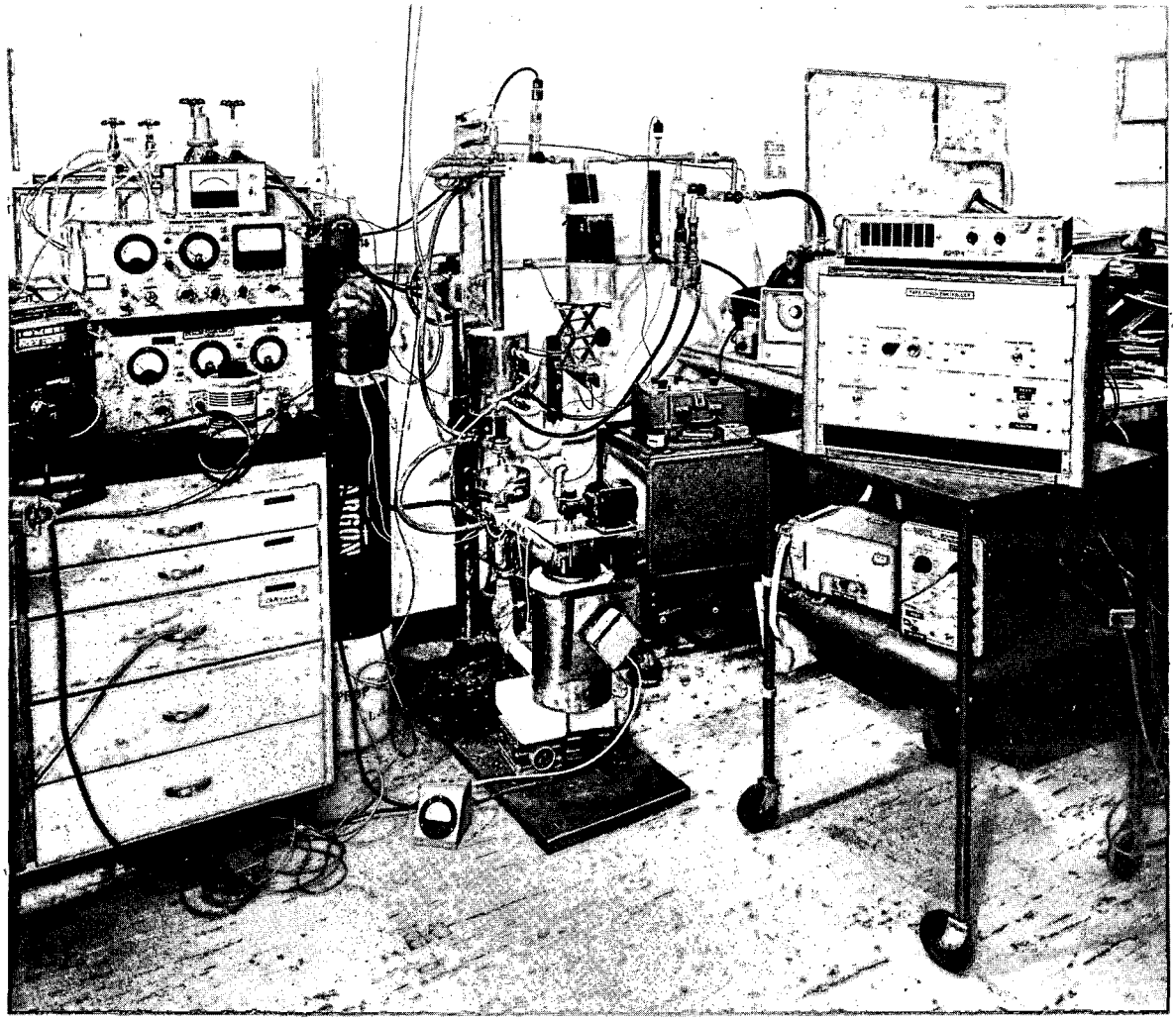

XBB 736-3675

Fig. 3

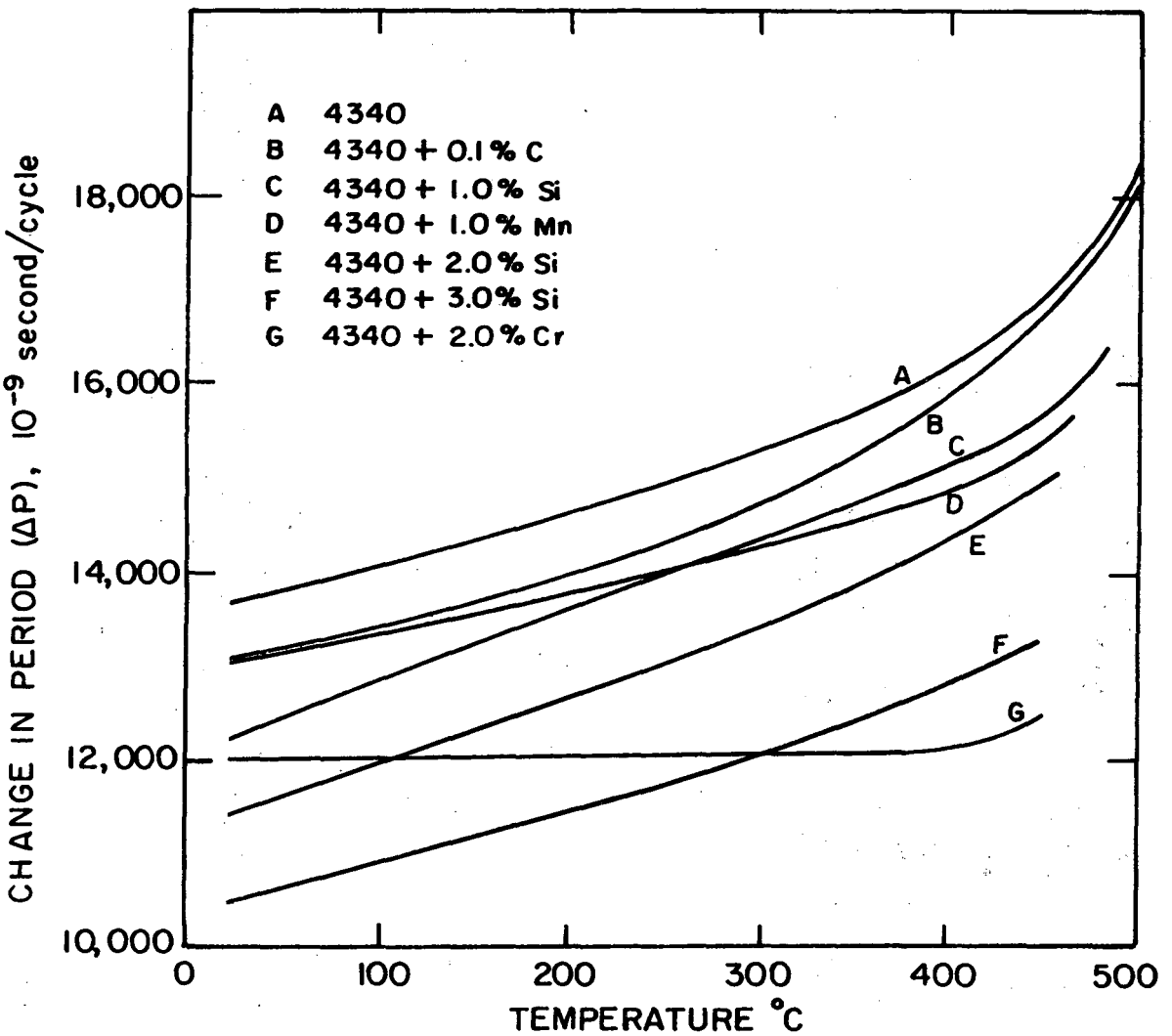

XBL 746-6515

Fig. 4

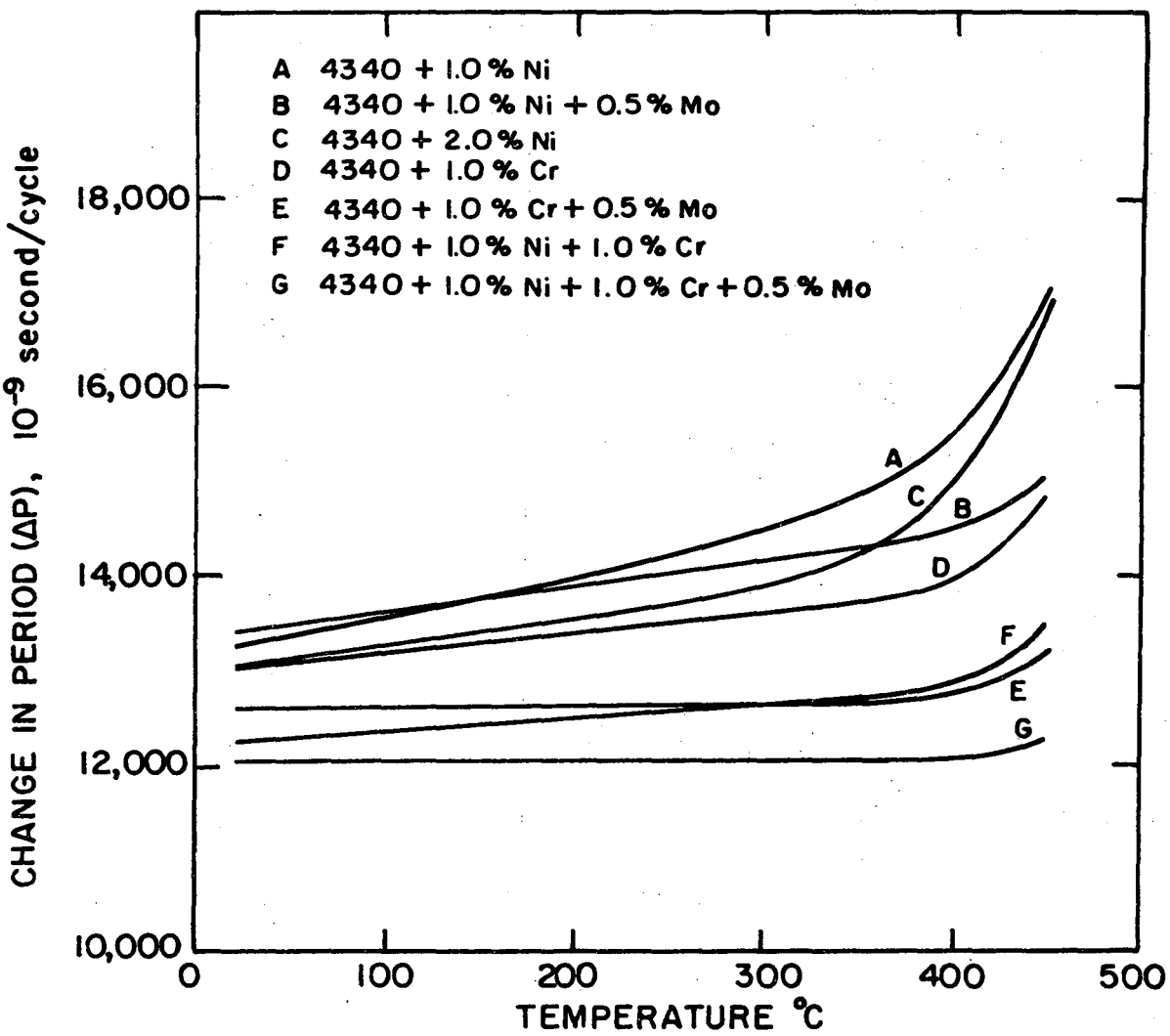

XBL 746-6514

Fig. 5

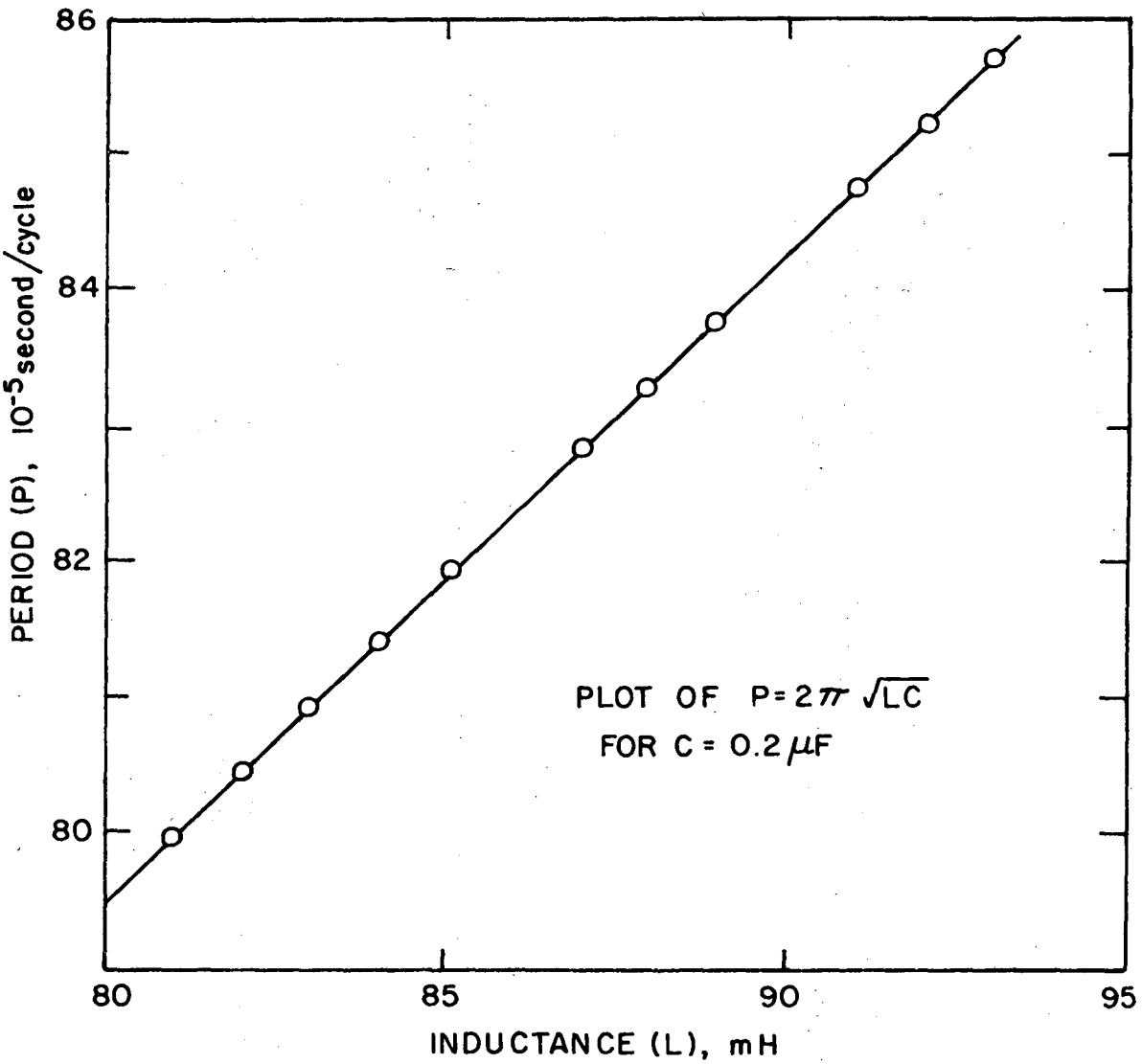

XBL 746-6517

Fig. 6

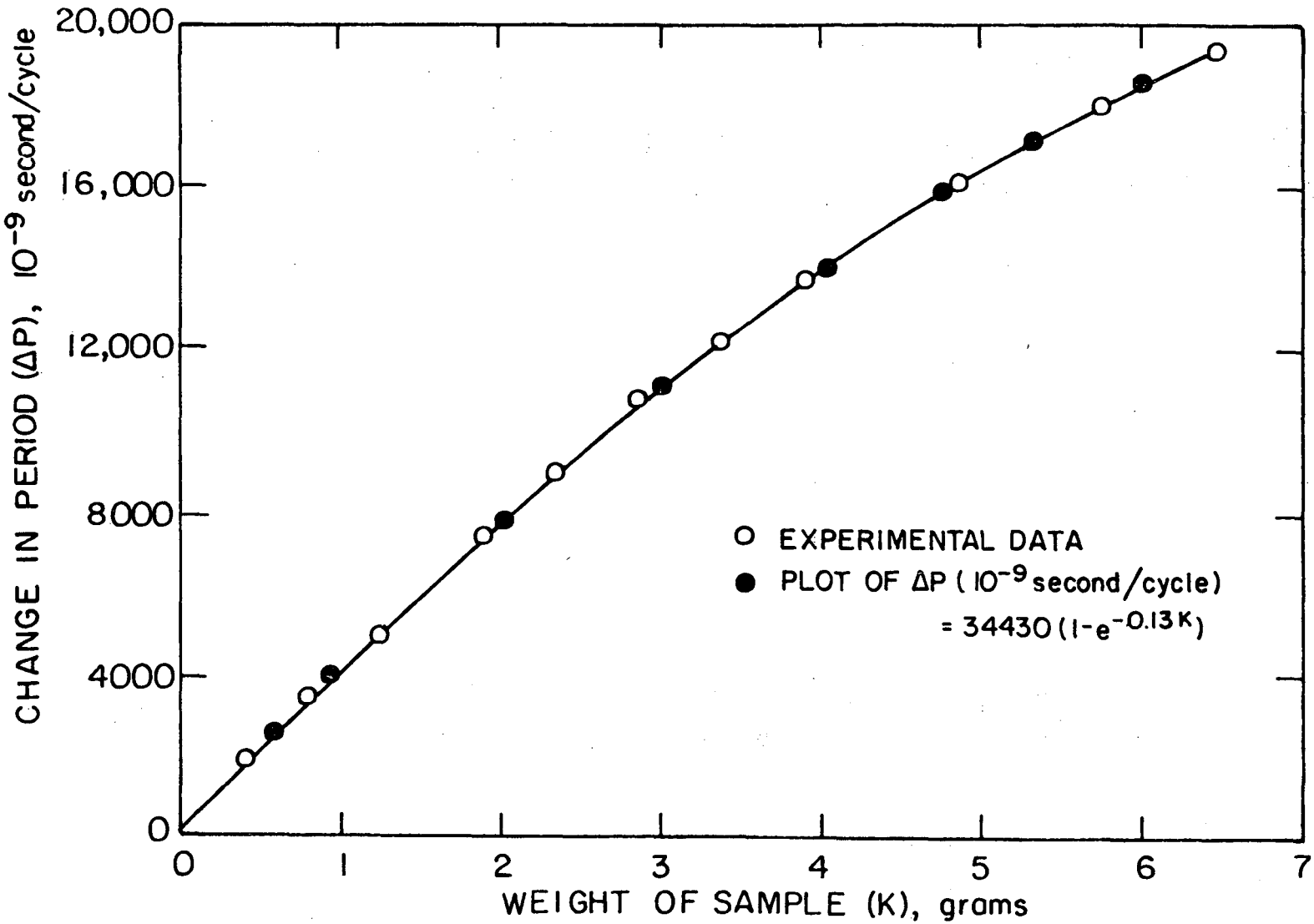

XBL 746-6518

Fig. 7

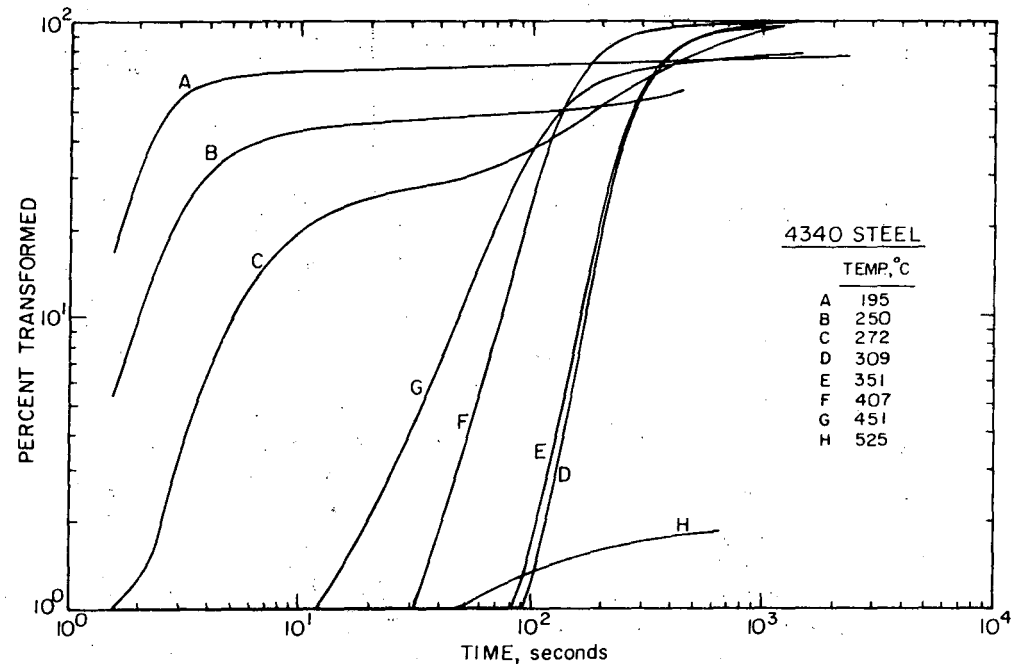
PERCENT TRANSFORMED
TIME, seconds
4340 STEEL
TEMP, °C
A 195
B 250
C 272
D 309
E 351
F 407
G 451
H 525

(a)

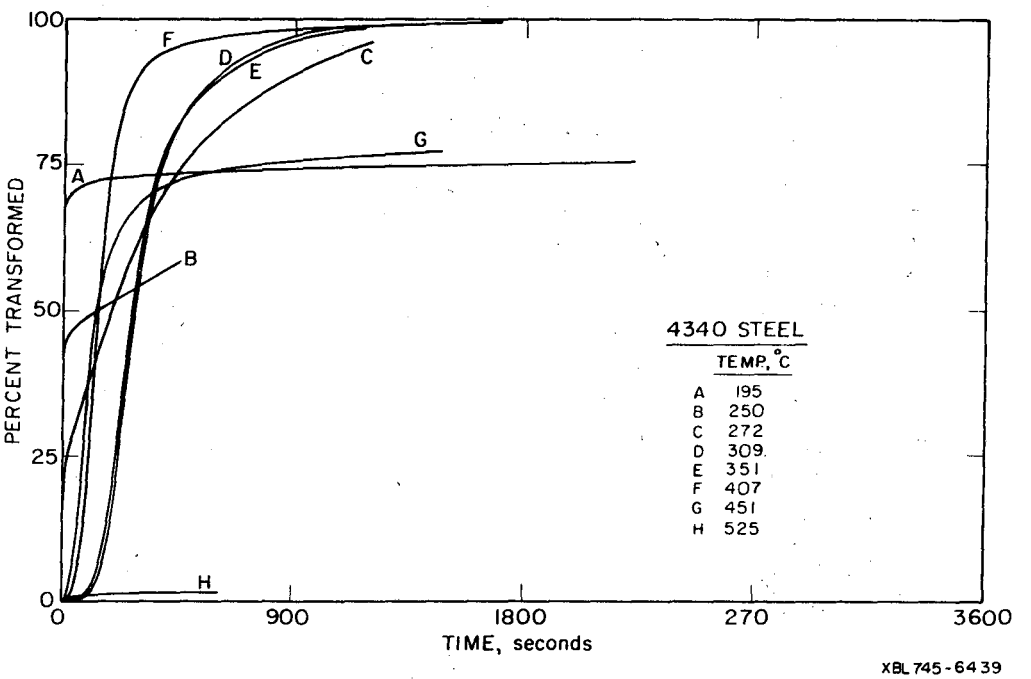
PERCENT TRANSFORMED
TIME, seconds
4340 STEEL
TEMP, °C
A 195
B 250
C 272
D 309
E 351
F 407
G 451
H 525
XBL745-6439

(b)

Fig. 8A

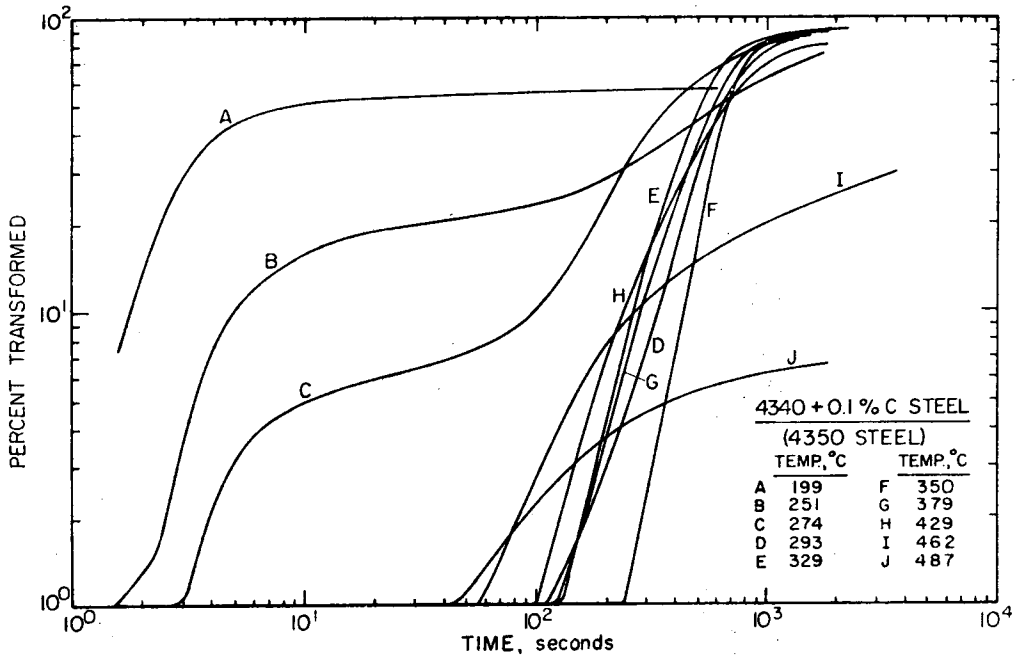
PERCENT TRANSFORMED
TIME, seconds
4340 + 0.1 % C STEEL
(4350 STEEL)
TEMP.,°C
A 199
B 251
C 274
D 293
E 329
F 350
G 379
H 429
I 462
J 487

(a)

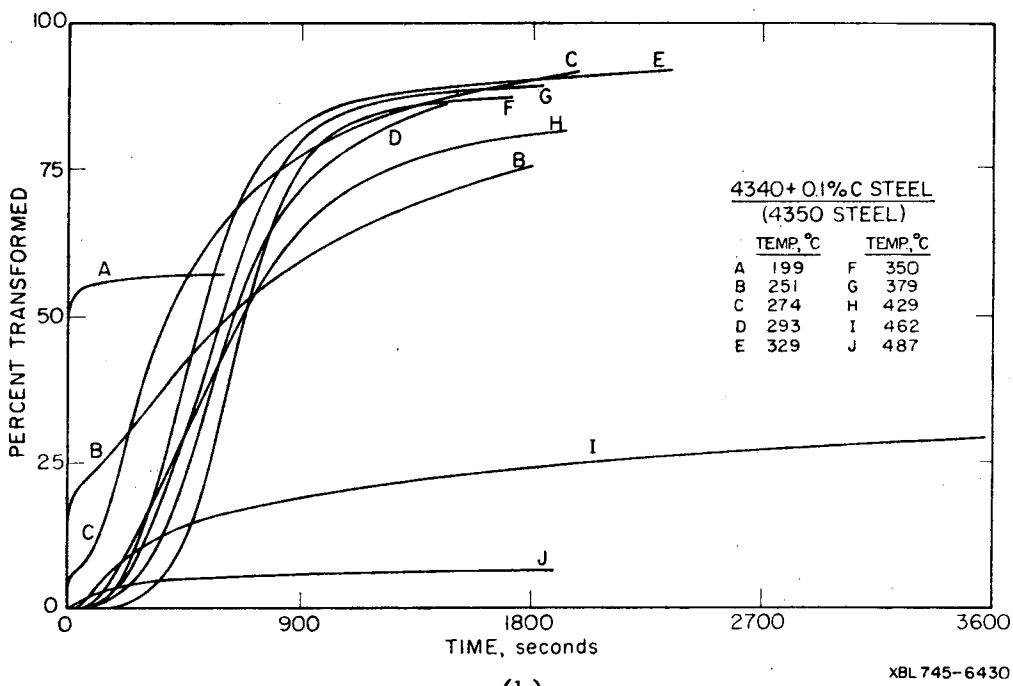
PERCENT TRANSFORMED
TIME, seconds
4340+0.1%C STEEL
(4350 STEEL)
TEMP.,°C
A 199
B 251
C 274
D 293
E 329
F 350
G 379
H 429
I 462
J 487
XBL 745-6430

(b)

Fig. 8B

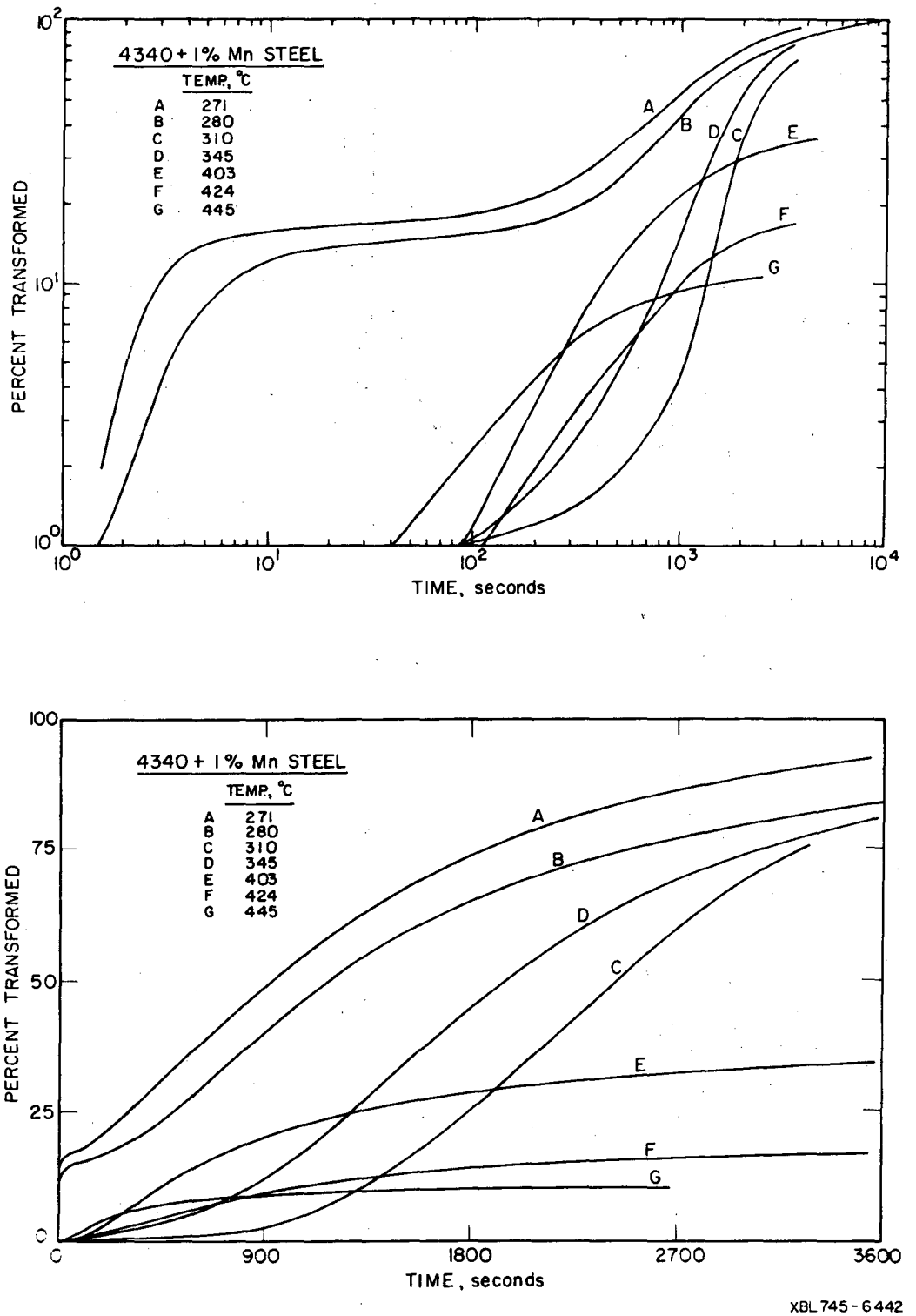
4340 + 1% Mn STEEL
TEMP, °C
A 271
B 280
C 310
D 345
E 403
F 424
G 445
PERCENT TRANSFORMED
TIME, seconds
4340 + 1% Mn STEEL
TEMP, °C
A 271
B 280
C 310
D 345
E 403
F 424
G 445
PERCENT TRANSFORMED
TIME, seconds
XBL 745-6442

Fig. 8C

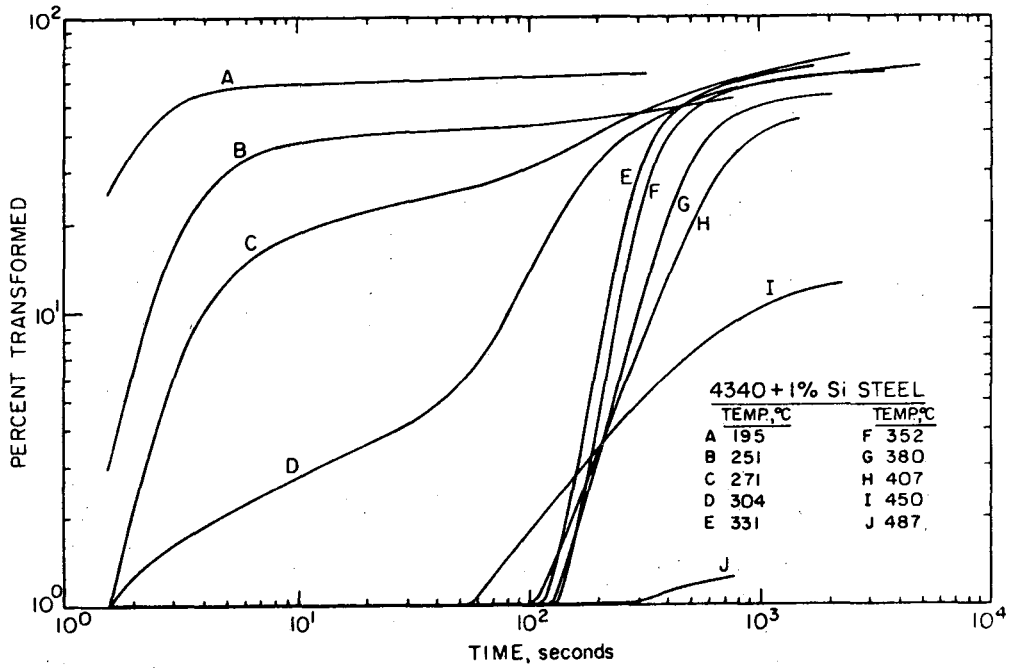

(a)

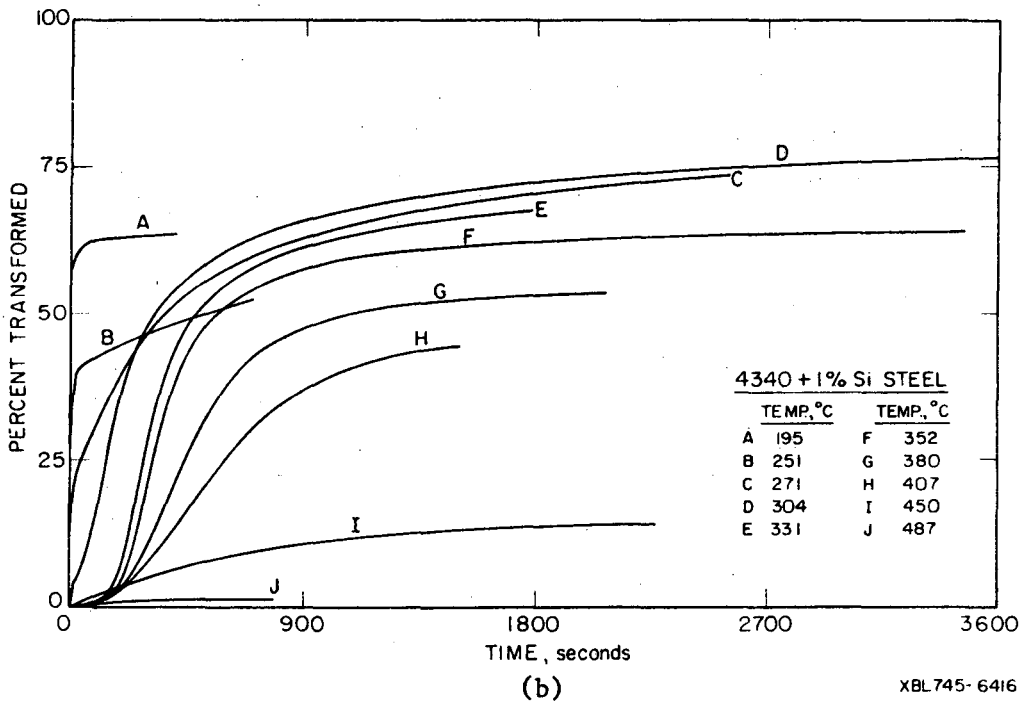

(b)

XBL745-6416

Fig. 8D

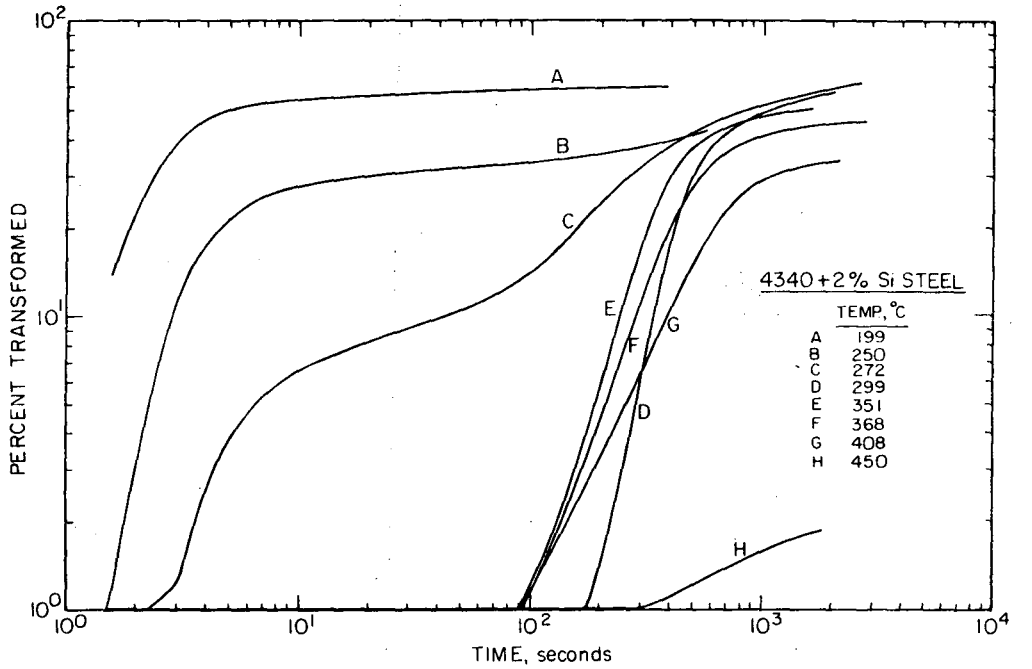
PERCENT TRANSFORMED
TIME, seconds
4340+2% Si STEEL
TEMP, °C
A 199
B 250
C 272
D 299
E 351
F 368
G 408
H 450

(a)

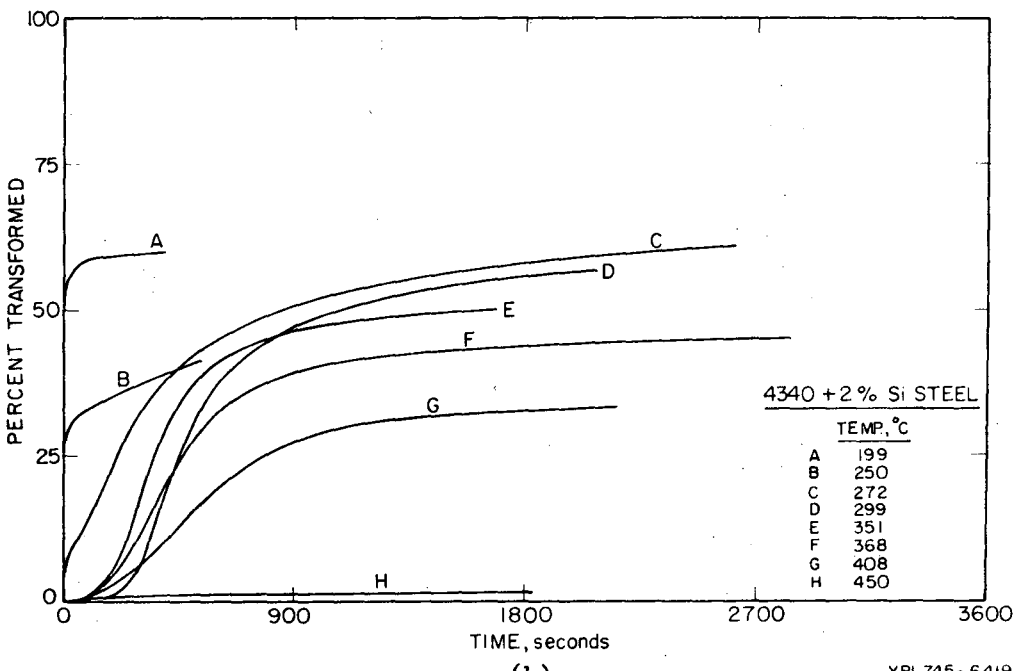
PERCENT TRANSFORMED
TIME, seconds
4340 +2% Si STEEL
TEMP, °C
A 199
B 250
C 272
D 299
E 351
F 368
G 408
H 450
XBL745-6419

(b)

Fig. 8E

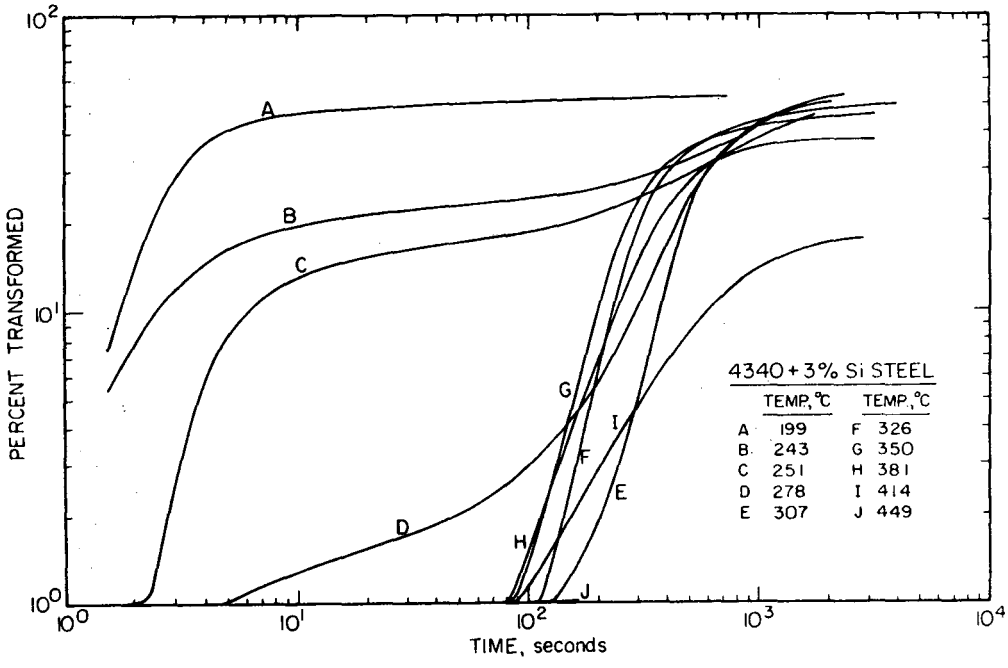
PERCENT TRANSFORMED
TIME, seconds
4340 + 3% Si STEEL
TEMP, °C
TEMP, °C
A 199
B 243
C 251
D 278
E 307
F 326
G 350
H 381
I 414
J 449

(a)

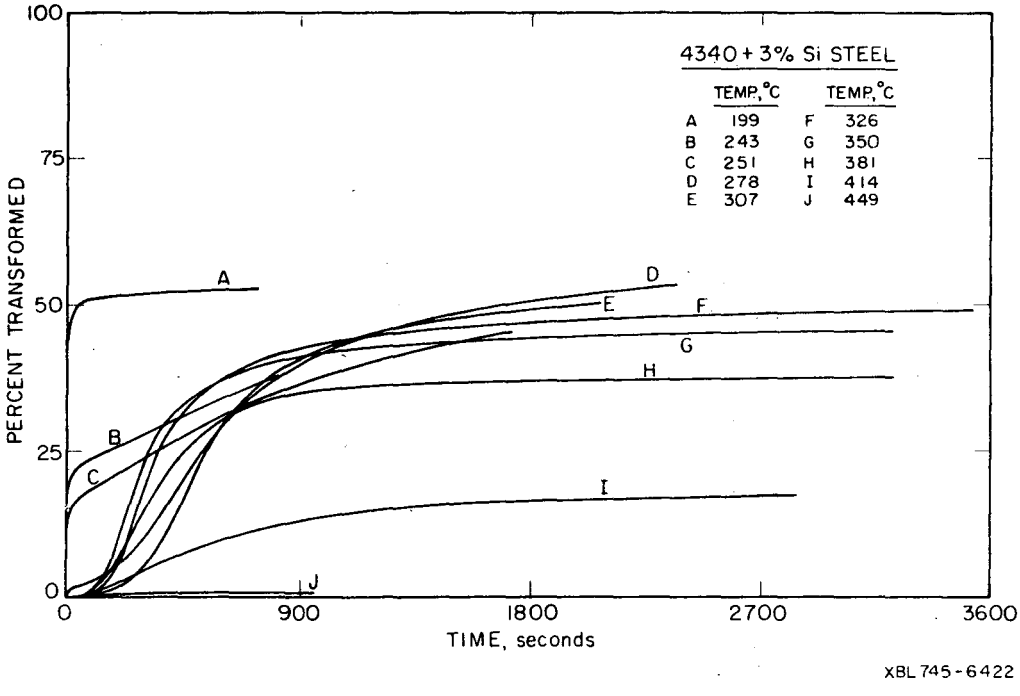
PERCENT TRANSFORMED
TIME, seconds
4340 + 3% Si STEEL
TEMP, °C
TEMP, °C
A 199
B 243
C 251
D 278
E 307
F 326
G 350
H 381
I 414
J 449
XBL 745-6422

(b)

Fig. 8F

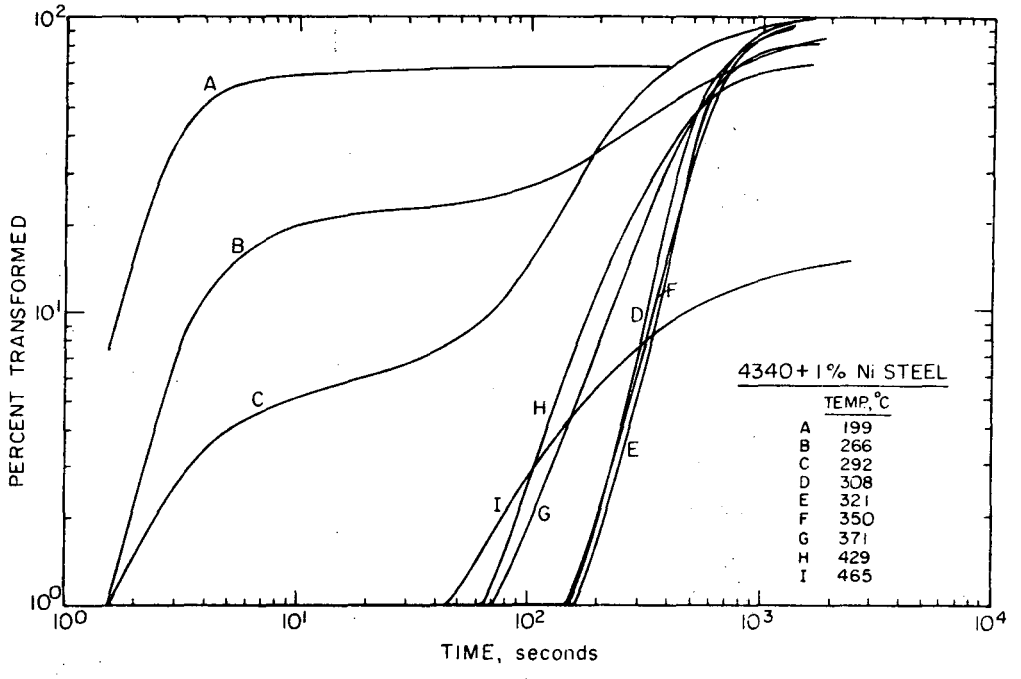
PERCENT TRANSFORMED
TIME, seconds
4340+1% Ni STEEL
TEMP, °C
A 199
B 266
C 292
D 308
E 321
F 350
G 371
H 429
I 465

(a)

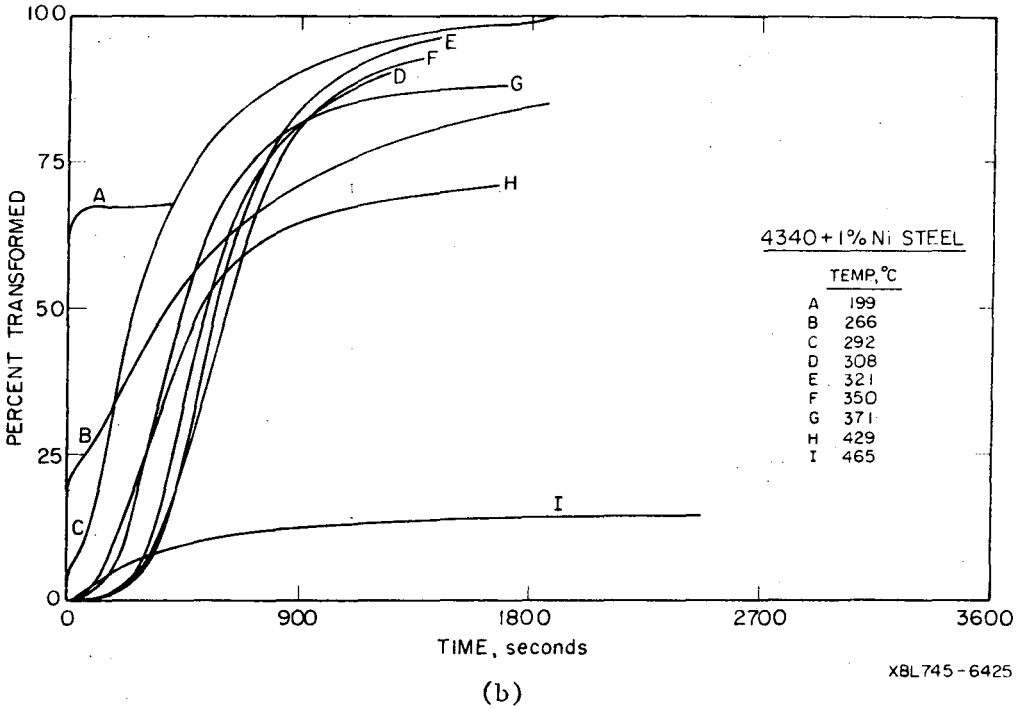
PERCENT TRANSFORMED
TIME, seconds
4340+1% Ni STEEL
TEMP, °C
A 199
B 266
C 292
D 308
E 321
F 350
G 371
H 429
I 465
XBL745-6425

(b)

Fig. 8G

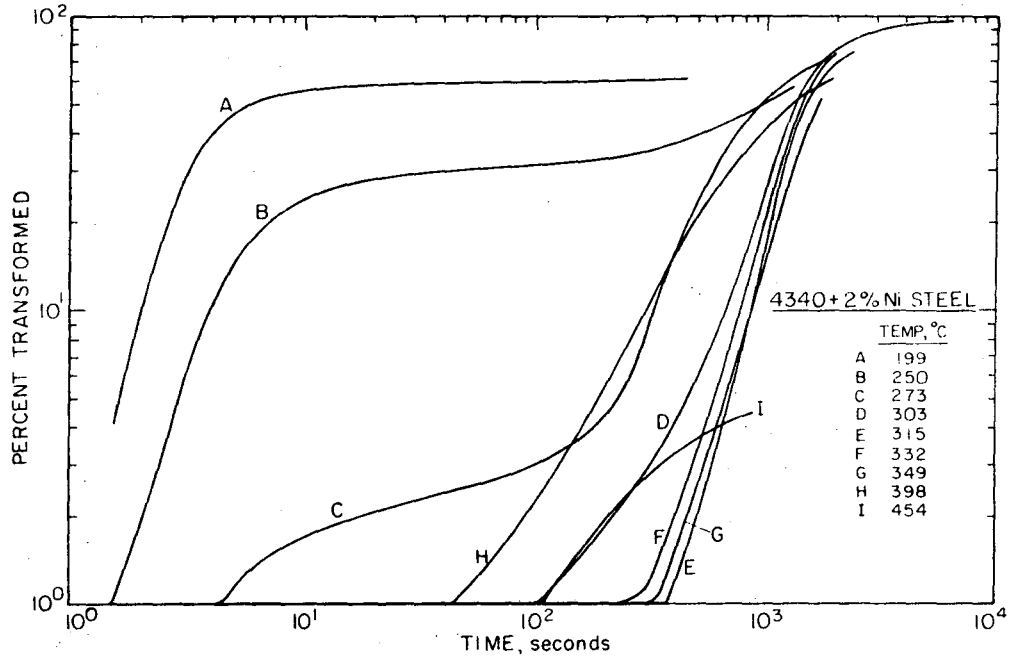
PERCENT TRANSFORMED
TIME, seconds
4340+2%Ni STEEL
TEMP, °C
A 199
B 250
C 273
D 303
E 315
F 332
G 349
H 398
I 454

(a)

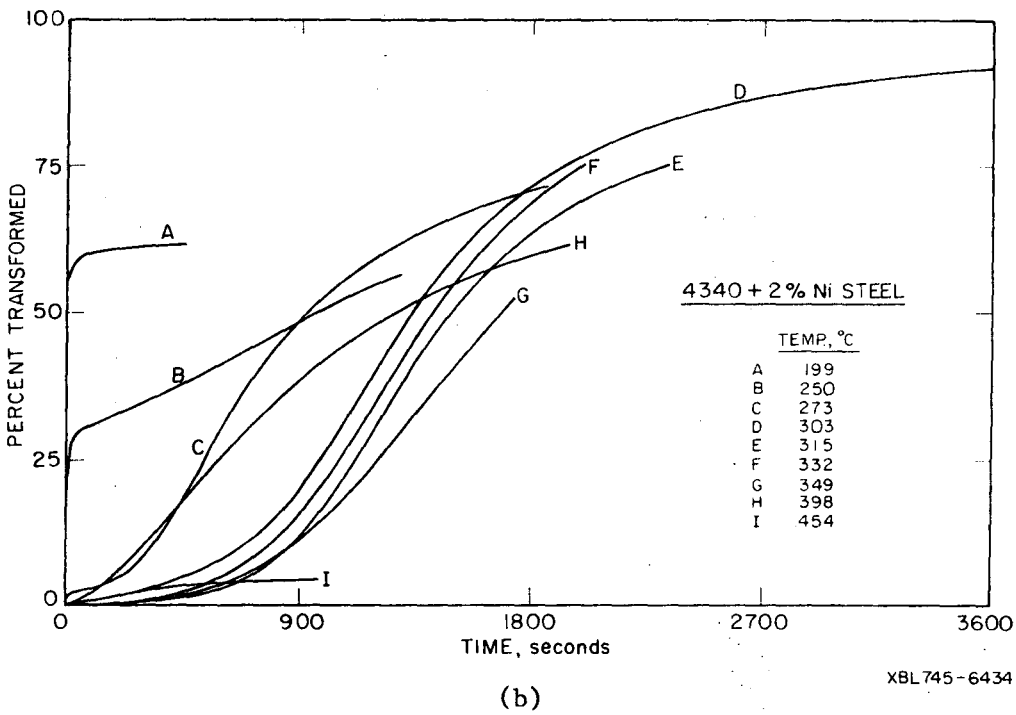
PERCENT TRANSFORMED
TIME, seconds
4340+2% Ni STEEL
TEMP, °C
A 199
B 250
C 273
D 303
E 315
F 332
G 349
H 398
I 454
XBL745-6434

(b)

Fig. 8H

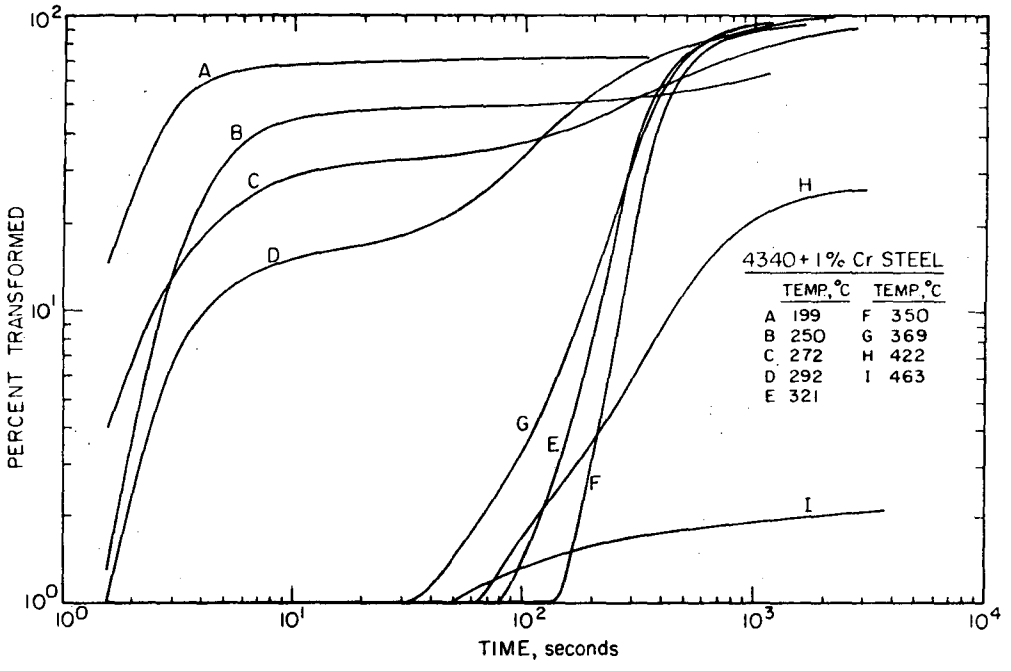
PERCENT TRANSFORMED
TIME, seconds
4340+1% Cr STEEL
TEMP.,°C TEMP.,°C
A 199 F 350
B 250 G 369
C 272 H 422
D 292 I 463
E 321

(a)

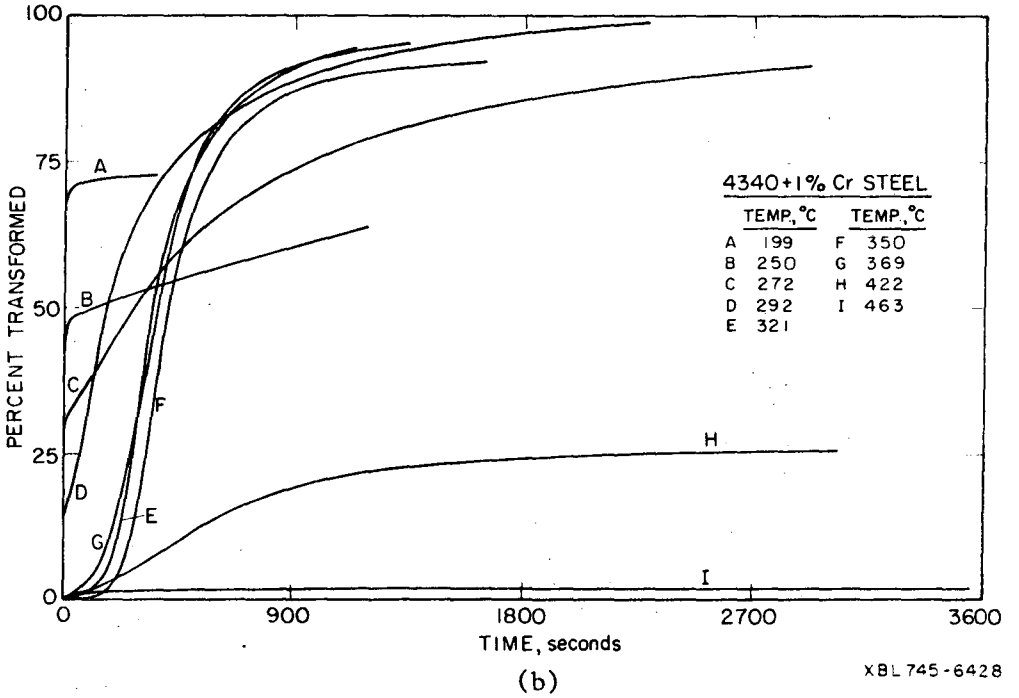
PERCENT TRANSFORMED
TIME, seconds
4340+1% Cr STEEL
TEMP.,°C TEMP.,°C
A 199 F 350
B 250 G 369
C 272 H 422
D 292 I 463
E 321
XBL 745-6428

(b)

Fig. 81

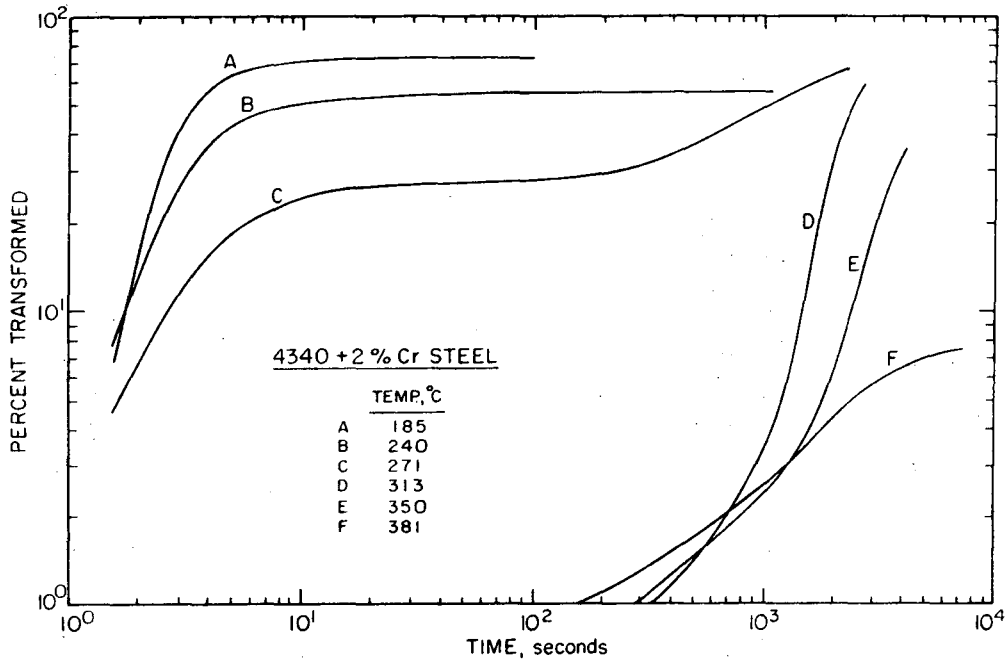
PERCENT TRANSFORMED
TIME, seconds
4340 + 2 % Cr STEEL
TEMP, °C
A 185
B 240
C 271
D 313
E 350
F 381

(a)

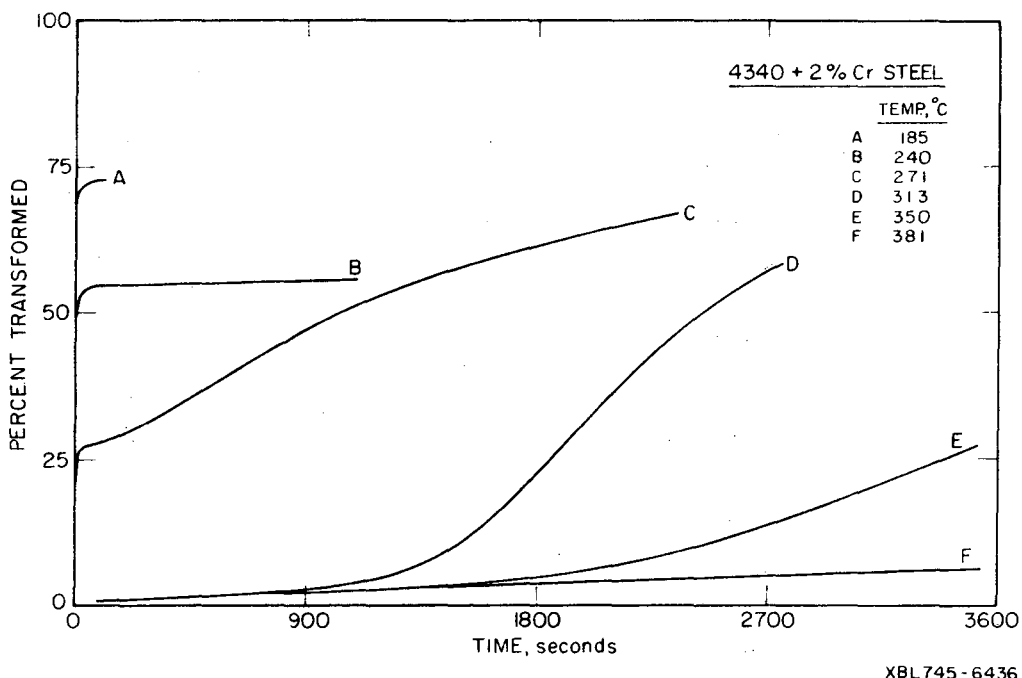
PERCENT TRANSFORMED
TIME, seconds
4340 + 2 % Cr STEEL
TEMP, °C
A 185
B 240
C 271
D 313
E 350
F 381
XBL745-6436

(b)

Fig. 8J

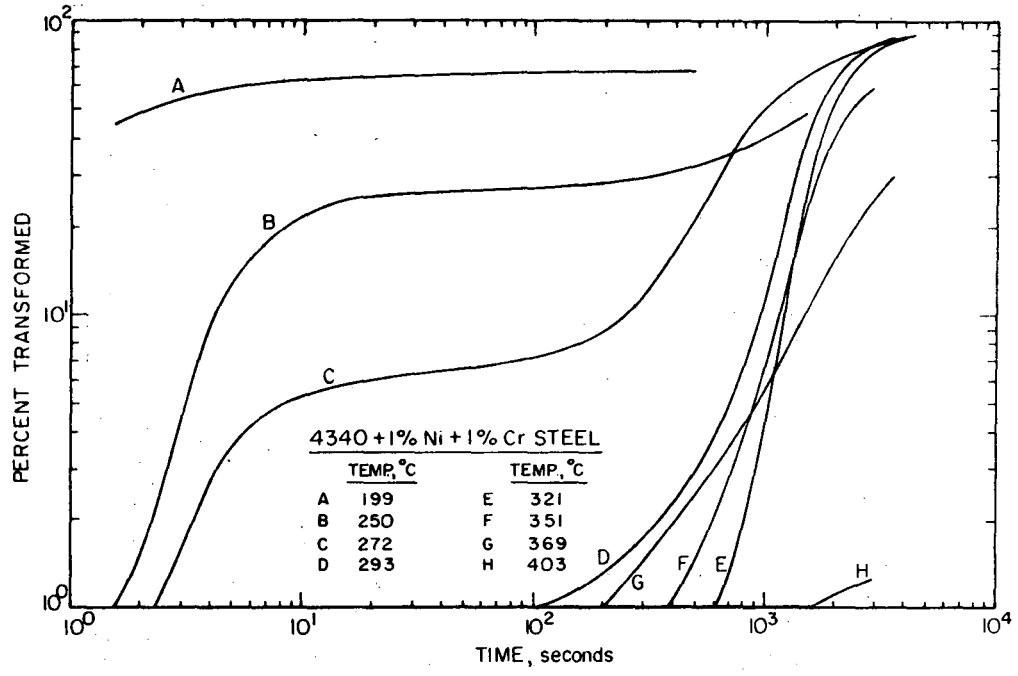
4340 + 1% Ni + 1% Cr STEEL
TEMP, °C
A 199
B 250
C 272
D 293
TEMP, °C
E 321
F 351
G 369
H 403
PERCENT TRANSFORMED
TIME, seconds

(a)

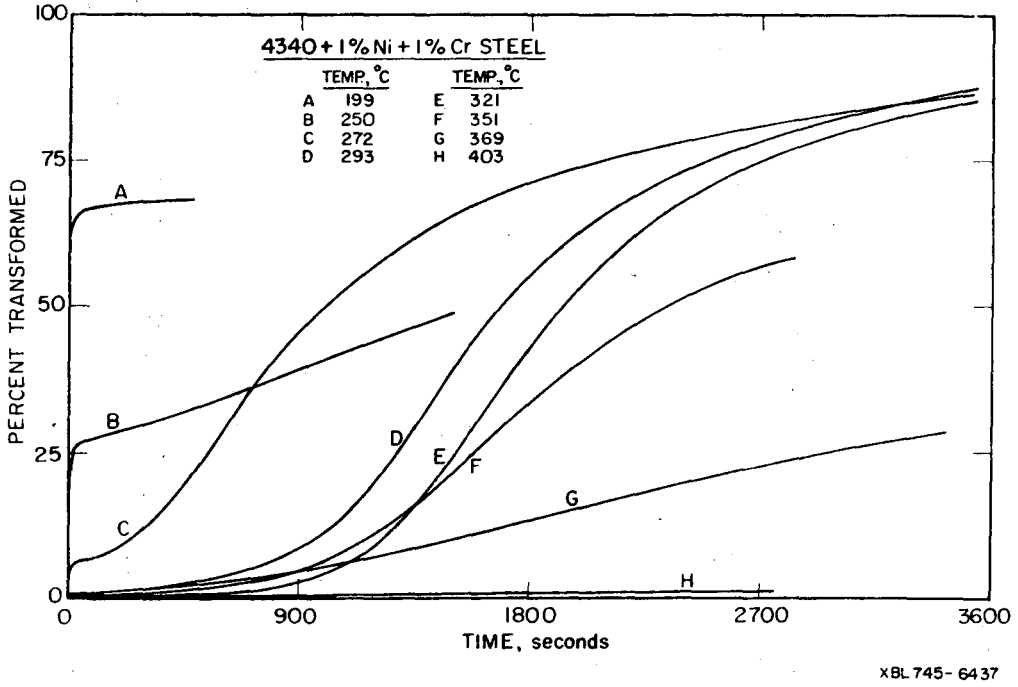
4340 + 1% Ni + 1% Cr STEEL
TEMP, °C
A 199
B 250
C 272
D 293
TEMP, °C
E 321
F 351
G 369
H 403
PERCENT TRANSFORMED
TIME, seconds
XBL 745-6437

(b)

Fig. 8K

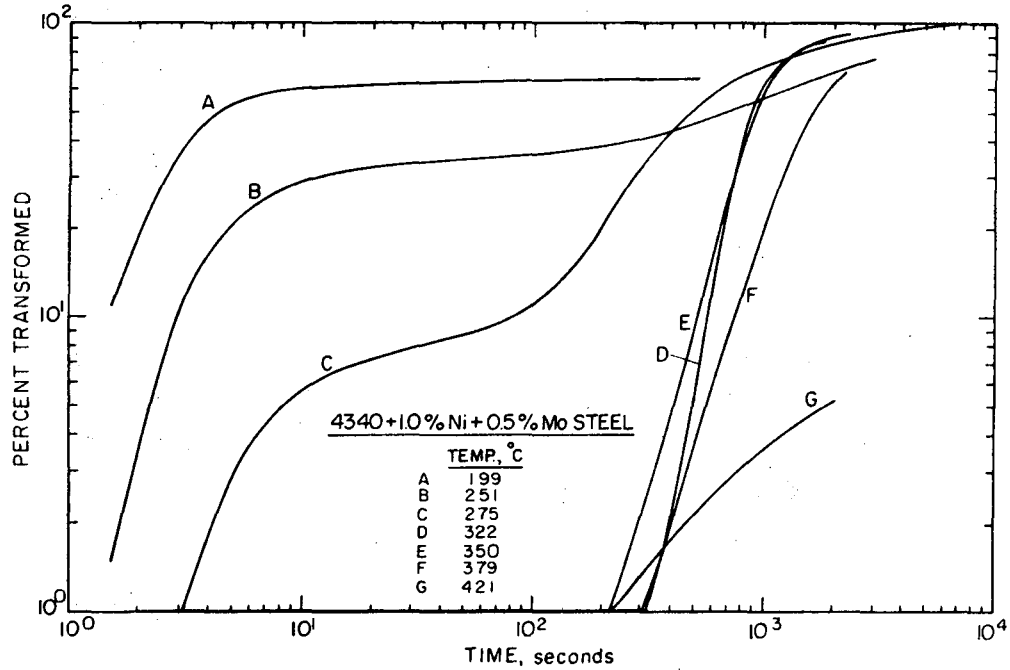
PERCENT TRANSFORMED
TIME, seconds
4340+1.0% Ni+0.5% Mo STEEL
TEMP, °C
A 199
B 251
C 275
D 322
E 350
F 379
G 421

(a)

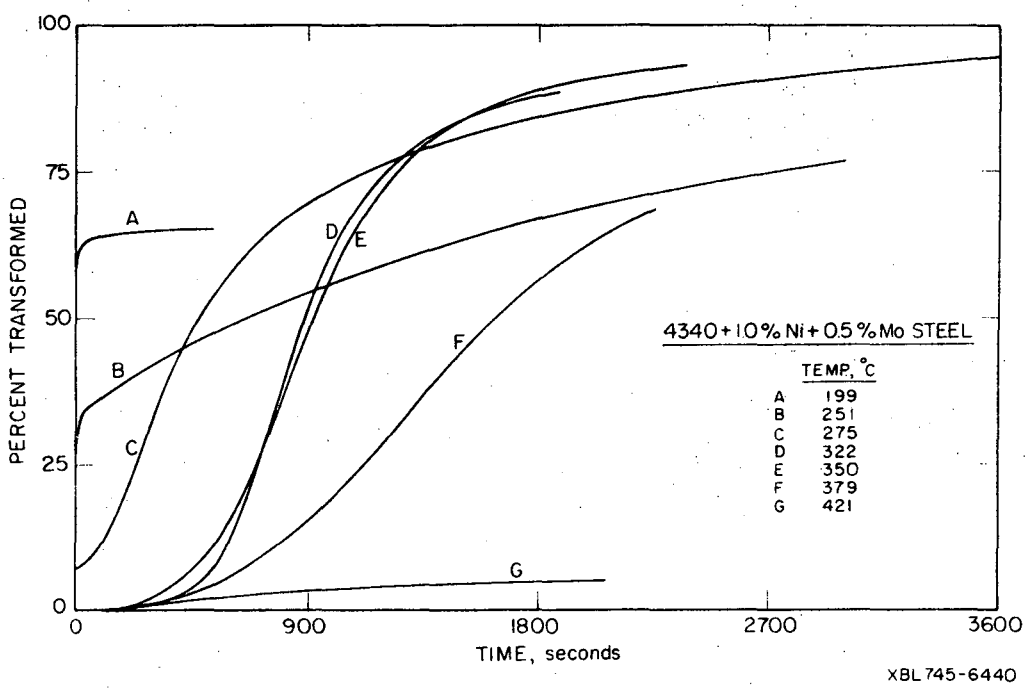
PERCENT TRANSFORMED
TIME, seconds
4340+1.0% Ni+0.5% Mo STEEL
TEMP, °C
A 199
B 251
C 275
D 322
E 350
F 379
G 421
XBL 745-6440

(b)

Fig. 8L

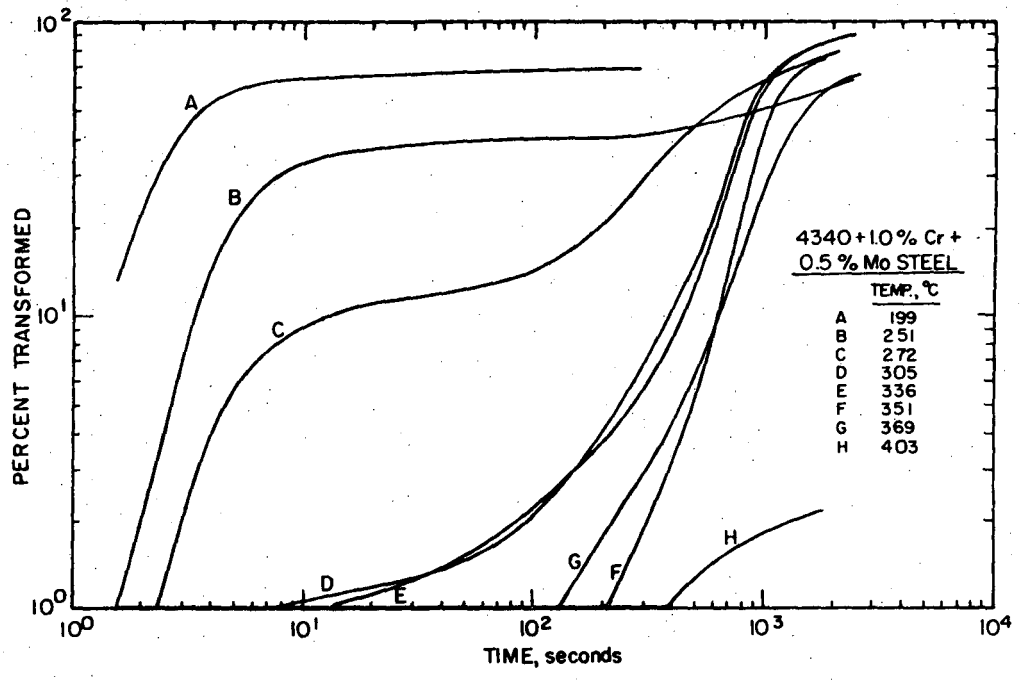
PERCENT TRANSFORMED
TIME, seconds
4340+1.0% Cr+
0.5% Mo STEEL
TEMP., °C
A 199
B 251
C 272
D 305
E 336
F 351
G 369
H 403

(a)

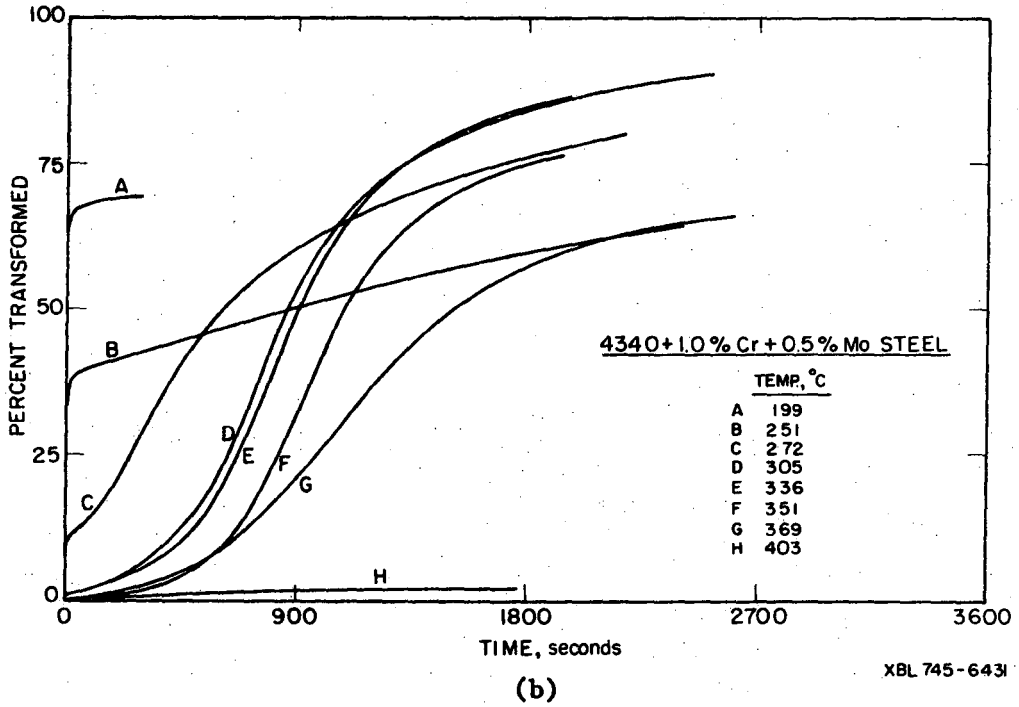
PERCENT TRANSFORMED
TIME, seconds
4340+1.0% Cr+0.5% Mo STEEL
TEMP., °C
A 199
B 251
C 272
D 305
E 336
F 351
G 369
H 403
XBL 745-6431

(b)

Fig. 8M

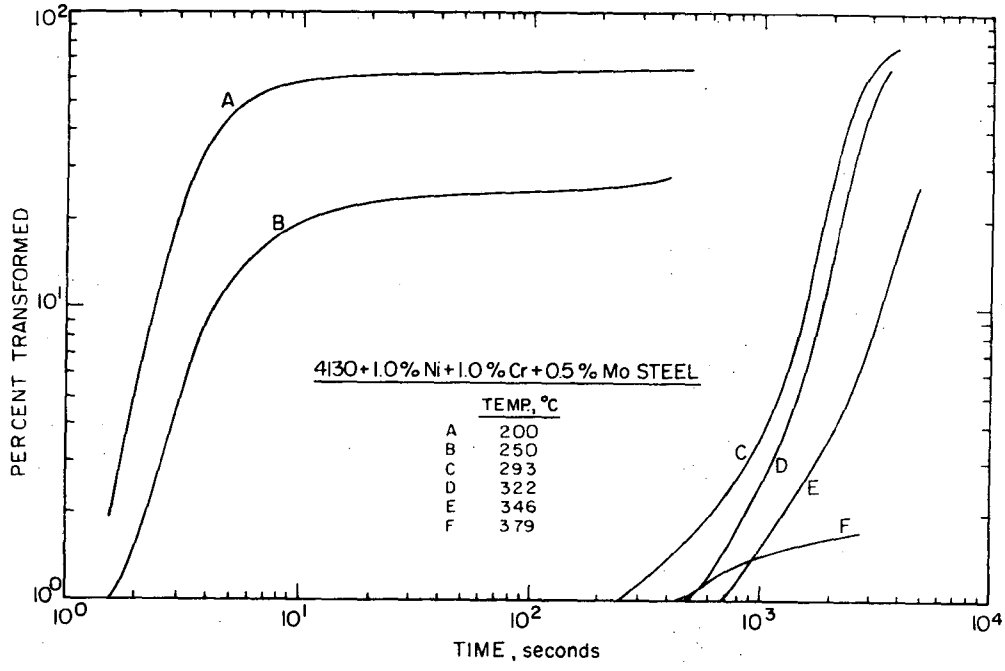
PERCENT TRANSFORMED
TIME, seconds
4130+1.0% Ni+1.0% Cr+0.5% Mo STEEL
TEMP, °C
A 200
B 250
C 293
D 322
E 346
F 379

(a)

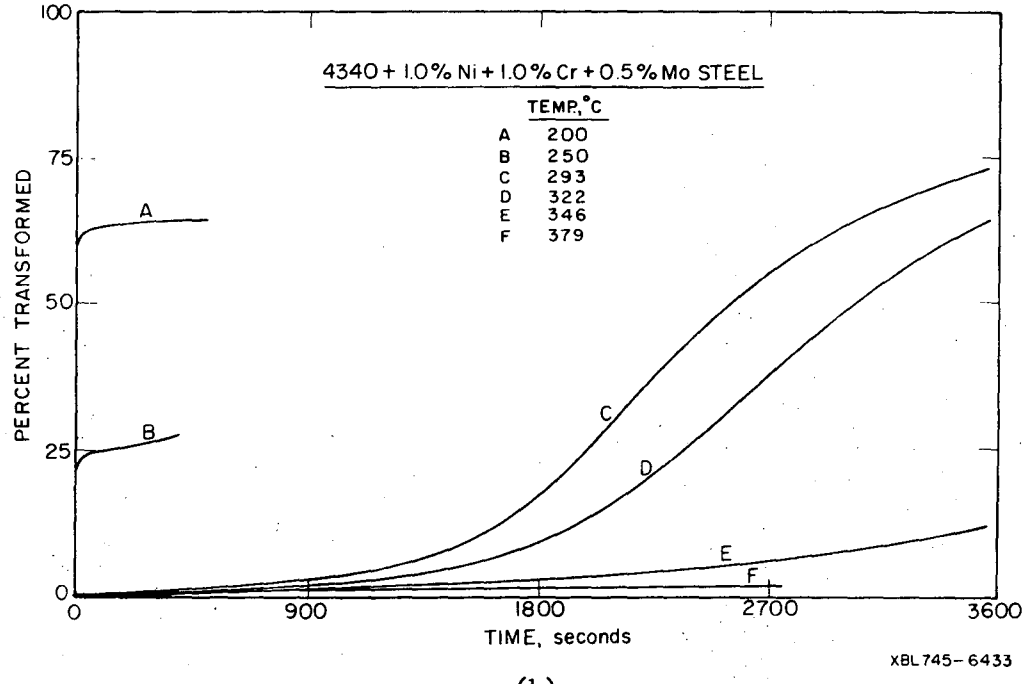
PERCENT TRANSFORMED
TIME, seconds
4340+1.0% Ni+1.0% Cr+0.5% Mo STEEL
TEMP, °C
A 200
B 250
C 293
D 322
E 346
F 379
XBL745-6433

(b)

Fig. 8N

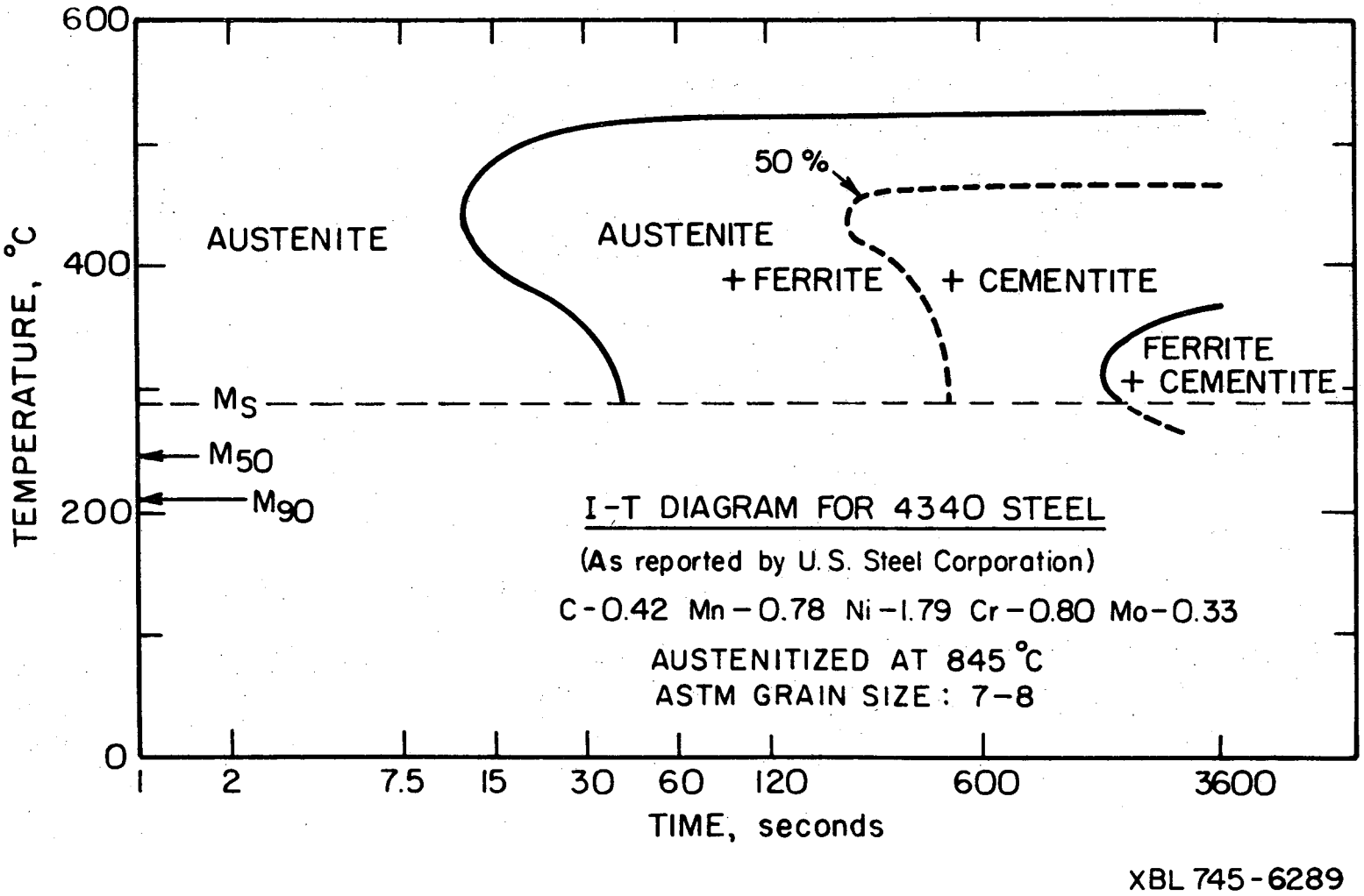
600
400
200
0
TEMPERATURE, °C
AUSTENITE
50 %
AUSTENITE
+ FERRITE
+ CEMENTITE
FERRITE
+ CEMENTITE
Ms
M50
M90
I-T DIAGRAM FOR 4340 STEEL
(As reported by U.S. Steel Corporation)
C-0.42 Mn-0.78 Ni-1.79 Cr-0.80 Mo-0.33
AUSTENITIZED AT 845 °C
ASTM GRAIN SIZE: 7-8
1
2
7.5
15
30
60
120
600
3600
TIME, seconds
XBL 745-6289

Fig. 9

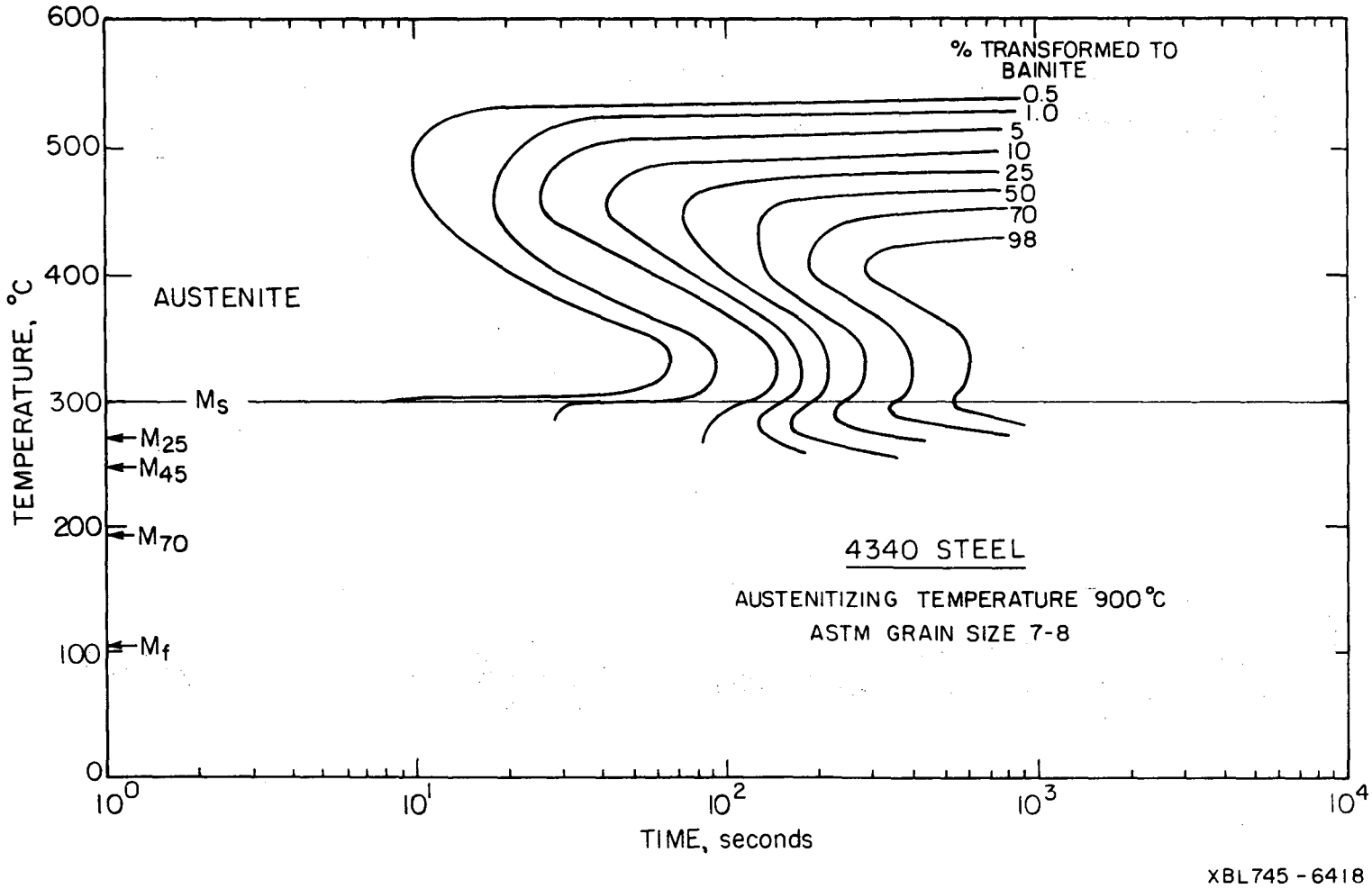
600
500
400
300
200
100
0
TEMPERATURE, °C
% TRANSFORMED TO BAINITE
0.5
1.0
5
10
25
50
70
98
AUSTENITE
M_S
M_{25}
M_{45}
M_{70}
M_f
4340 STEEL
AUSTENITIZING TEMPERATURE 900°C
ASTM GRAIN SIZE 7-8
10^0
10^1
10^2
10^3
10^4
TIME, seconds
XBL745-6418

Fig. 10

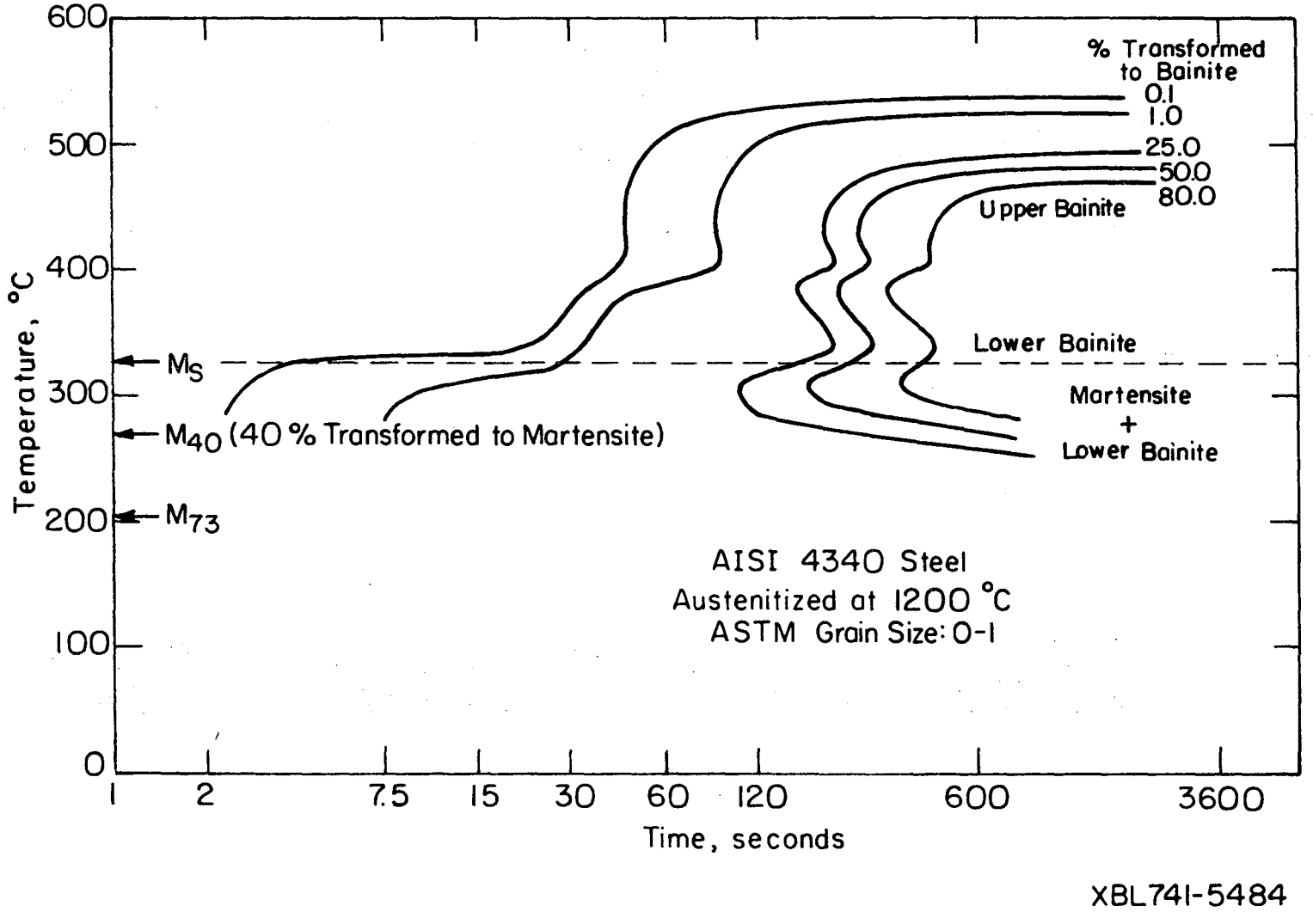
600
500
400
300
200
100
0
Temperature, °C
% Transformed to Bainite
0.1
1.0
25.0
50.0
80.0
Upper Bainite
Lower Bainite
Martensite + Lower Bainite
M_S
M_{40} (40 % Transformed to Martensite)
M_{73}
AISI 4340 Steel
Austenitized at 1200 °C
ASTM Grain Size: 0-1
1
2
7.5
15
30
60
120
600
3600
Time, seconds
XBL741-5484

Fig. 11

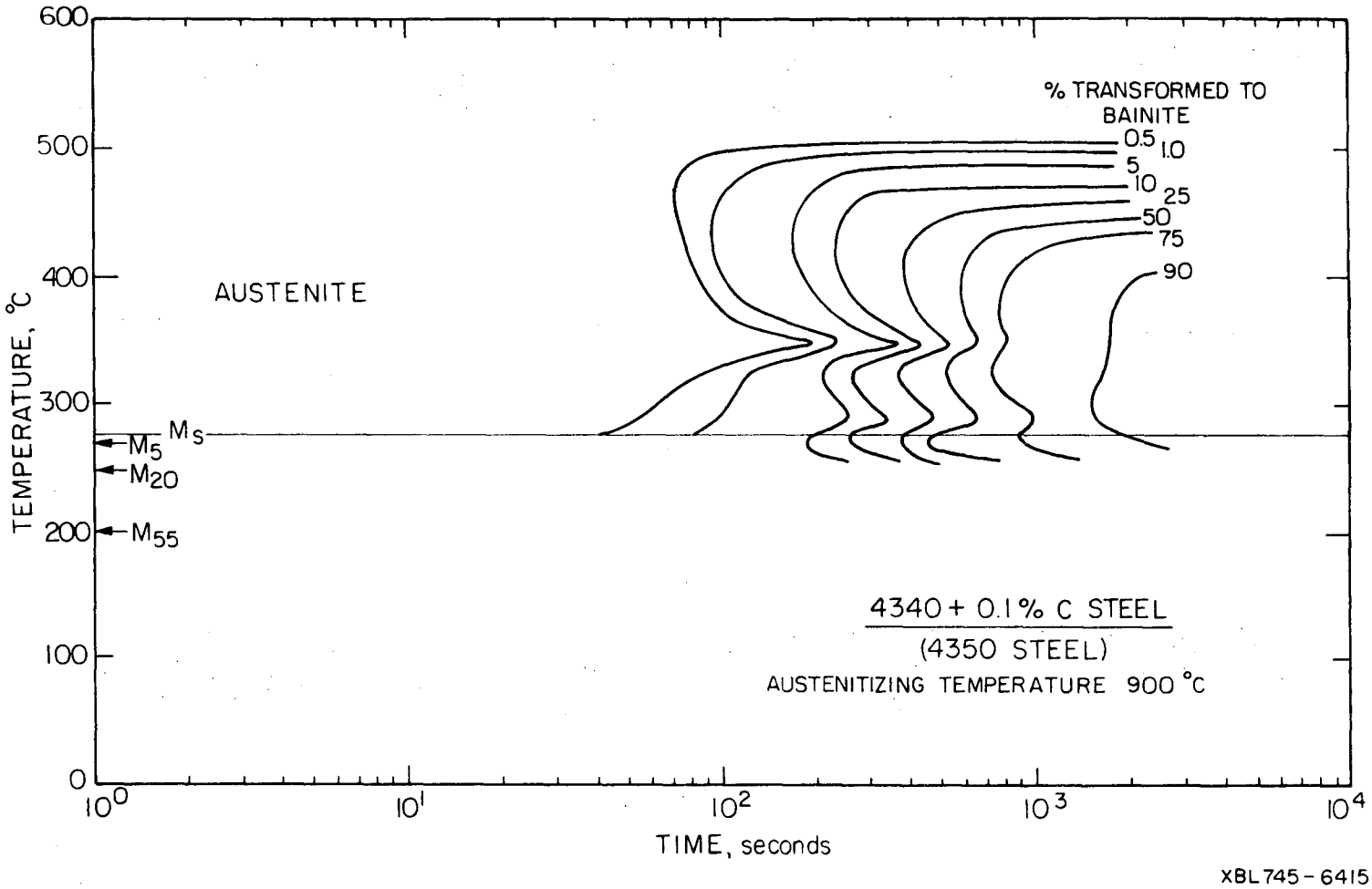
600
500
400
300
200
100
0
TEMPERATURE, °C
AUSTENITE
% TRANSFORMED TO
BAINITE
0.5
1.0
5
10
25
50
75
90
M_S
M_5
M_{20}
M_{55}
4340 + 0.1% C STEEL
(4350 STEEL)
AUSTENITIZING TEMPERATURE 900 °C
10^0
10^1
10^2
10^3
10^4
TIME, seconds
XBL745-6415

Fig. 12A

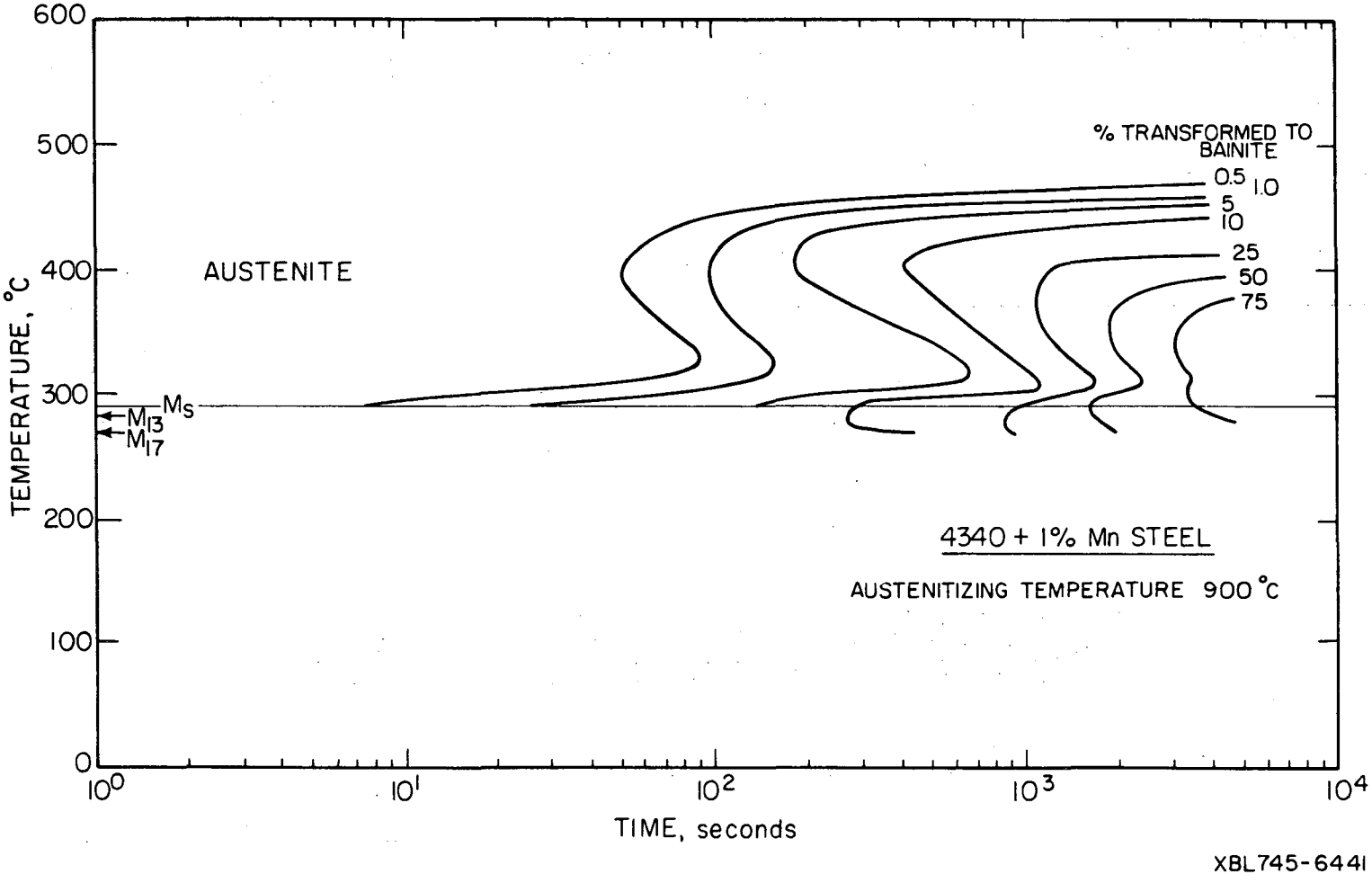
600
500
400
300
200
100
0
TEMPERATURE, °C
AUSTENITE
% TRANSFORMED TO BAINITE
0.5
1.0
5
10
25
50
75
Ms
M13
M17
4340 + 1% Mn STEEL
AUSTENITIZING TEMPERATURE 900 °C
10^0
10^1
10^2
10^3
10^4
TIME, seconds
XBL745-6441

Fig. 12B

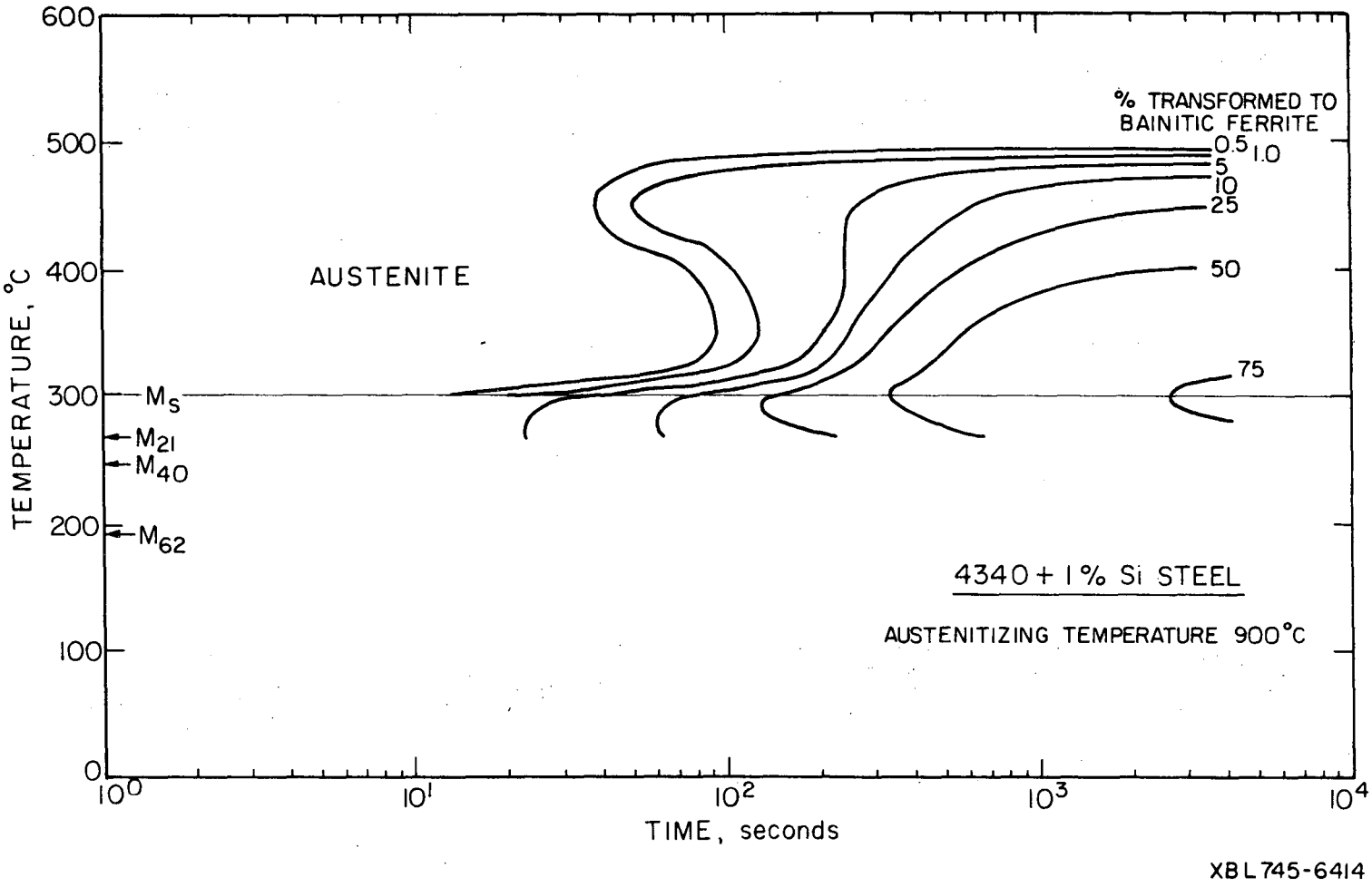
600
500
400
300
200
100
0
TEMPERATURE, °C
AUSTENITE
% TRANSFORMED TO
BAINITIC FERRITE
0.5
1.0
5
10
25
50
75
M_S
M_{21}
M_{40}
M_{62}
4340 + 1% Si STEEL
AUSTENITIZING TEMPERATURE 900°C
10^0
10^1
10^2
10^3
10^4
TIME, seconds
XBL745-6414

Fig. 12C

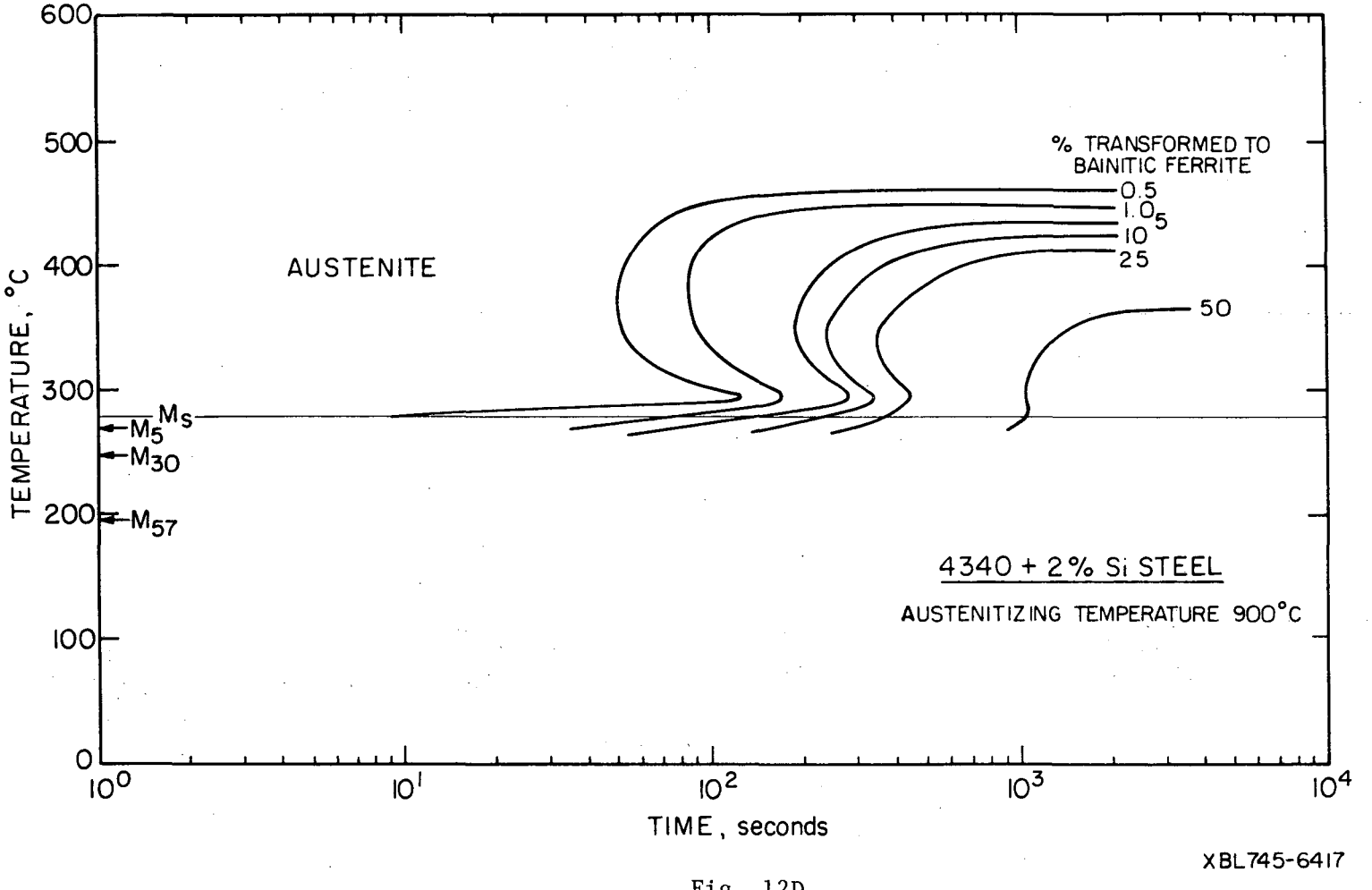
600
500
400
300
200
100
0
TEMPERATURE, °C
AUSTENITE
% TRANSFORMED TO
BAINITIC FERRITE
0.5
1.0
5
10
25
50
Ms
M5
M30
M57
4340 + 2% Si STEEL
AUSTENITIZING TEMPERATURE 900°C
10^0
10^1
10^2
10^3
10^4
TIME, seconds
XBL745-6417

Fig. 12D

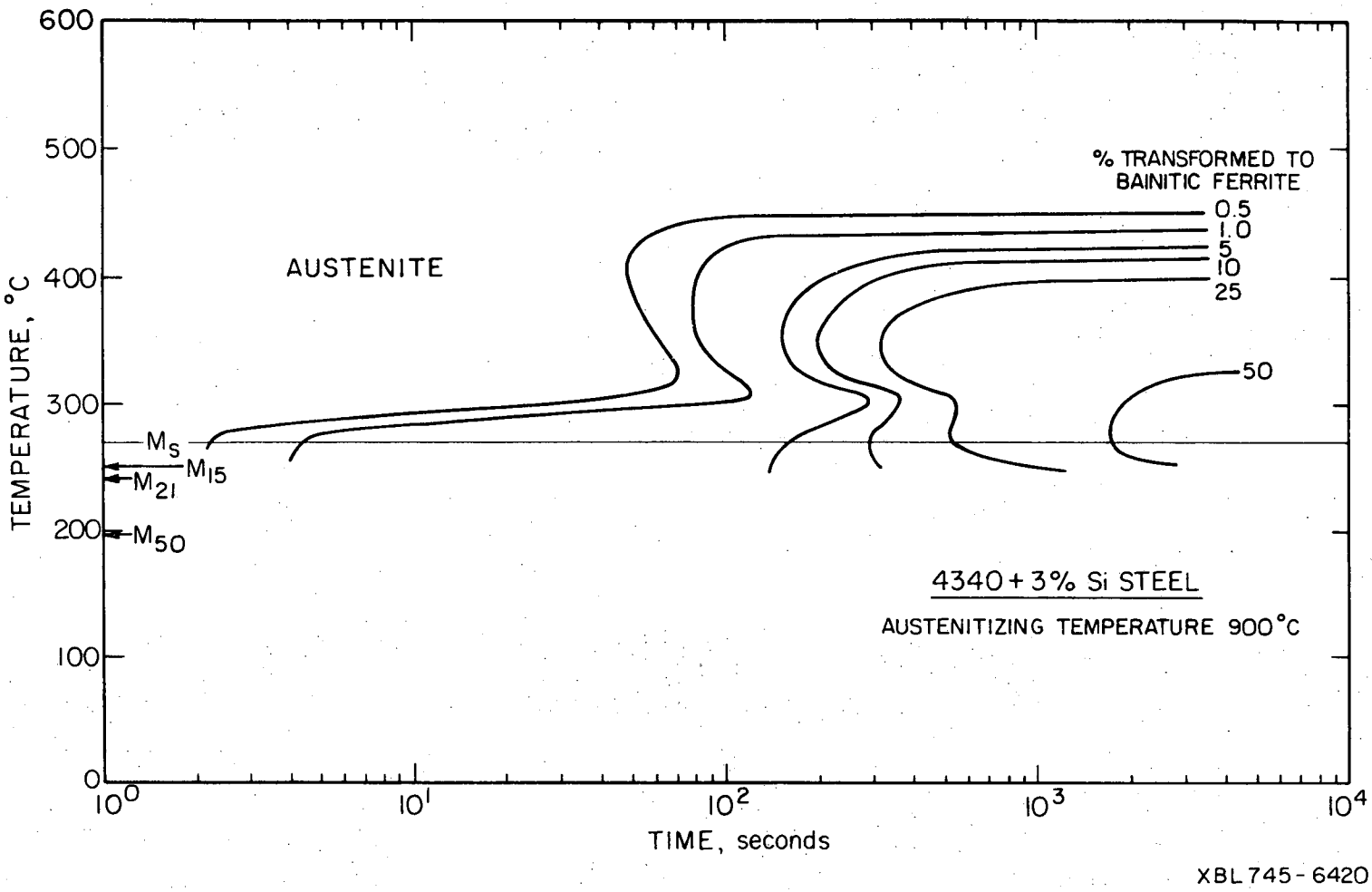
600
500
400
300
200
100
0
TEMPERATURE, °C
AUSTENITE
% TRANSFORMED TO
BAINITIC FERRITE
0.5
1.0
5
10
25
50
M_S
M_{15}
M_{21}
M_{50}
4340 + 3% Si STEEL
AUSTENITIZING TEMPERATURE 900°C
10^0
10^1
10^2
10^3
10^4
TIME, seconds
XBL 745-6420

Fig. 12E

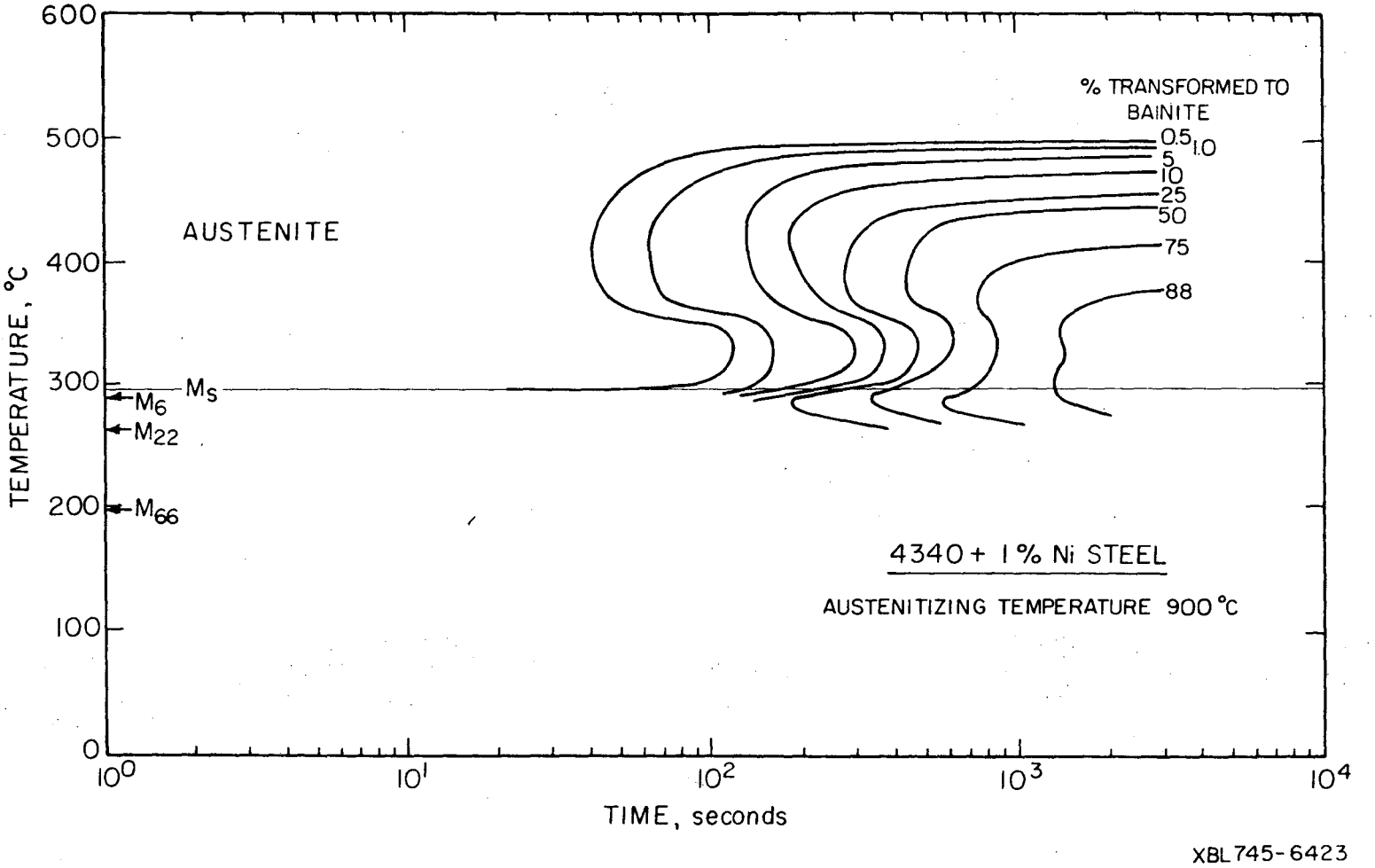
600
500
400
300
200
100
0
TEMPERATURE, °C
AUSTENITE
% TRANSFORMED TO BAINITE
0.5
1.0
5
10
25
50
75
88
Ms
M6
M22
M66
4340 + 1% Ni STEEL
AUSTENITIZING TEMPERATURE 900°C
10^0
10^1
10^2
10^3
10^4
TIME, seconds
XBL745-6423

Fig. 12F

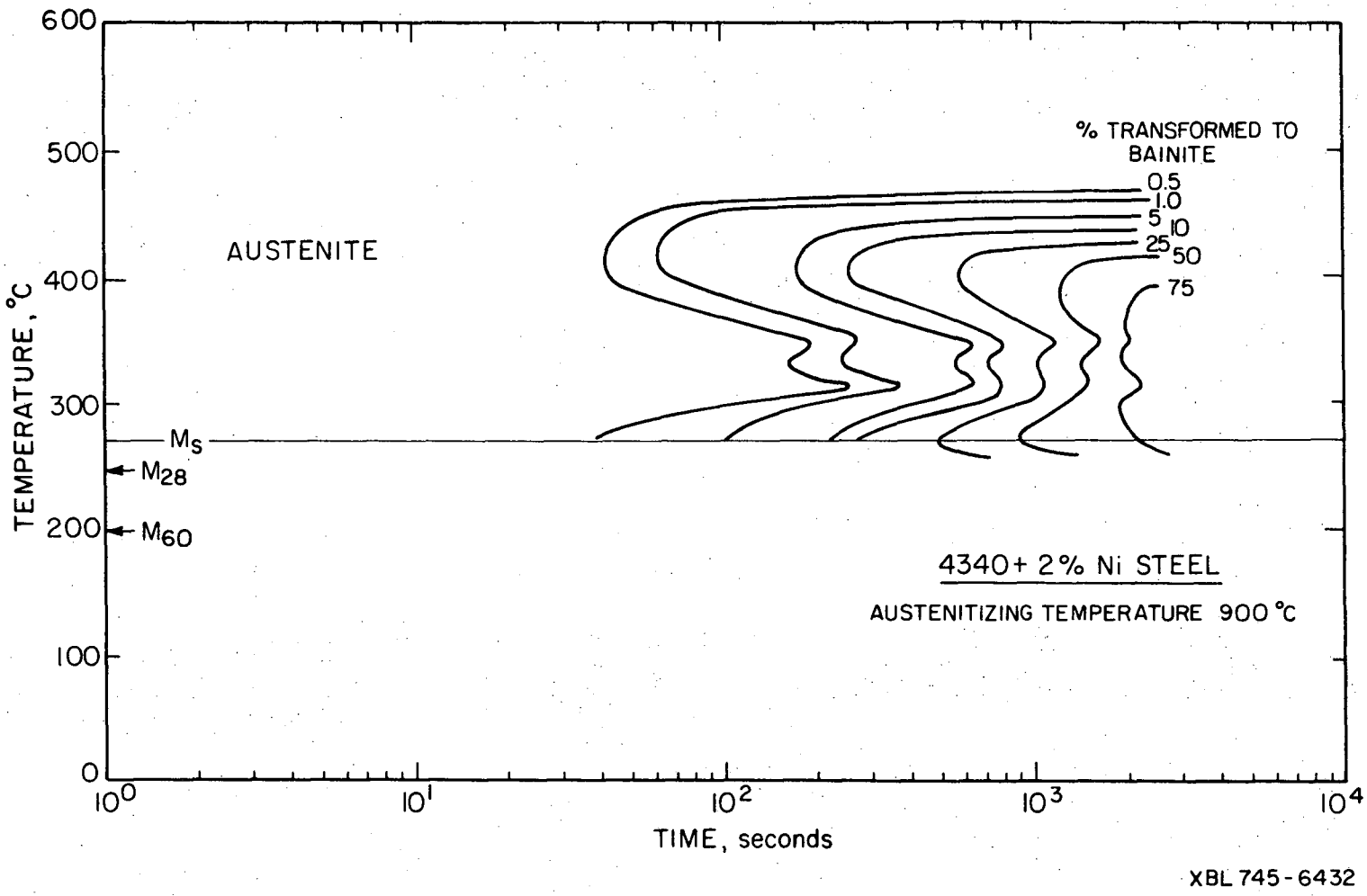
600
500
400
300
200
100
0
TEMPERATURE, °C
AUSTENITE
% TRANSFORMED TO BAINITE
0.5
1.0
5
10
25
50
75
M_S
M_{28}
M_{60}
4340+ 2% Ni STEEL
AUSTENITIZING TEMPERATURE 900 °C
10^0
10^1
10^2
10^3
10^4
TIME, seconds
XBL 745-6432

Fig. 12G

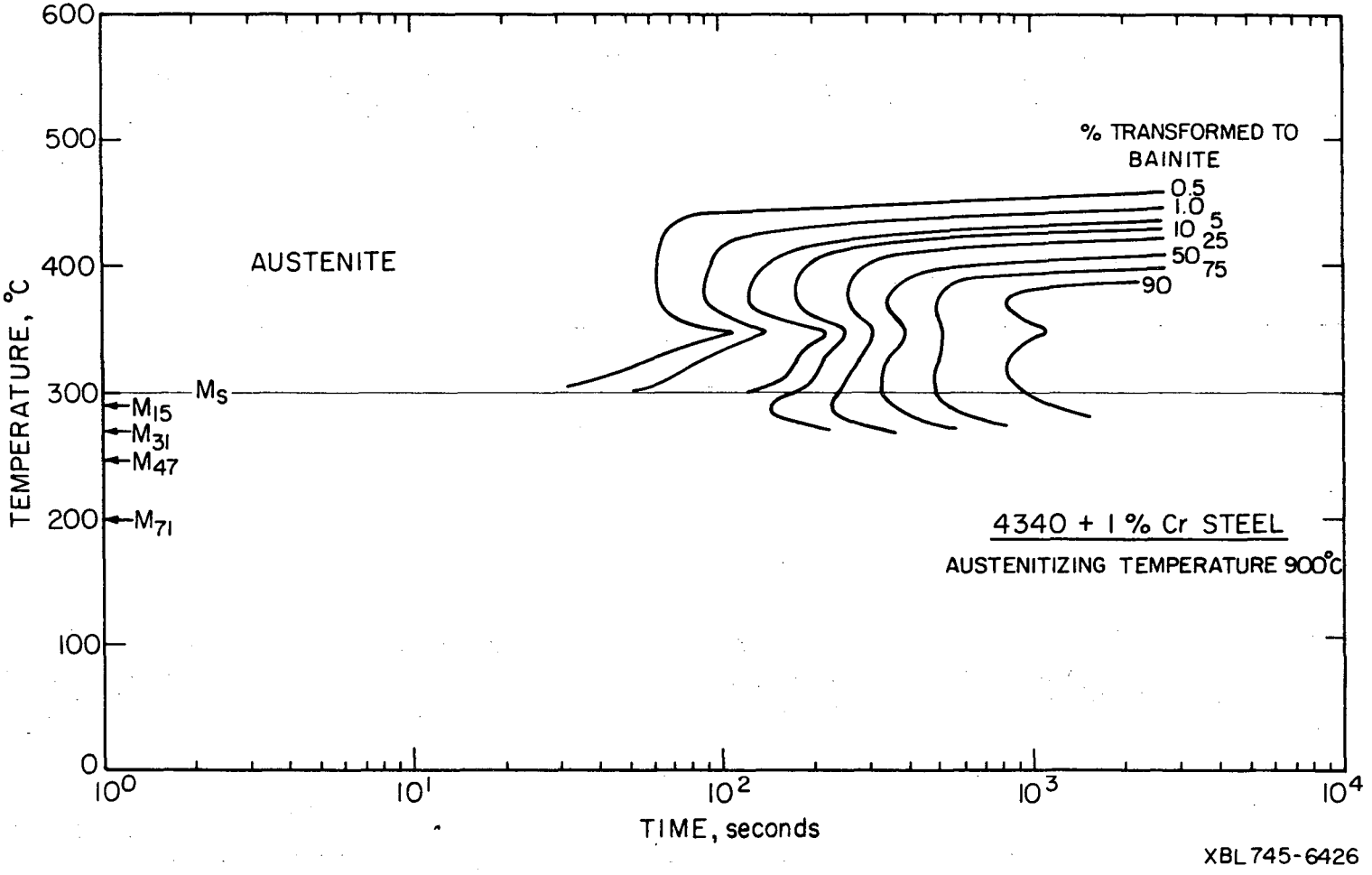
600
500
400
300
200
100
0
TEMPERATURE, °C
AUSTENITE
% TRANSFORMED TO
BAINITE
0.5
1.0
10
5
25
50
75
90
M_S
M_{15}
M_{31}
M_{47}
M_{71}
4340 + 1 % Cr STEEL
AUSTENITIZING TEMPERATURE 900°C
10^0
10^1
10^2
10^3
10^4
TIME, seconds
XBL745-6426

Fig. 12H

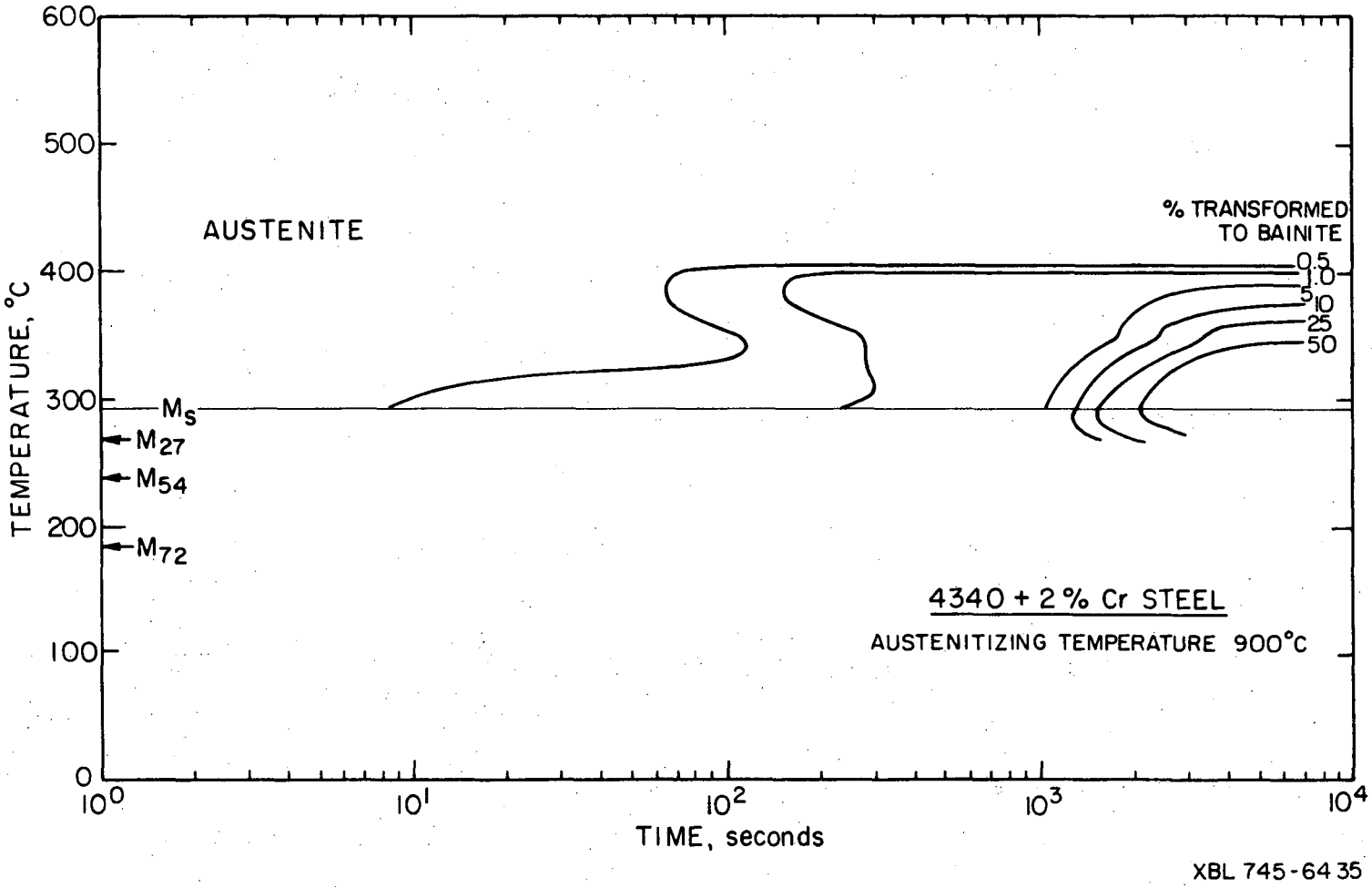
600
500
400
300
200
100
0
AUSTENITE
% TRANSFORMED TO BAINITE
0.5
1.0
5
10
25
50
M_S
M_{27}
M_{54}
M_{72}
4340 + 2 % Cr STEEL
AUSTENITIZING TEMPERATURE 900°C
TEMPERATURE, °C
10^0
10^1
10^2
10^3
10^4
TIME, seconds
XBL 745-6435

Fig. 12I

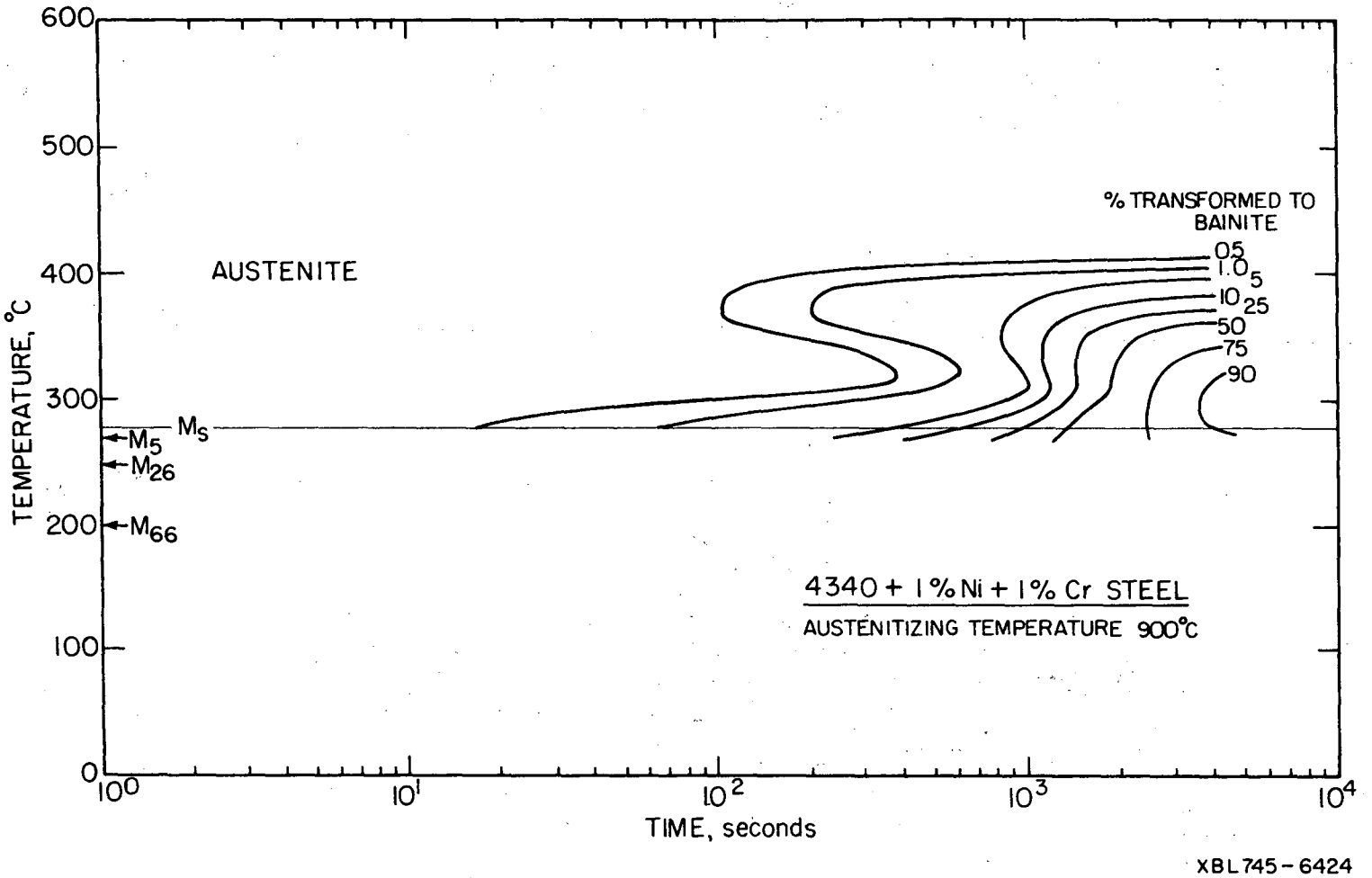
600
500
400
300
200
100
0
TEMPERATURE, °C
AUSTENITE
% TRANSFORMED TO BAINITE
05
1.0 5
10 25
50
75
90
Ms
M5
M26
M66
4340 + 1% Ni + 1% Cr STEEL
AUSTENITIZING TEMPERATURE 900°C
10^0
10^1
10^2
10^3
10^4
TIME, seconds
XBL745-6424

Fig. 12J

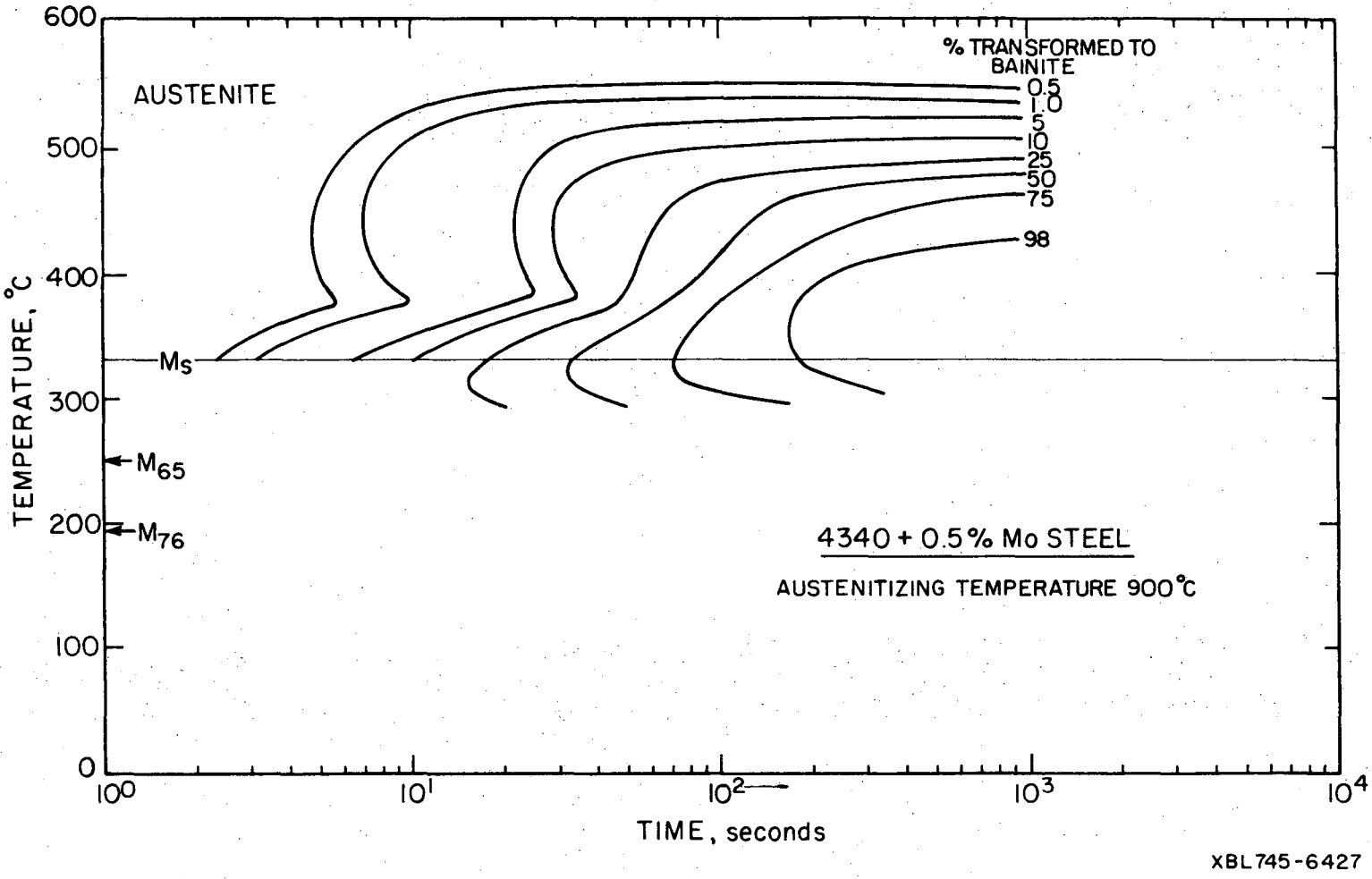
600
500
400
300
200
100
0
TEMPERATURE, °C
AUSTENITE
% TRANSFORMED TO BAINITE
0.5
1.0
5
10
25
50
75
98
M_S
M_{65}
M_{76}
4340 + 0.5% Mo STEEL
AUSTENITIZING TEMPERATURE 900°C
10^0
10^1
10^2
10^3
10^4
TIME, seconds
XBL745-6427

Fig. 12K

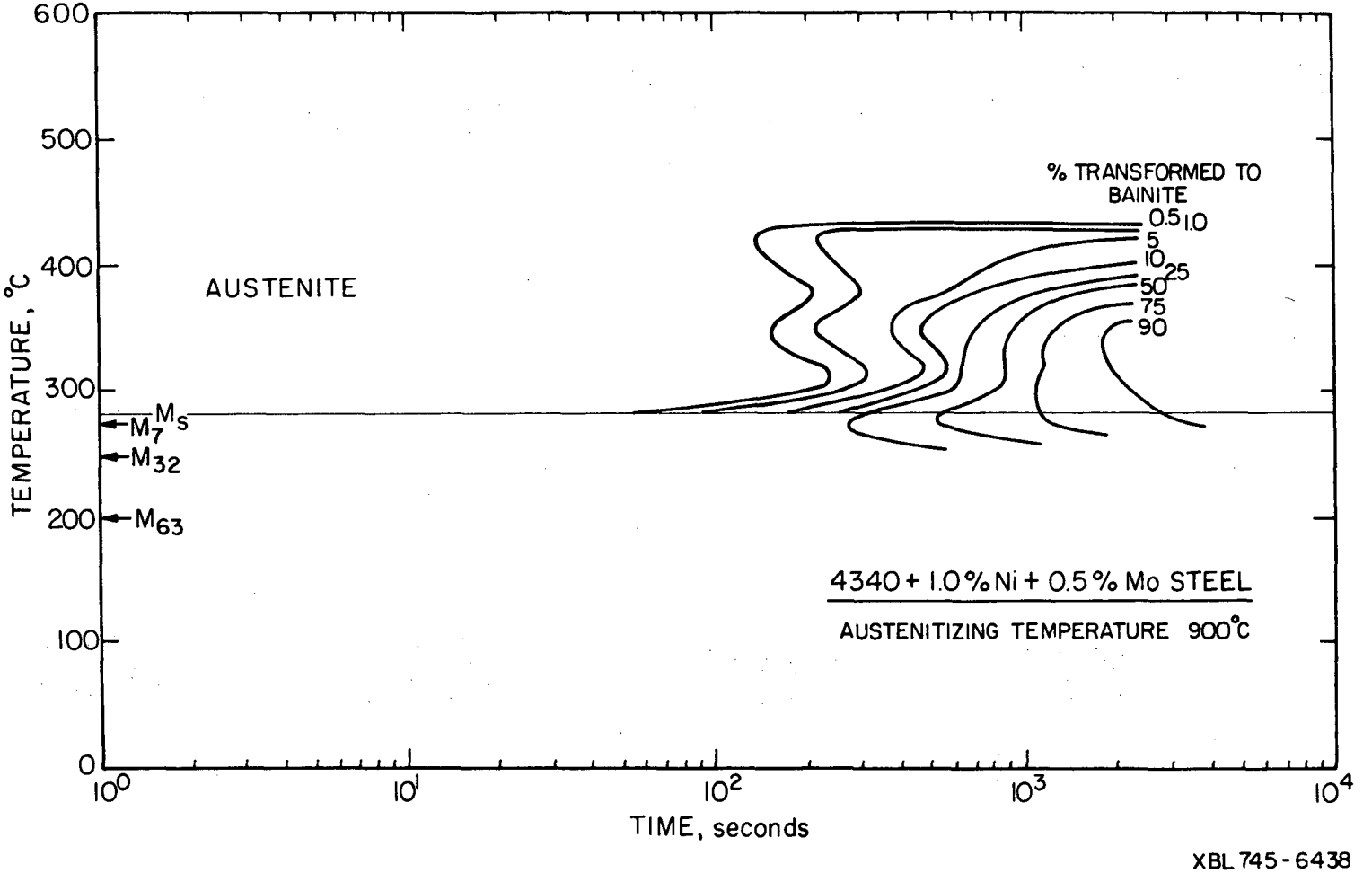
600
500
400
300
200
100
0
TEMPERATURE, °C
AUSTENITE
% TRANSFORMED TO BAINITE
0.5
1.0
5
10
25
50
75
90
M_S
M_7
M_{32}
M_{63}
4340 + 1.0% Ni + 0.5% Mo STEEL
AUSTENITIZING TEMPERATURE 900°C
10^0
10^1
10^2
10^3
10^4
TIME, seconds
XBL 745-6438

Fig. 12L

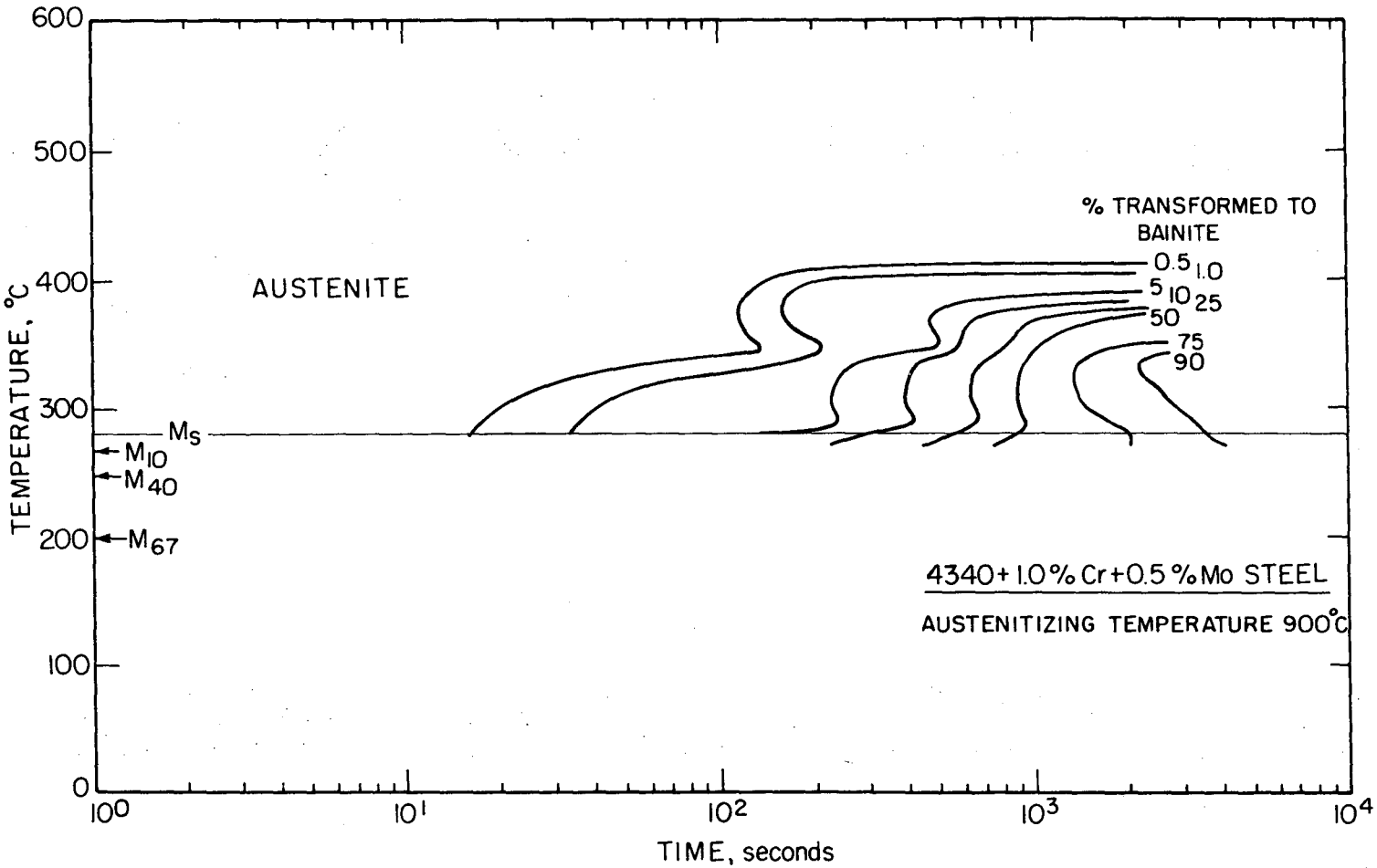
600
500
400
300
200
100
0
TEMPERATURE, °C
AUSTENITE
% TRANSFORMED TO
BAINITE
0.5
1.0
5
10
25
50
75
90
Ms
M10
M40
M67
4340+1.0% Cr+0.5 %Mo STEEL
AUSTENITIZING TEMPERATURE 900°C
10^0
10^1
10^2
10^3
10^4
TIME, seconds
XBL 745-6429

Fig. 12M

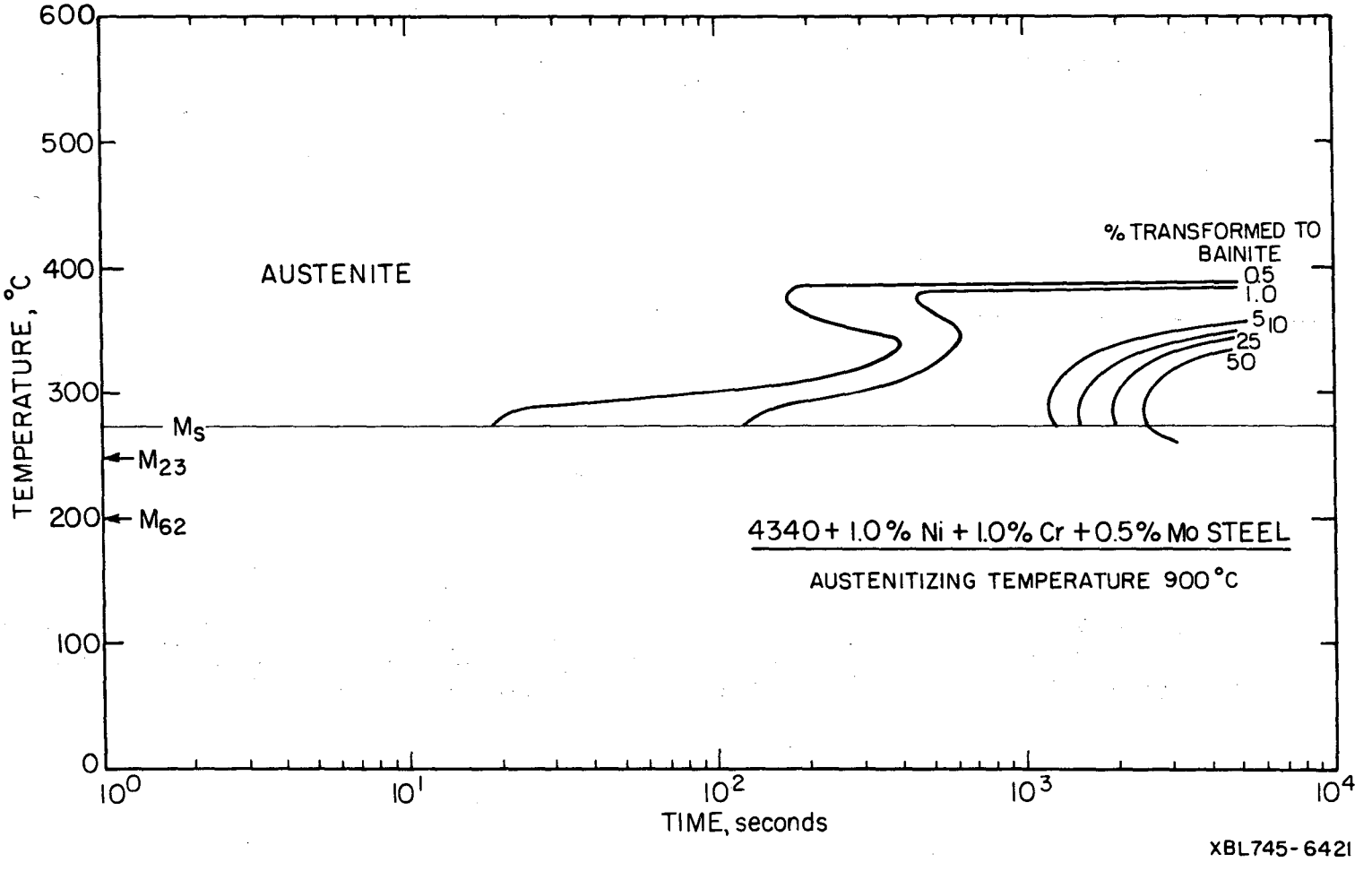
600
500
400
300
200
100
0
TEMPERATURE, °C
AUSTENITE
% TRANSFORMED TO BAINITE
0.5
1.0
5
10
25
50
M_S
M_{23}
M_{62}
4340 + 1.0% Ni + 1.0% Cr + 0.5% Mo STEEL
AUSTENITIZING TEMPERATURE 900°C
10^0
10^1
10^2
10^3
10^4
TIME, seconds
XBL745-6421

Fig. 12N

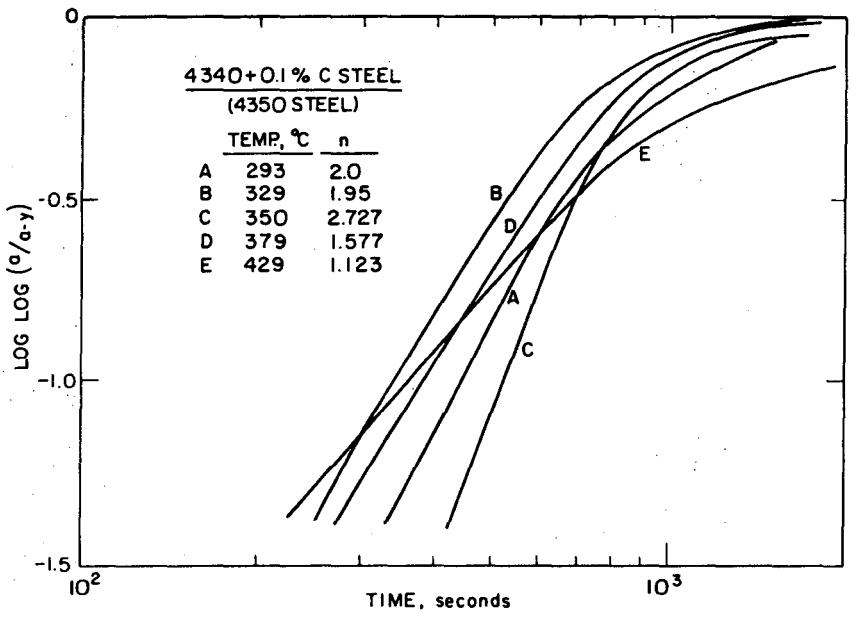
4340+0.1 % C STEEL
(4350 STEEL)
TEMP, °C n
A 293 2.0
B 329 1.95
C 350 2.727
D 379 1.577
E 429 1.123
LOG LOG (σ/σ-y)
0
-0.5
-1.0
-1.5
10²
10³
TIME, seconds
A
B
C
D
E

(a)

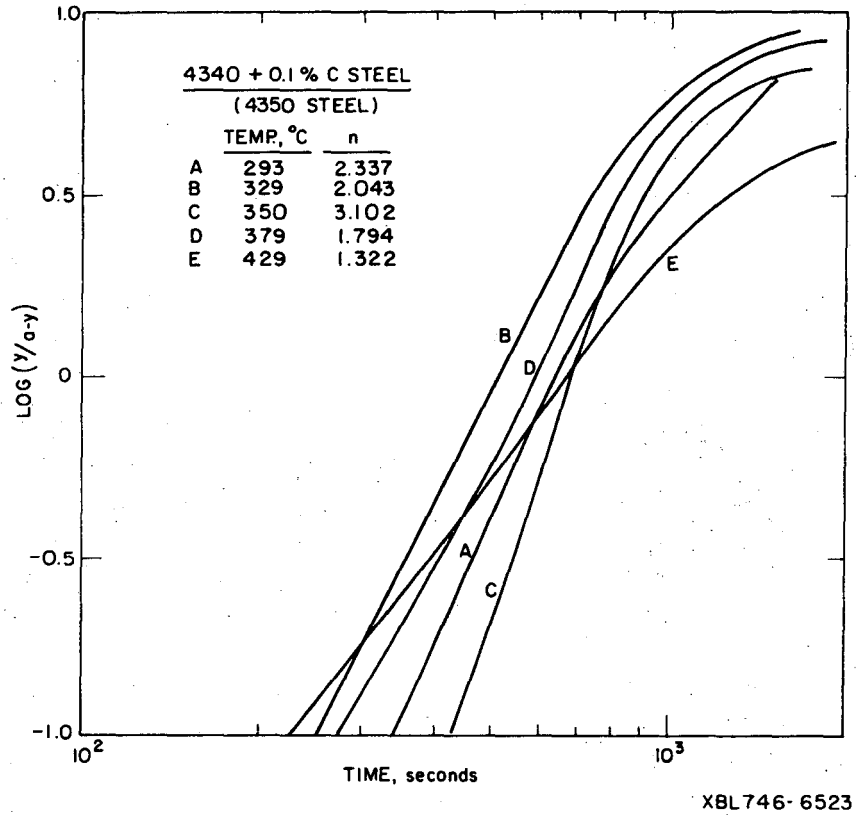
4340 + 0.1 % C STEEL
(4350 STEEL)
TEMP, °C n
A 293 2.337
B 329 2.043
C 350 3.102
D 379 1.794
E 429 1.322
LOG (Y/σ-y)
1.0
0.5
0
-0.5
-1.0
10²
10³
TIME, seconds
A
B
C
D
E
XBL746-6523

(b)

Fig. 13A

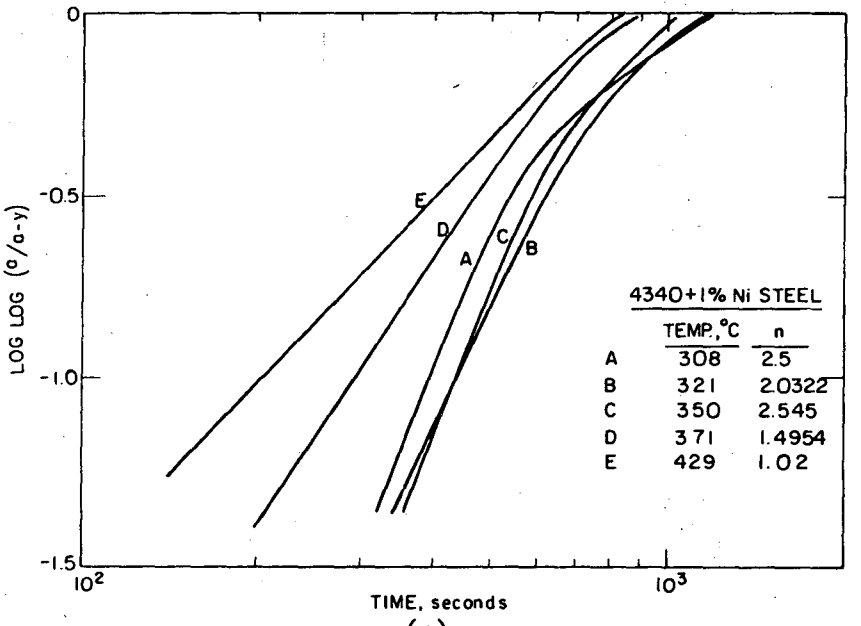
LOG LOG (σ/α-γ)
0
-0.5
-1.0
-1.5
10²
10³
TIME, seconds
A
B
C
D
E
4340+1% Ni STEEL
TEMP.,°C n
A 308 2.5
B 321 2.0322
C 350 2.545
D 371 1.4954
E 429 1.02

(a)

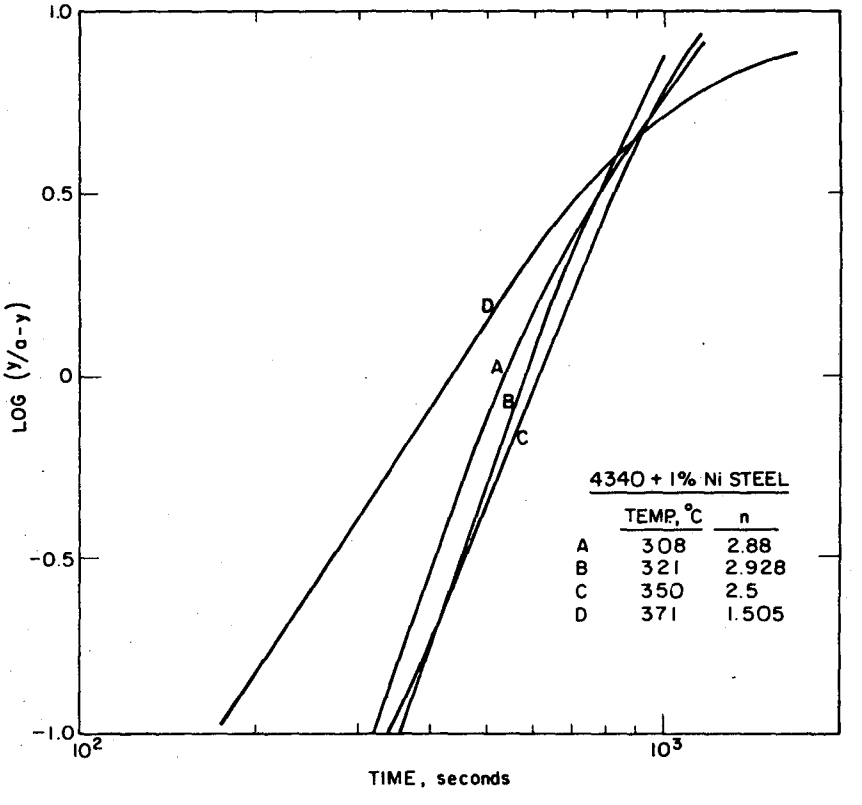
LOG (γ/α-γ)
1.0
0.5
0
-0.5
-1.0
10²
10³
TIME, seconds
A
B
C
D
4340 + 1% Ni STEEL
TEMP, °C n
A 308 2.88
B 321 2.928
C 350 2.5
D 371 1.505
XBL 746-6522

(b)

Fig. 13B

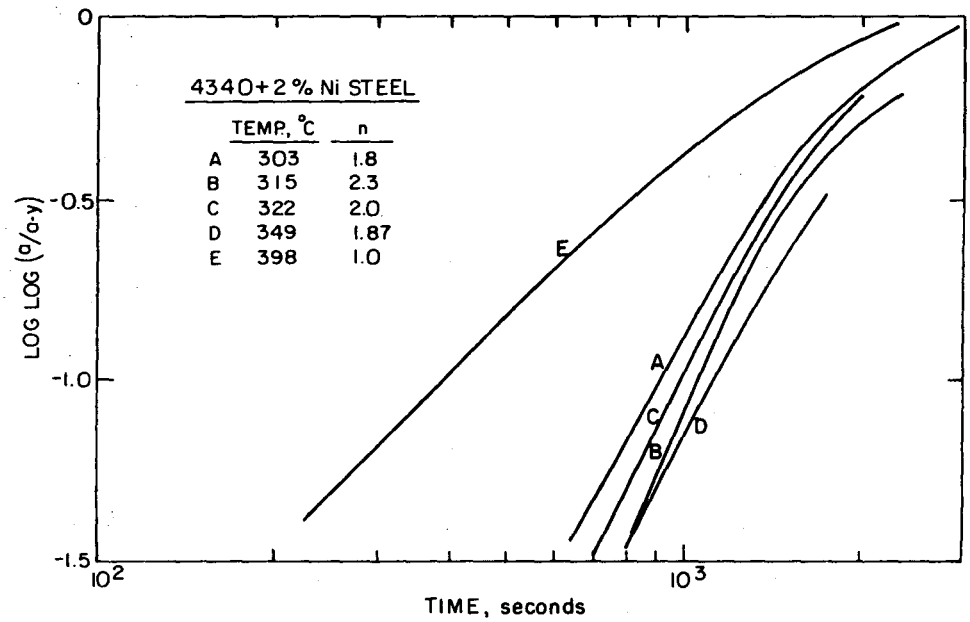
4340+2 % Ni STEEL
TEMP, °C n
A 303 1.8
B 315 2.3
C 322 2.0
D 349 1.87
E 398 1.0
LOG LOG (o/o-y)
0
-0.5
-1.0
-1.5
10^2
10^3
TIME, seconds
A
B
C
D
E

(a)

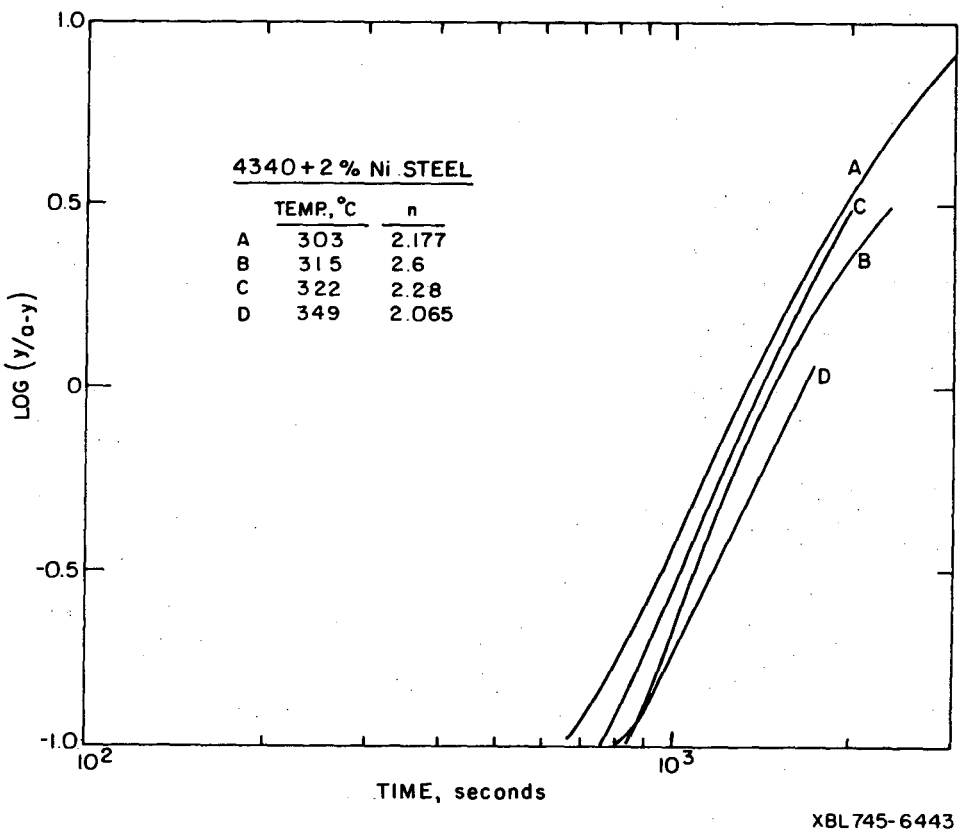
4340+2 % Ni STEEL
TEMP, °C n
A 303 2.177
B 315 2.6
C 322 2.28
D 349 2.065
LOG (y/o-y)
1.0
0.5
0
-0.5
-1.0
10^2
10^3
TIME, seconds
A
B
C
D
XBL745-6443

(b)

Fig. 13C

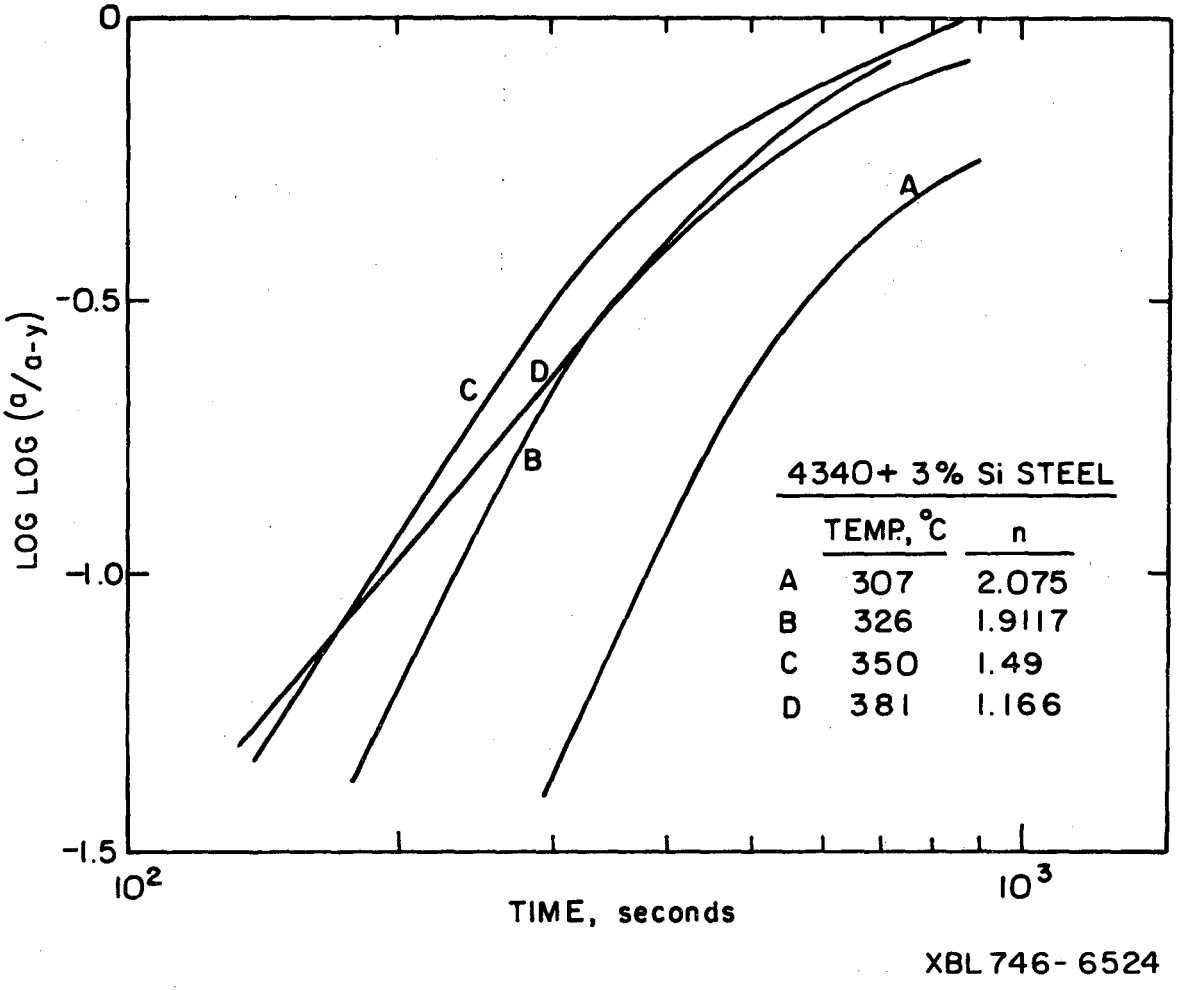
0
-0.5
-1.0
-1.5
LOG LOG (a/a-y)
10^2
10^3
TIME, seconds
A
B
C
D
4340+ 3% Si STEEL
TEMP, °C
n
A 307 2.075
B 326 1.9117
C 350 1.49
D 381 1.166
XBL 746-6524

Fig. 14

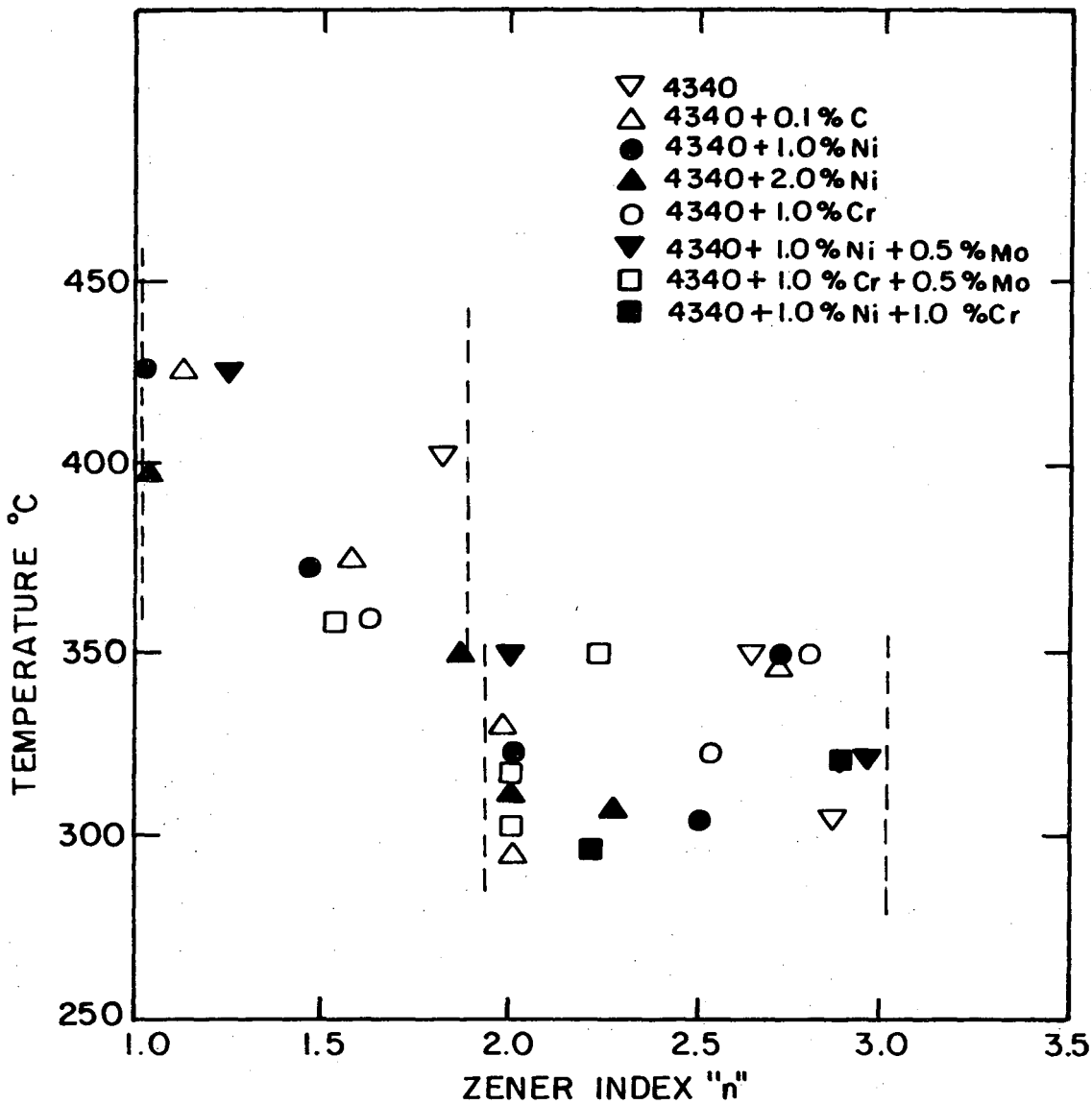

XBL 746-6516

Fig. 15

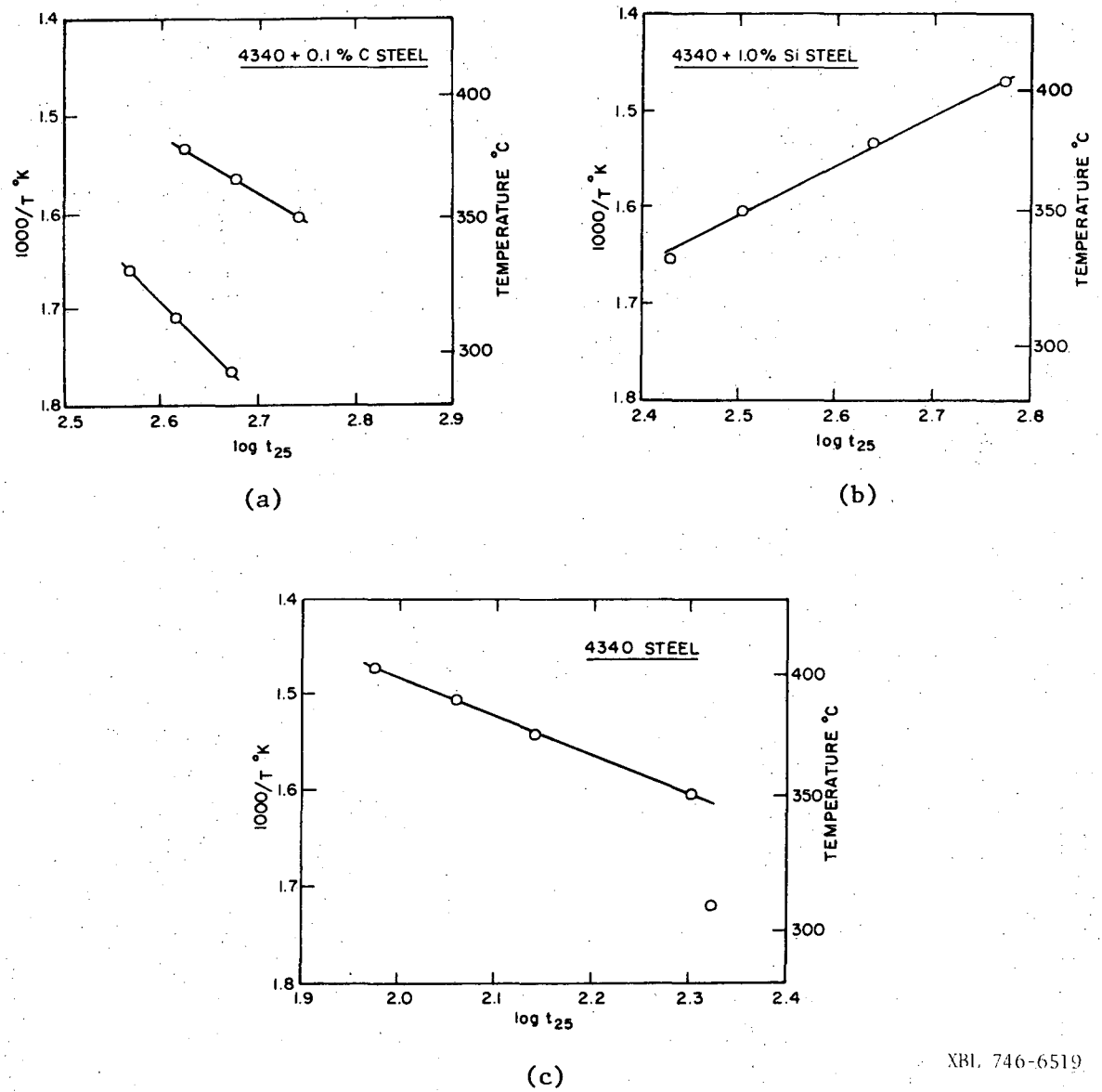
4340 + 0.1 % C STEEL
1000/T °K
TEMPERATURE °C
log t_{25}
(a)
4340 + 1.0% Si STEEL
1000/T °K
TEMPERATURE °C
log t_{25}
(b)
4340 STEEL
1000/T °K
TEMPERATURE °C
log t_{25}
(c)
XBL 746-6519

Fig. 16

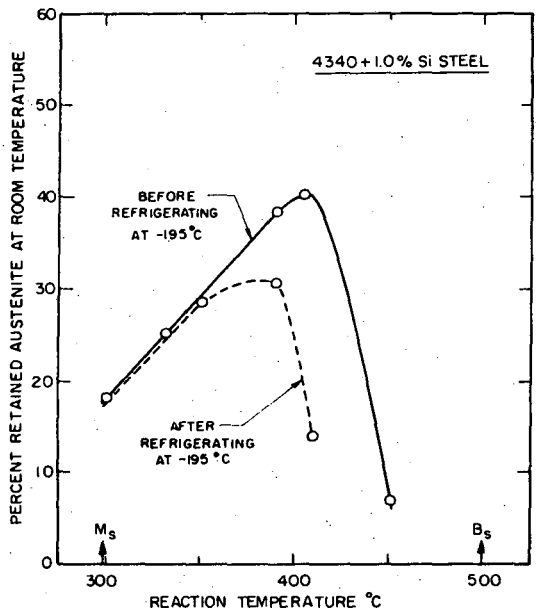

Fig. 17A

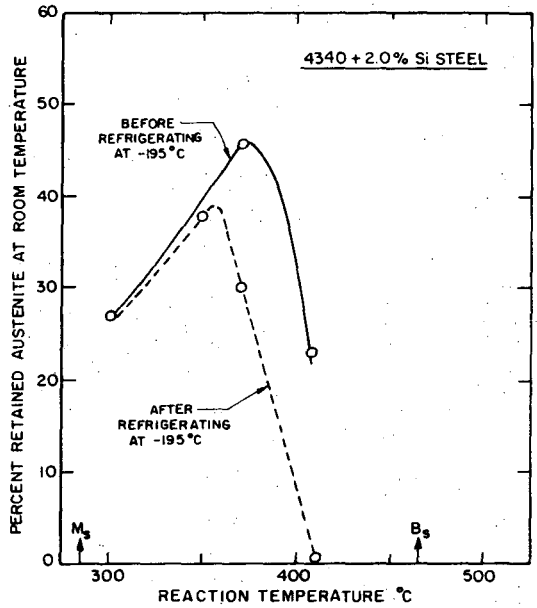

Fig. 17B

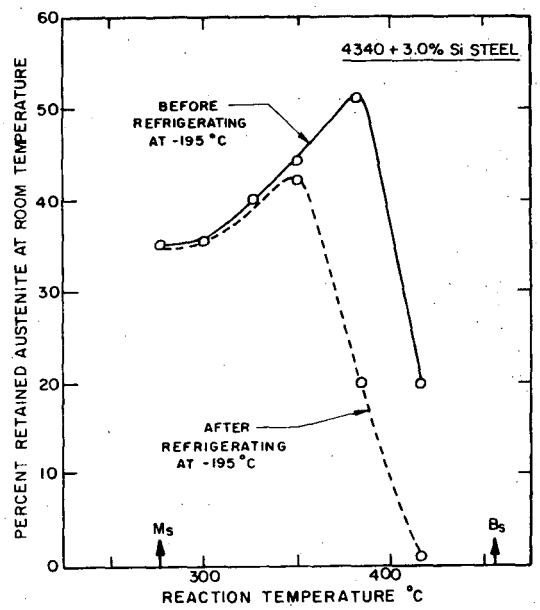

XBL 746-6520

Fig. 17C

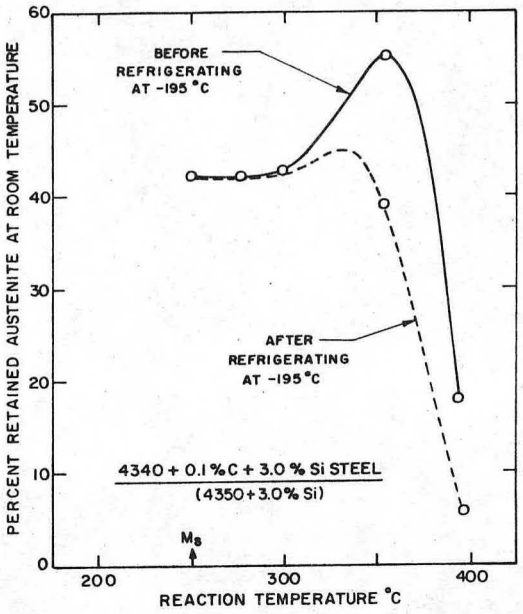

Fig. 17D

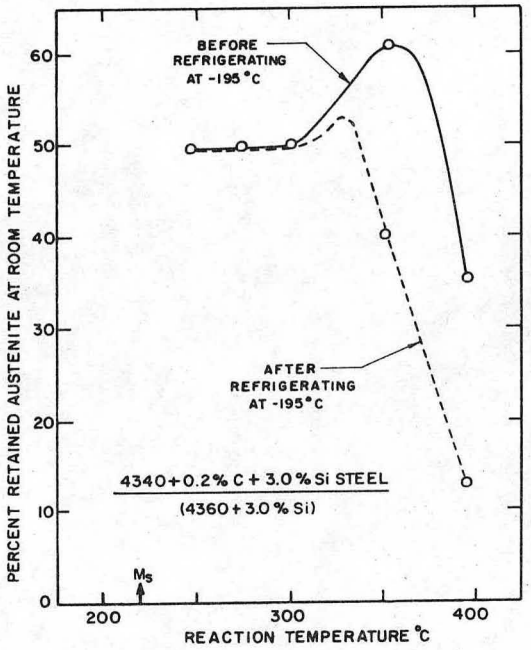

XBL 746-6521

Fig. 17E

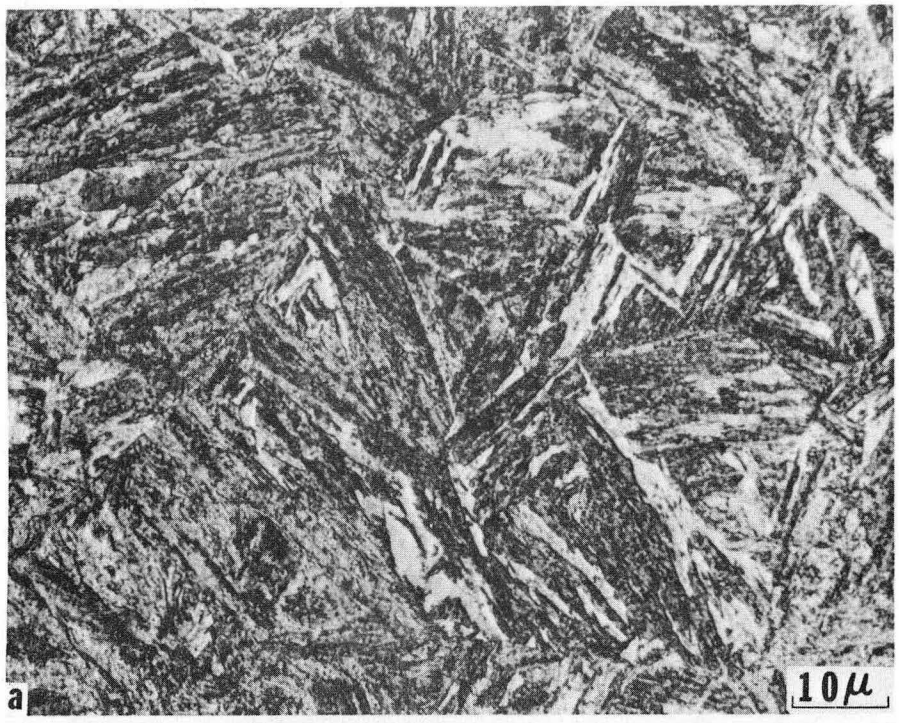

XB3 746-4182

Fig. 18

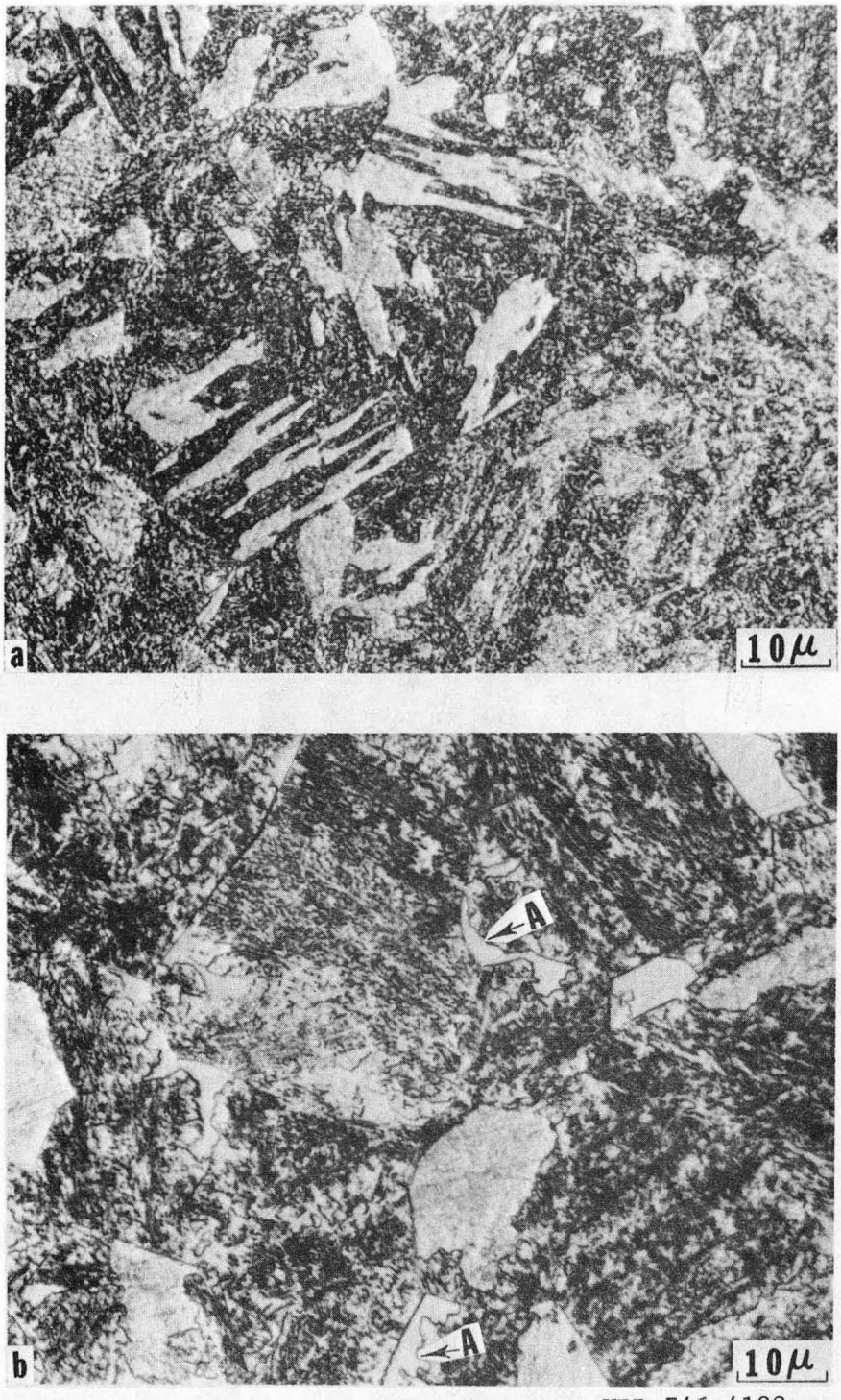

XBB 746-4188

Fig. 19

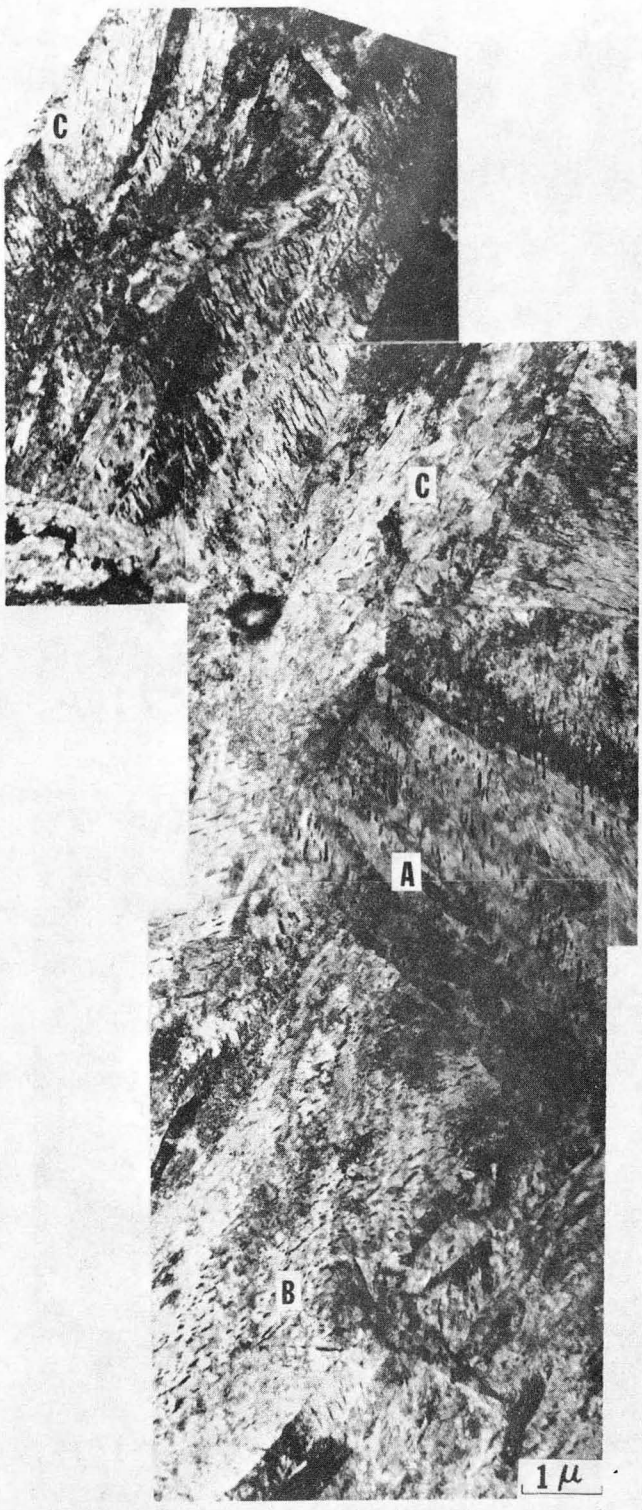

XBB 746-4175

Fig. 20

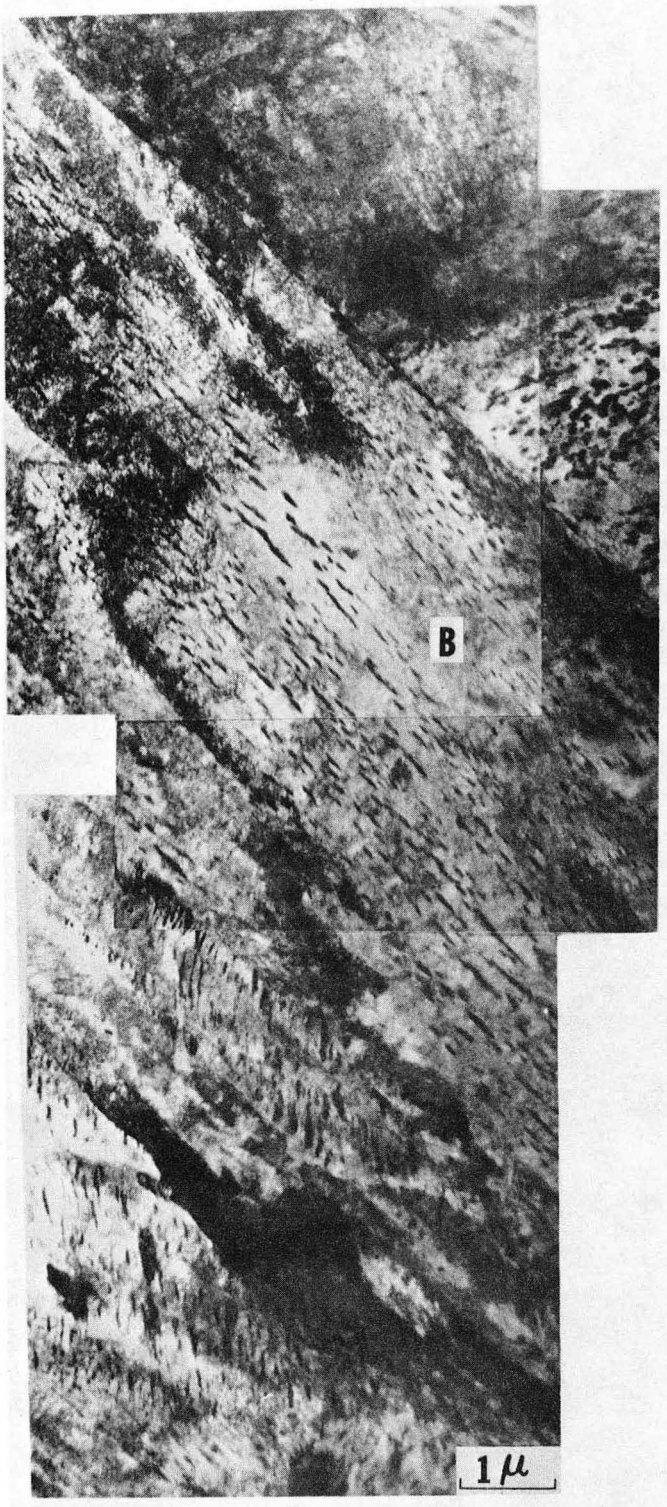

XBB 746-4174

Fig. 21

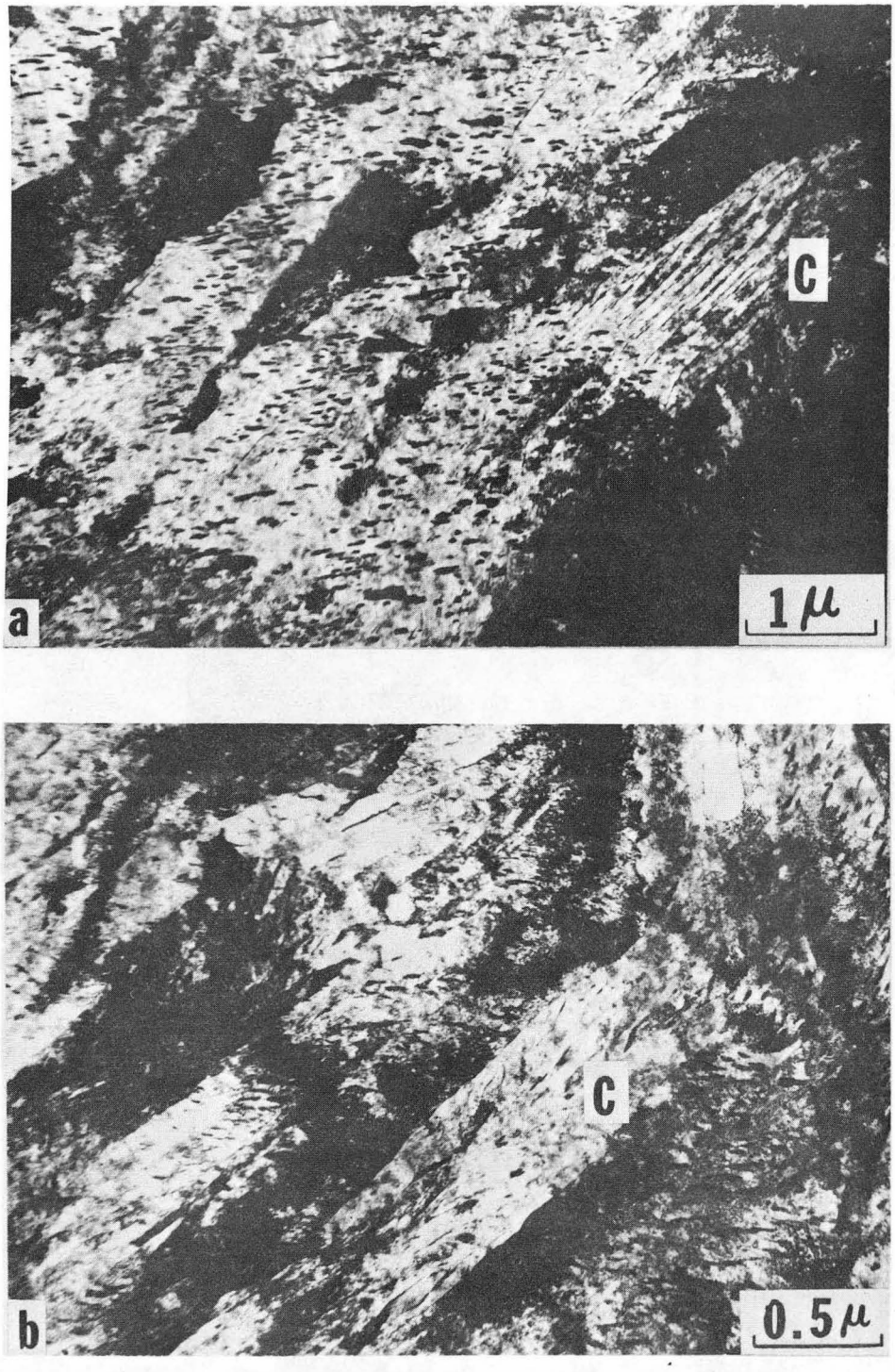

XBB 746-4190

Fig. 22

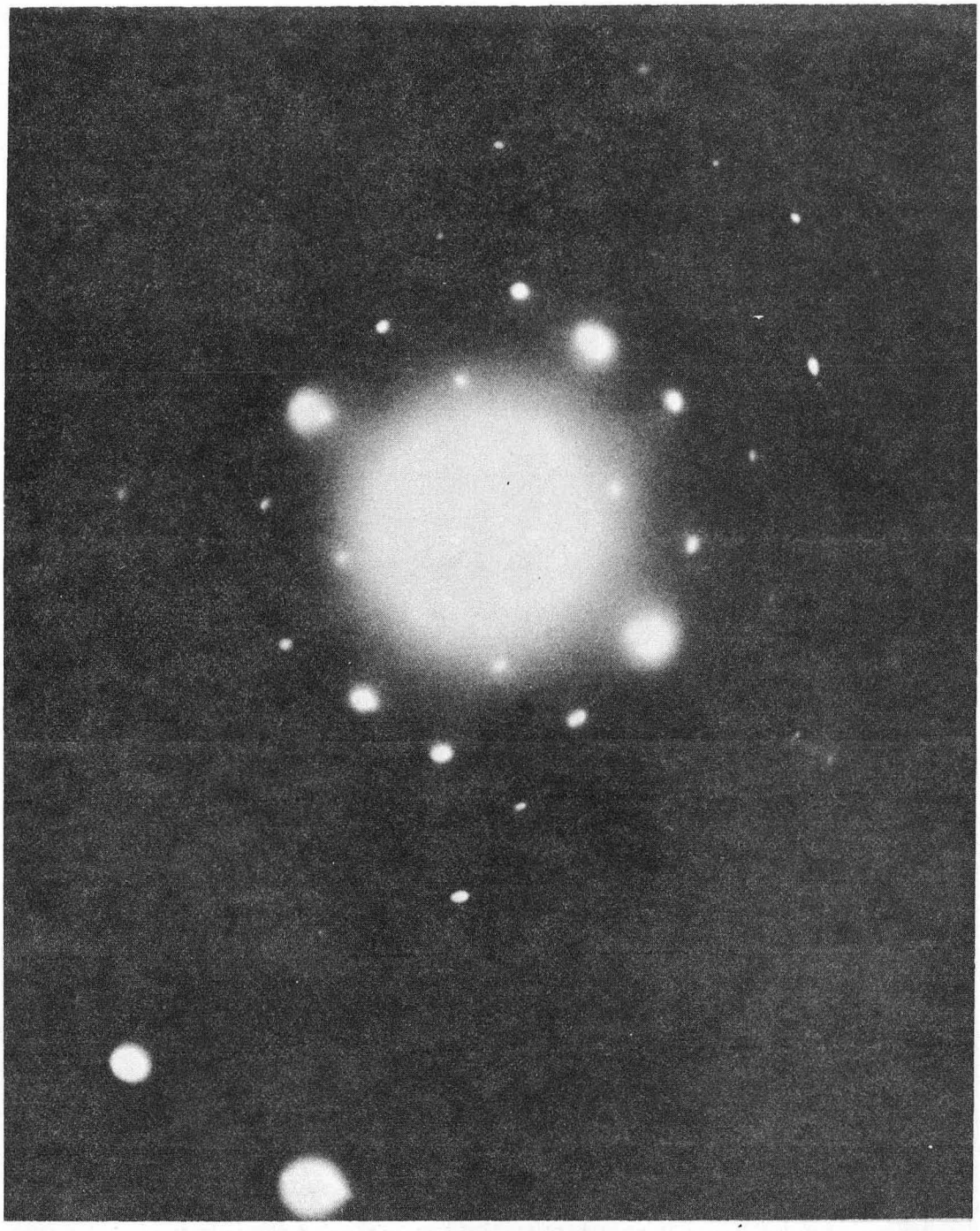

XBB 746-4192

Fig. 23

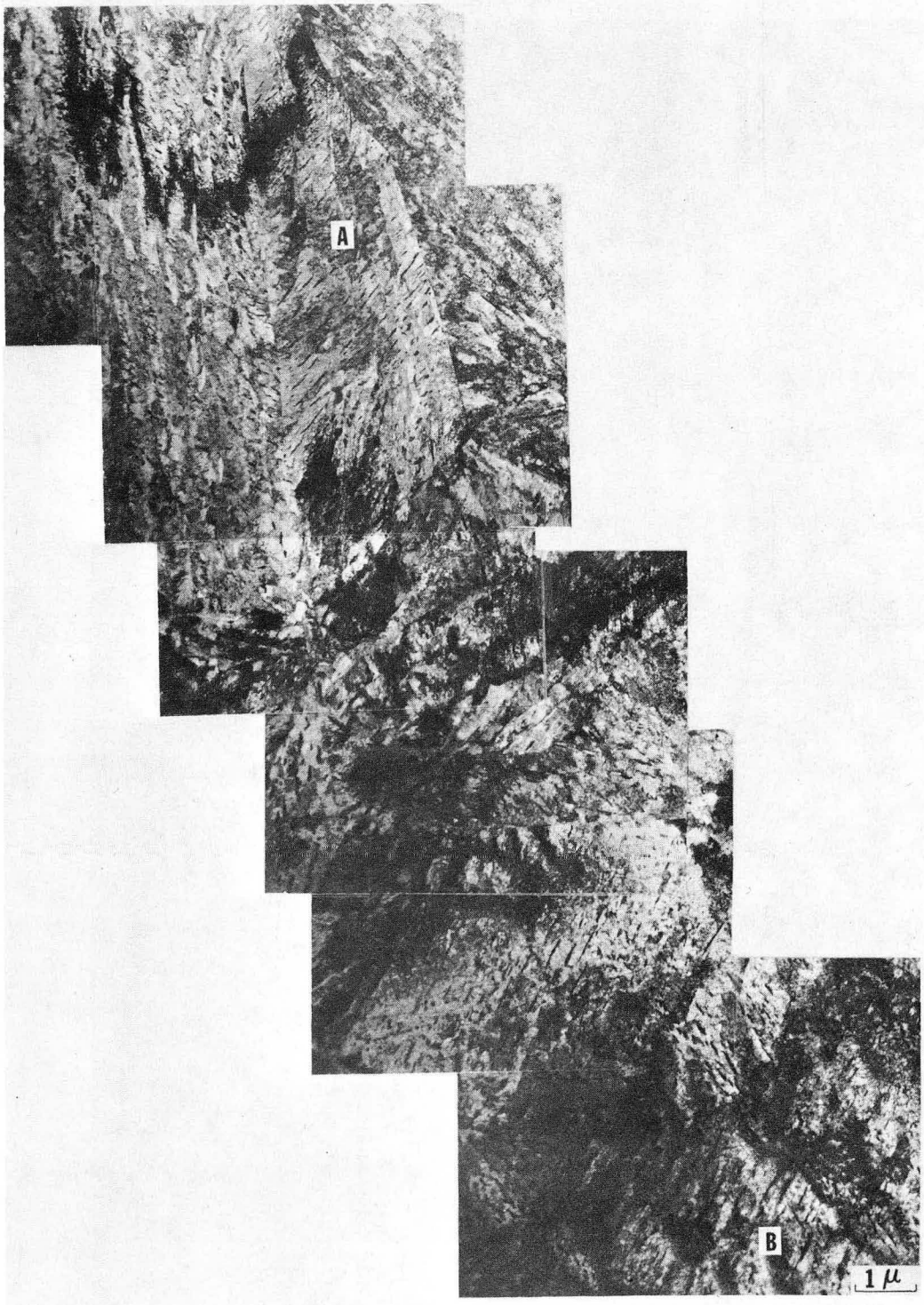

XBB 746-4177

Fig. 24

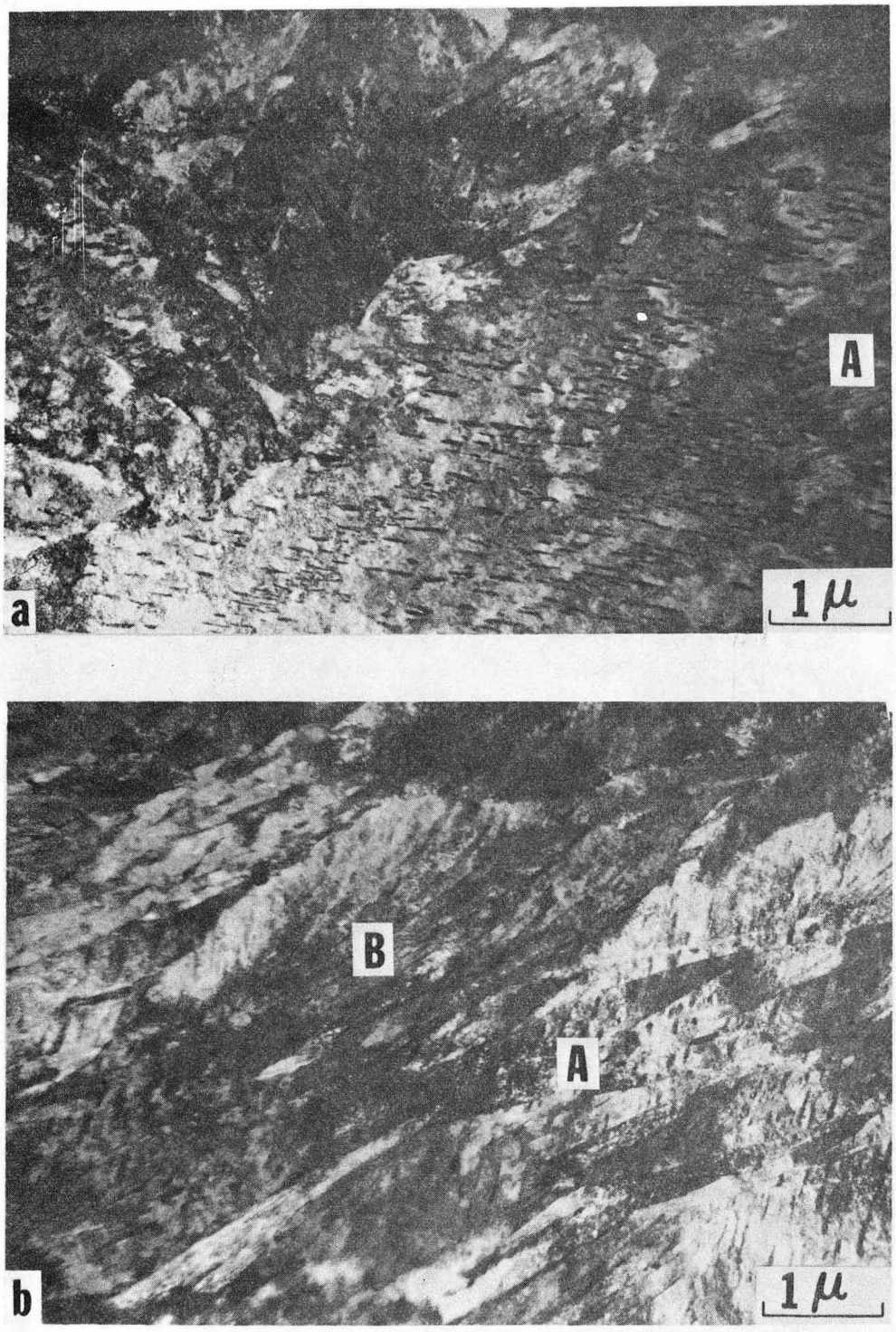

XBB 746-4186

Fig. 25

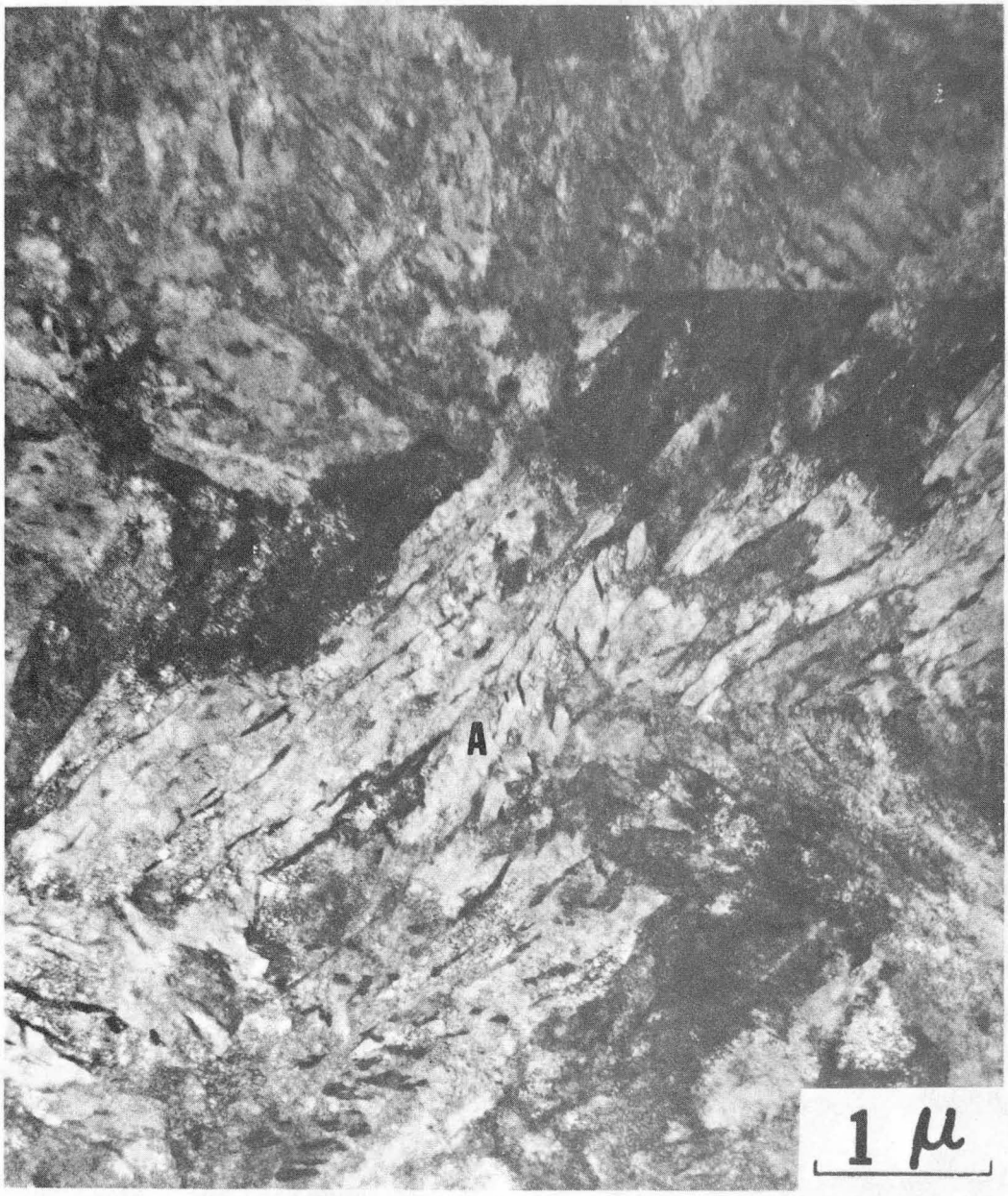

XBB 747-4732

Fig. 26

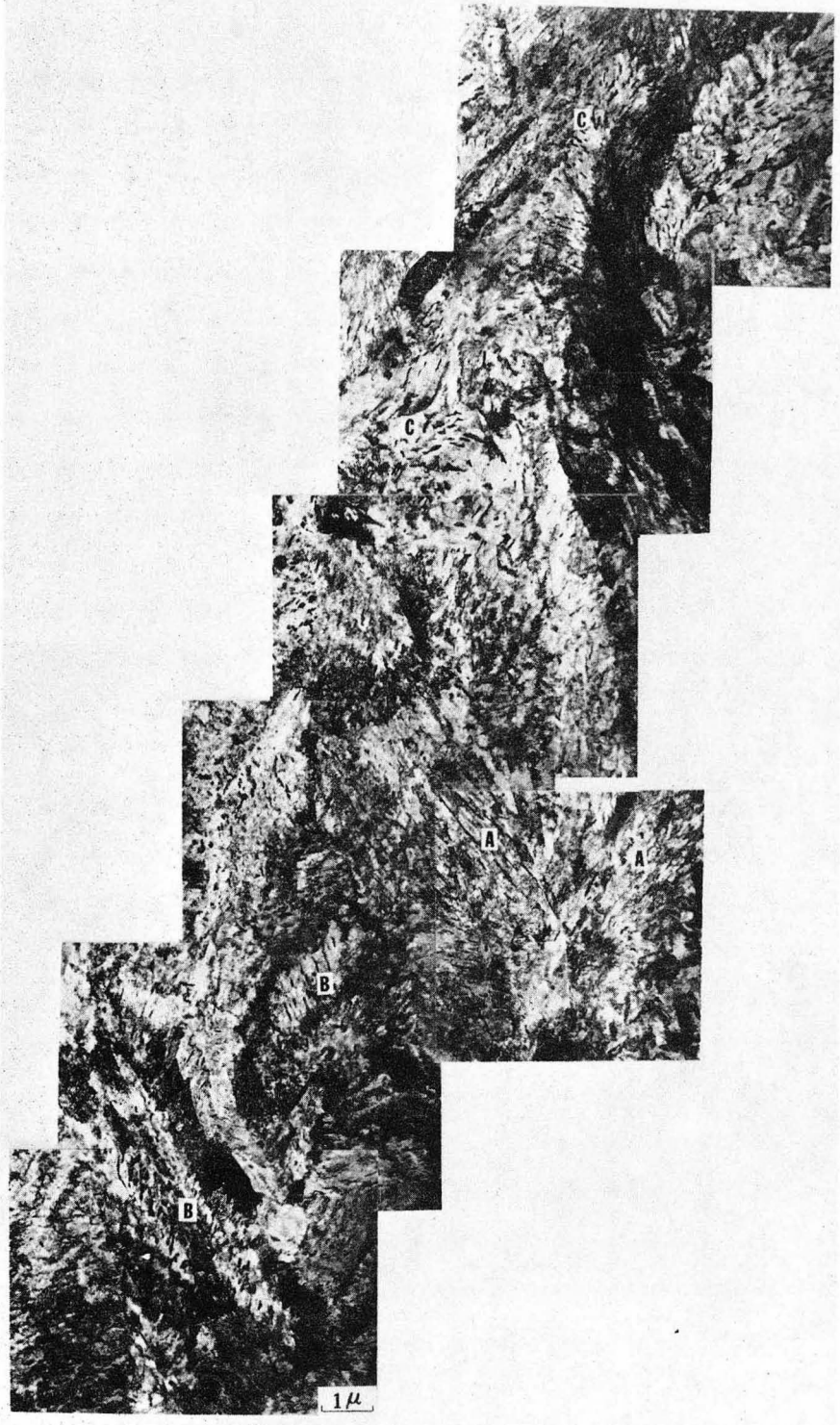

XBB 746-4176

Fig. 27

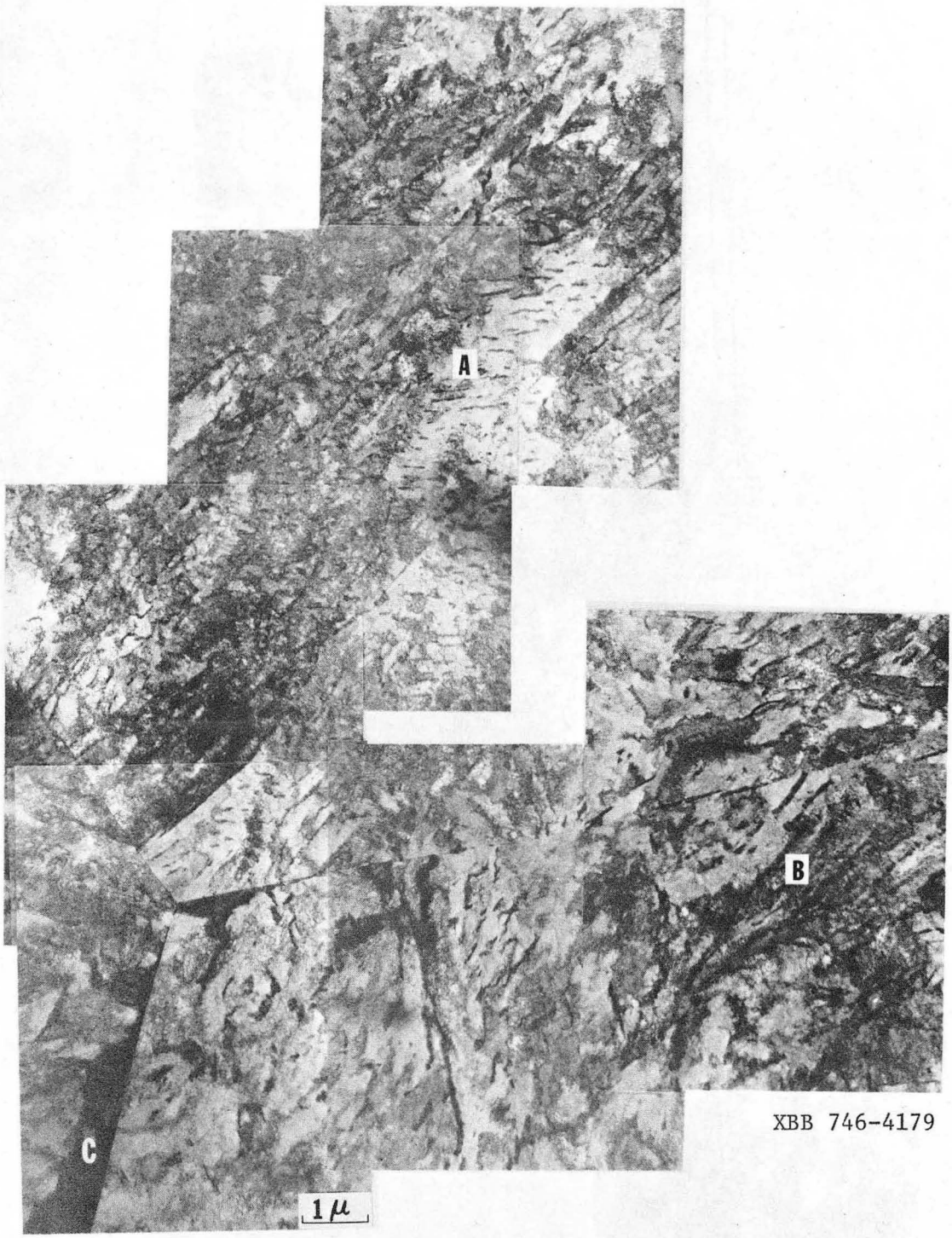

XBB 746-4179

Fig. 28

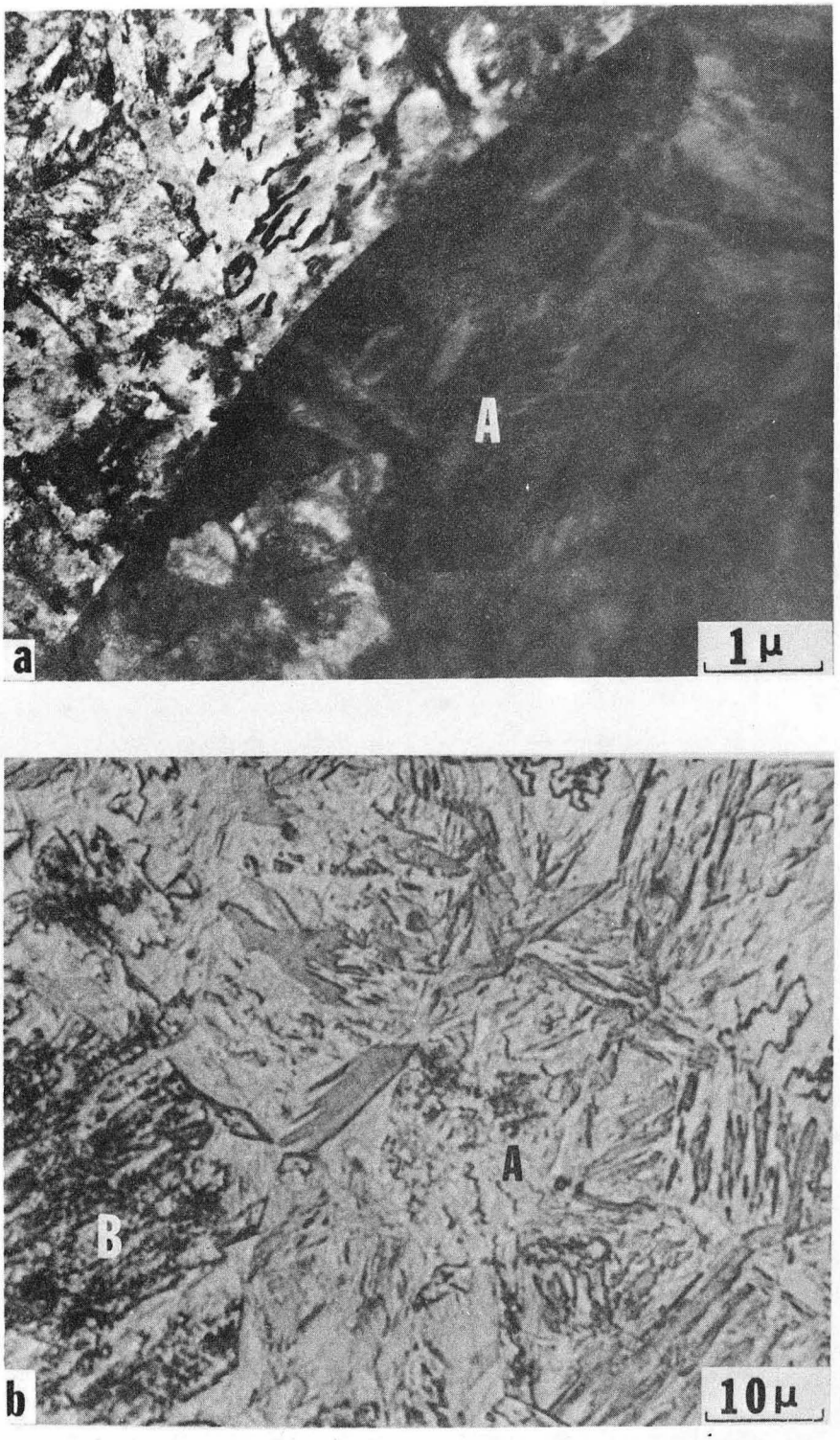

XBB 746-4187

Fig. 29

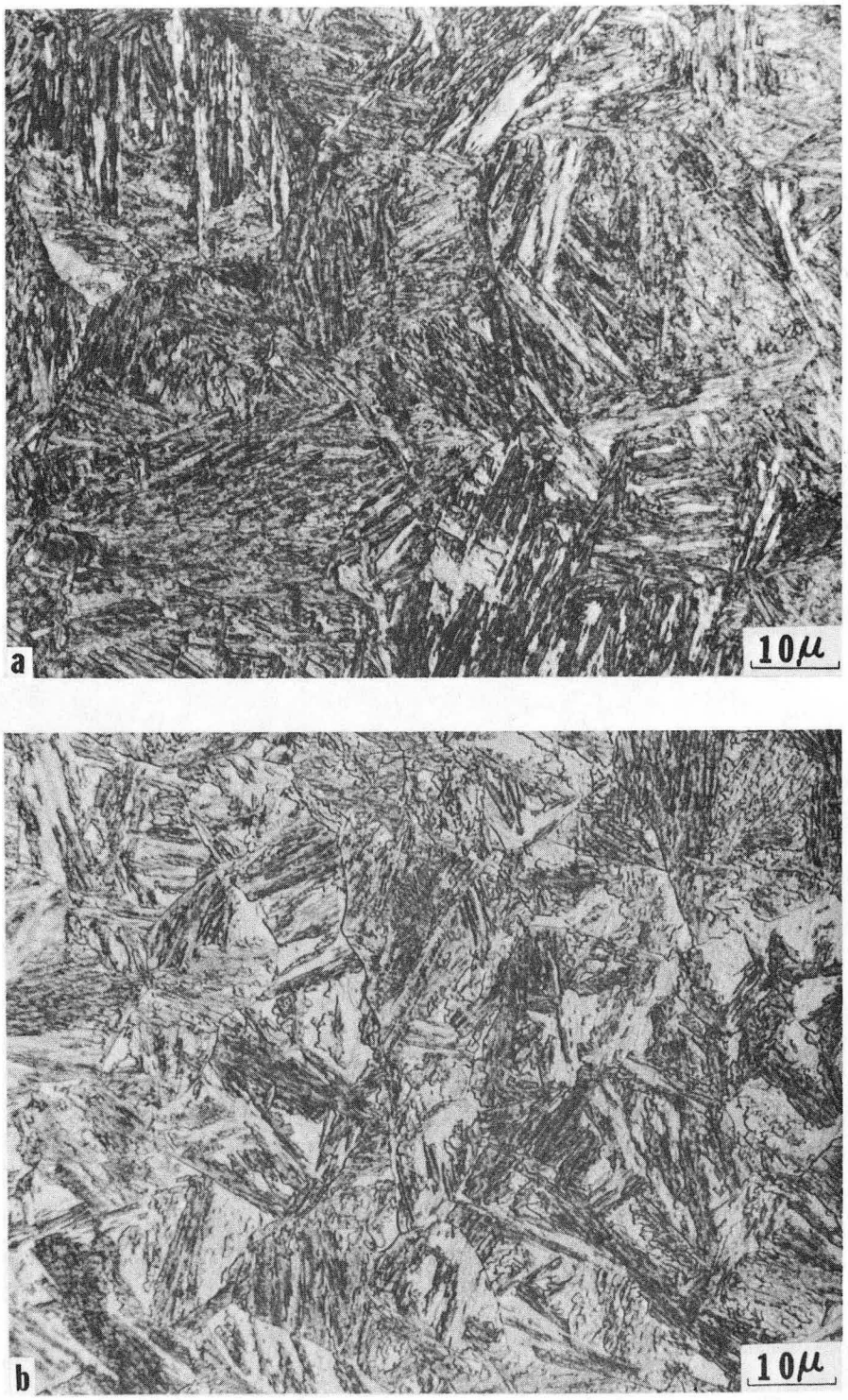

XBB 746-4181

Fig. 30

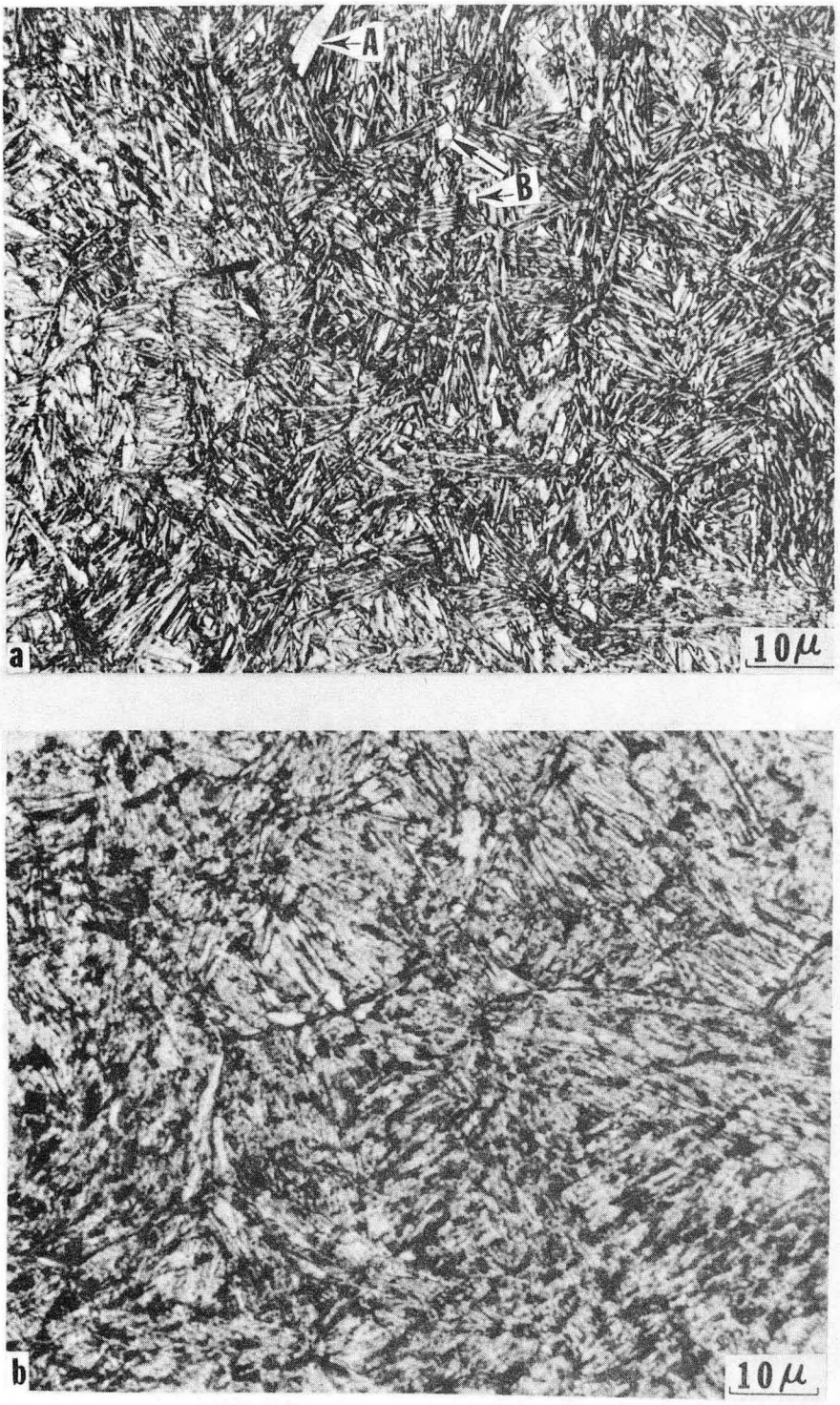

XBB 746-4185

Fig. 31

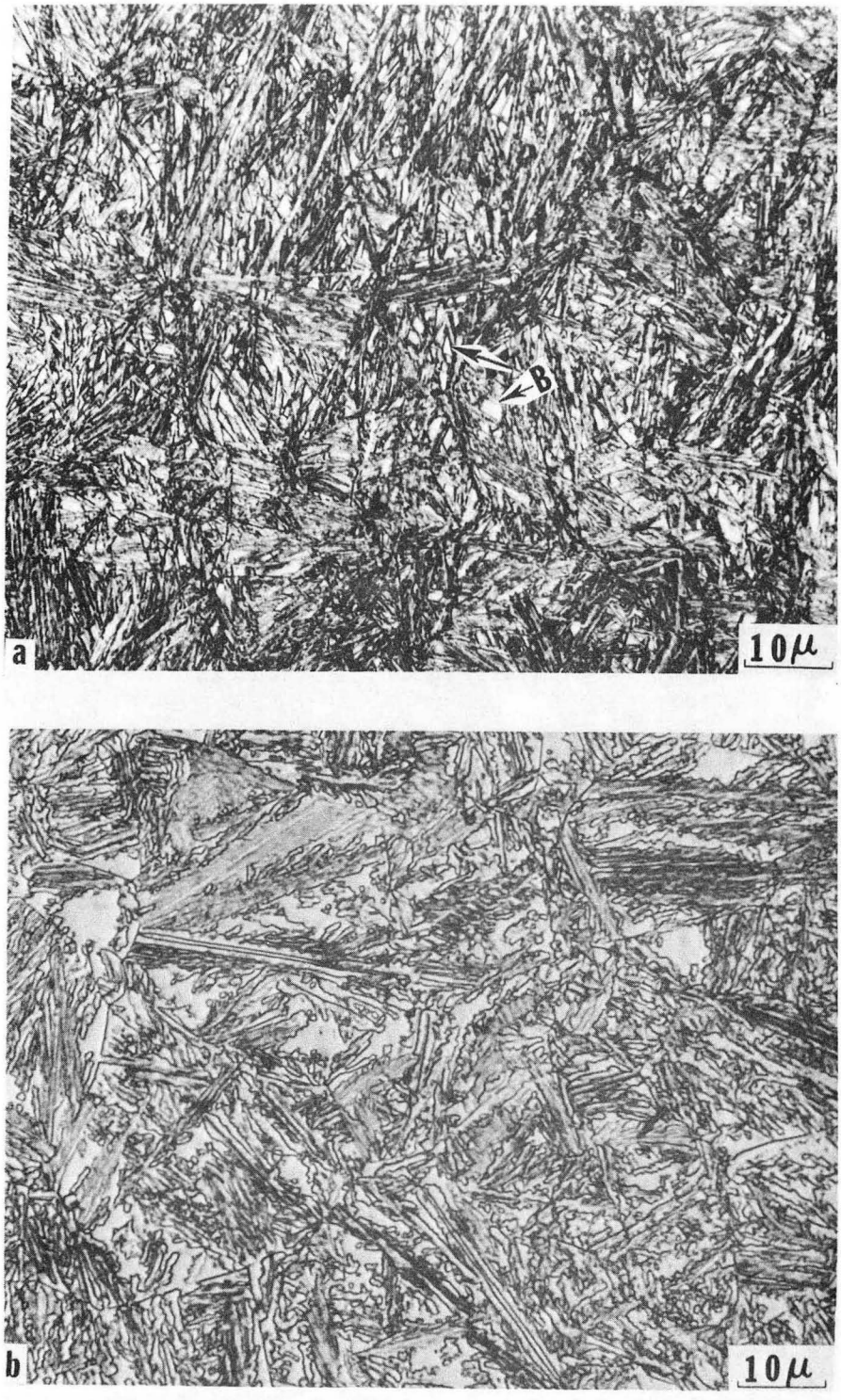

XBB 746-4183

Fig. 32

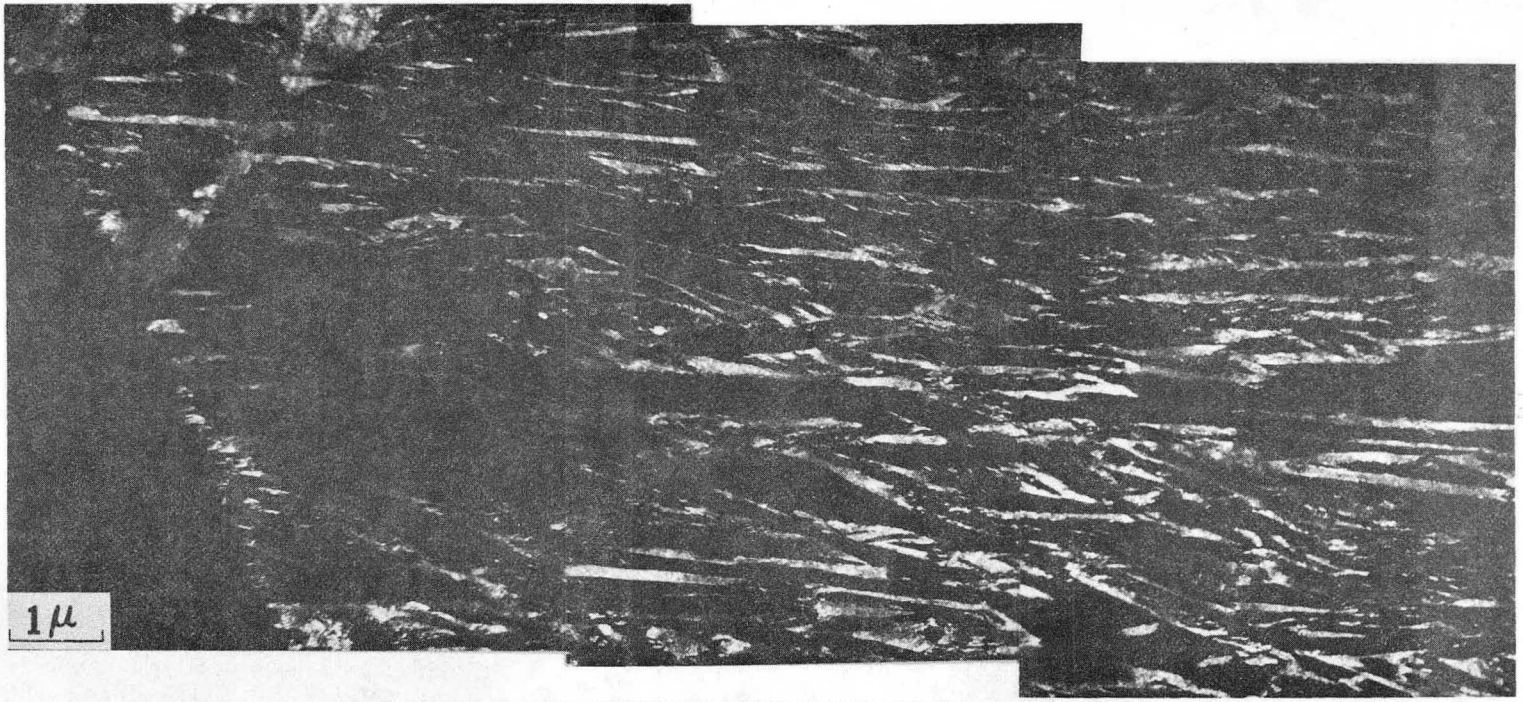

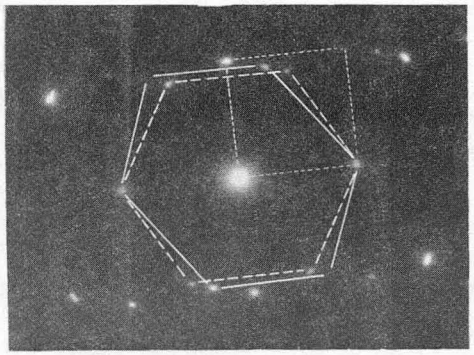

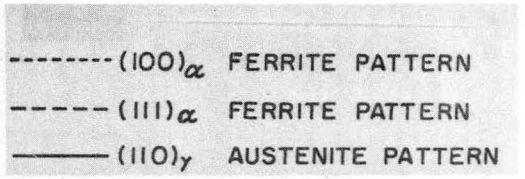

XBB 746-4178

Fig. 33

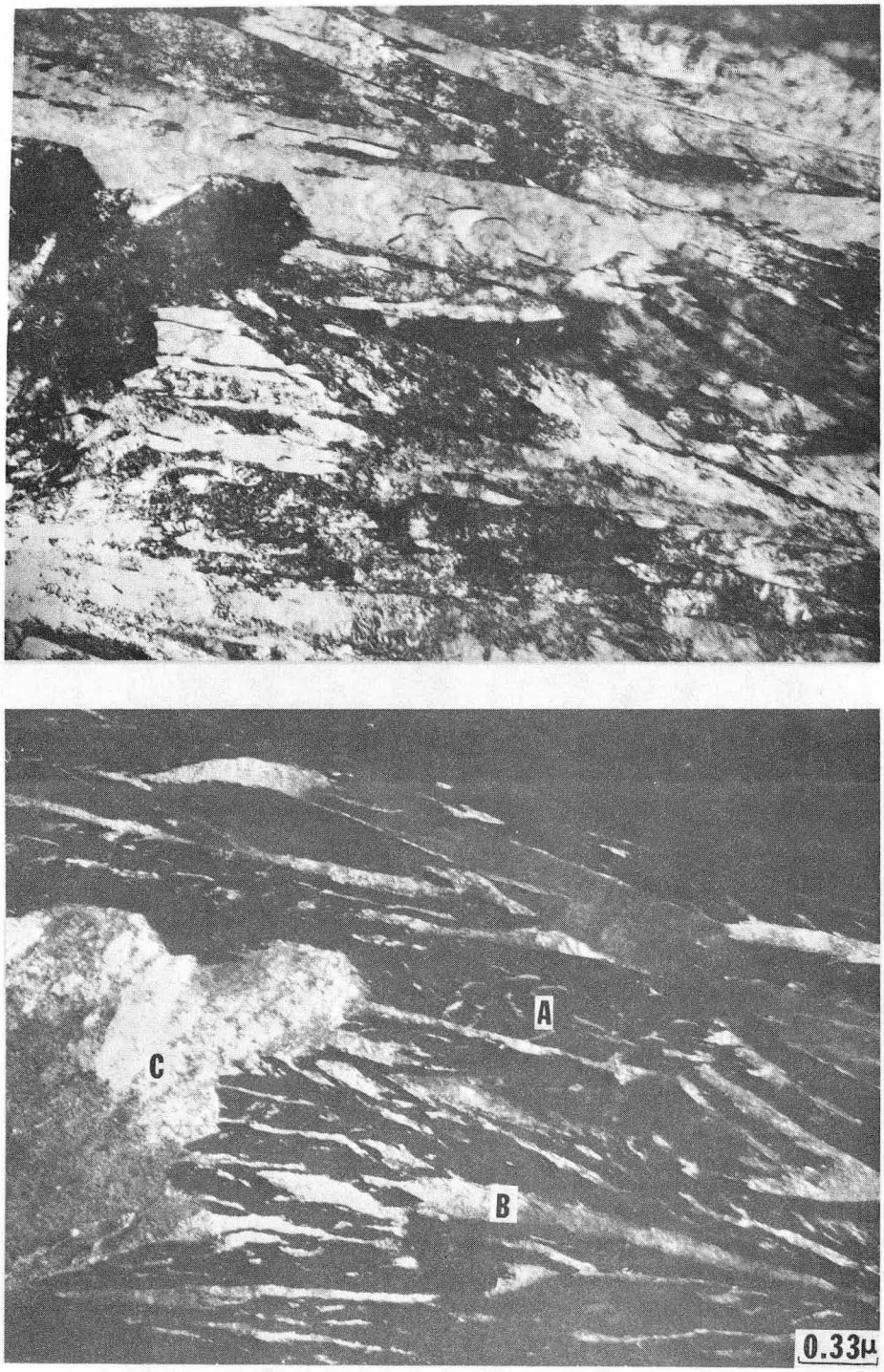

XBB 746-4189.

Fig. 34

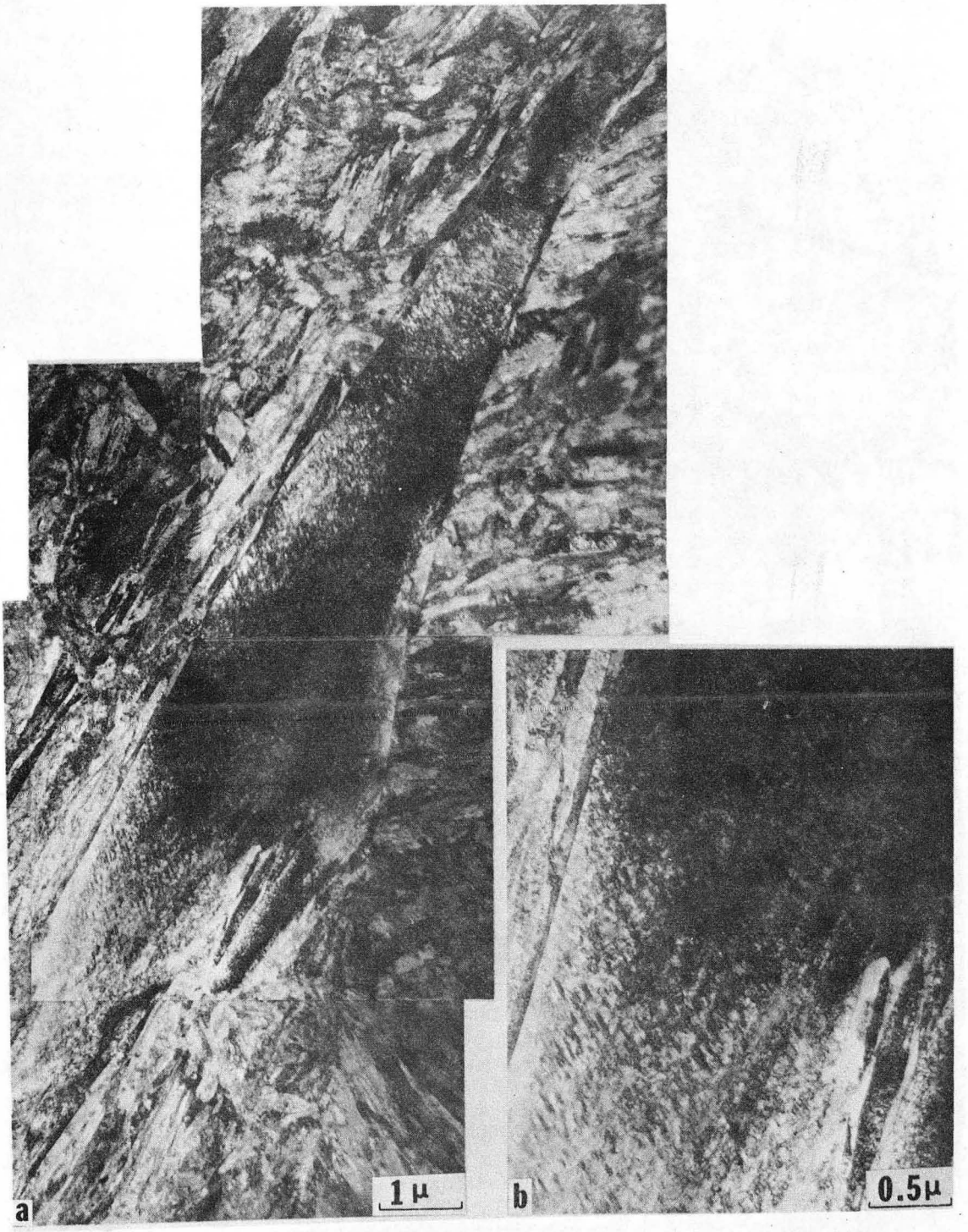

XBB 746-4180

Fig. 35

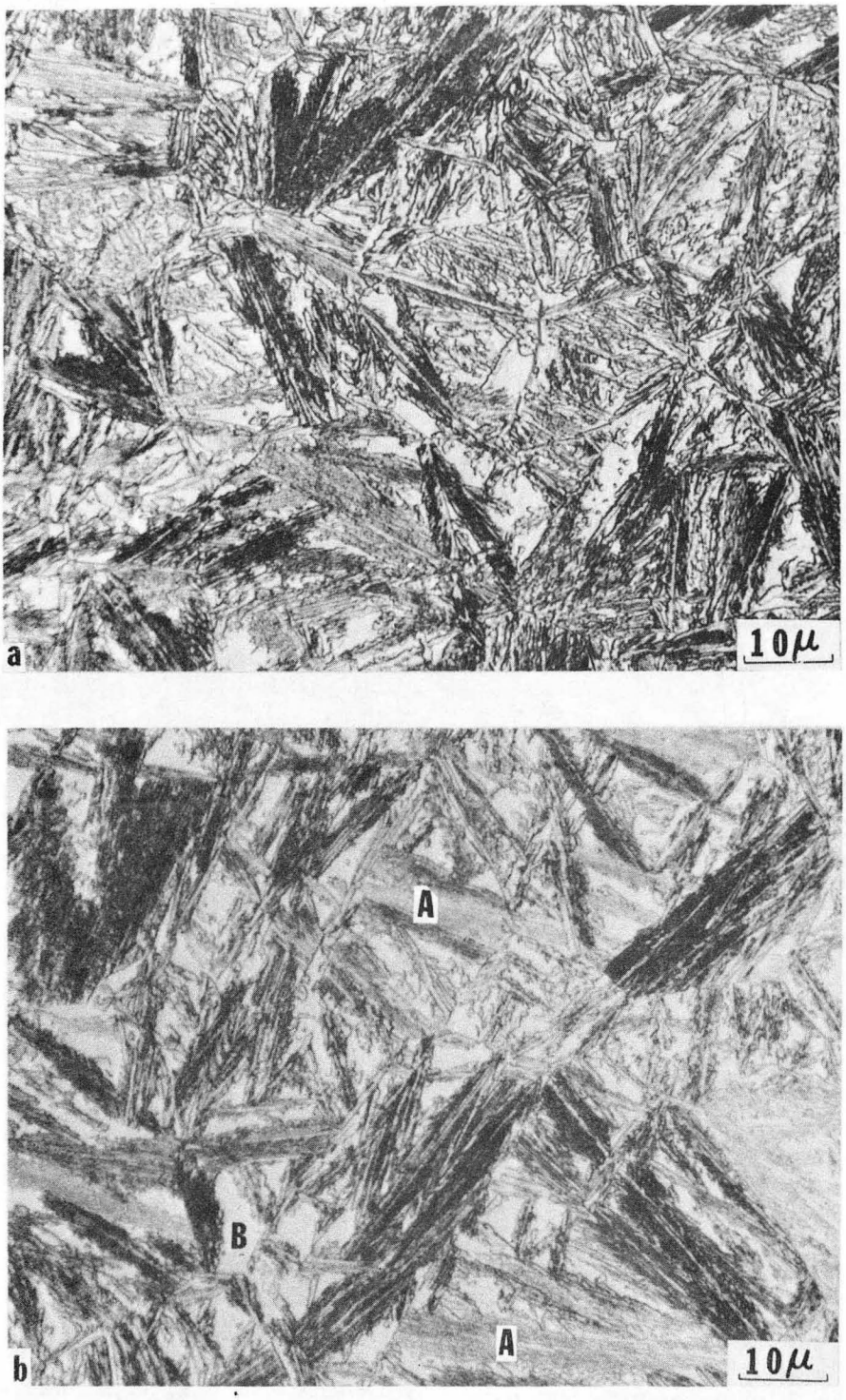

XBB 746-4184

Fig. 36

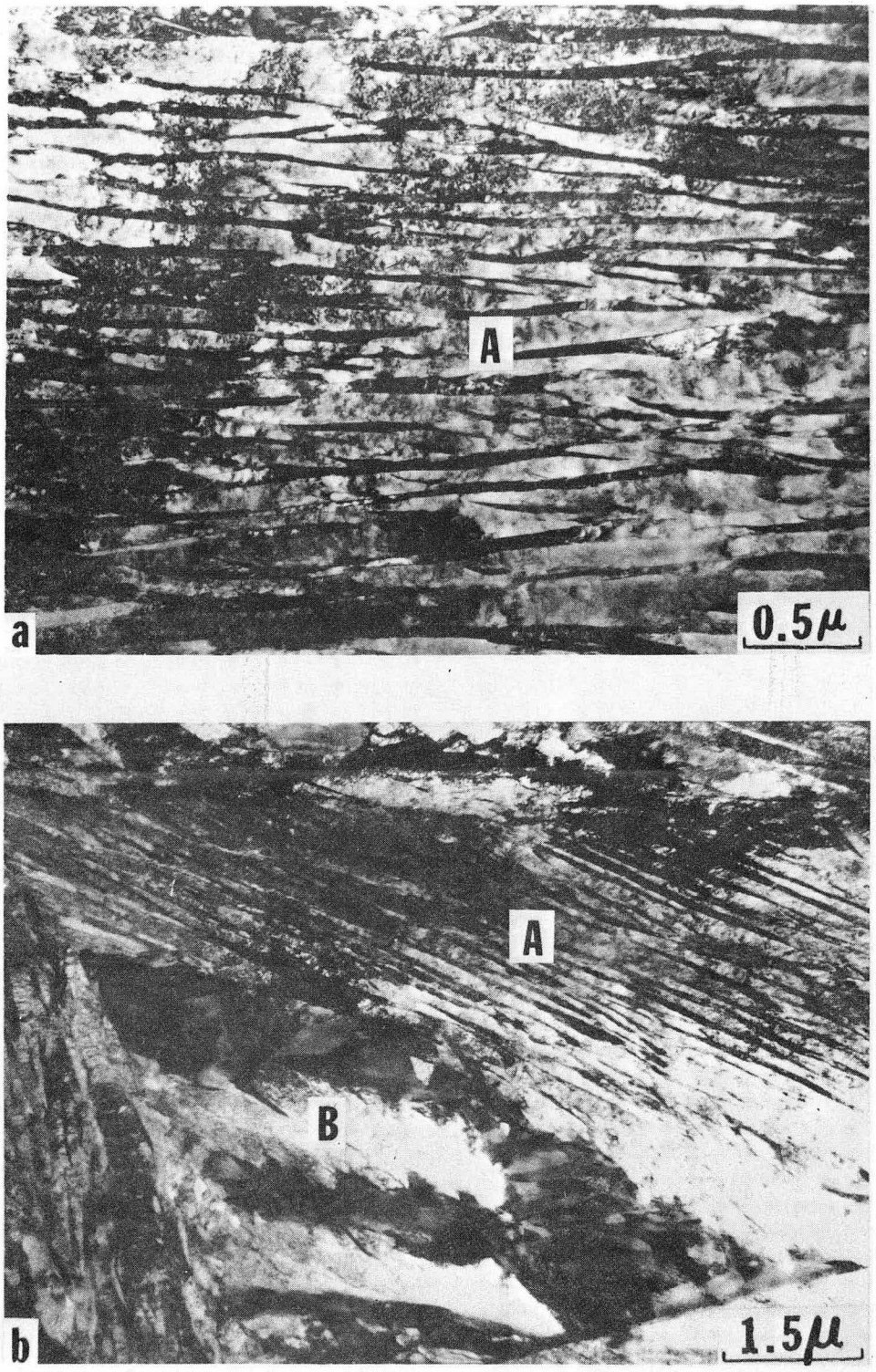

XBB 746-4191

Fig. 37

TECHNICAL INFORMATION DIVISION
LAWRENCE BERKELEY LABORATORY
UNIVERSITY OF CALIFORNIA
BERKELEY, CALIFORNIA 94720